MODELING AND ANALYSIS OF ACTUAL EVAPOTRANSPIRATION USING DATA DRIVEN AND WAVELET TECHNIQUES

A Thesis

Submitted to the College of Graduate Studies and Research

In Partial Fulfillment of the Requirements

for the

Degree of Master of Science

in the

Department of Civil and Geological Engineering

University of Saskatchewan,

Saskatoon, Saskatchewan, Canada

By

Zohreh Izadifar

PERMISSION TO USE

The author has agreed that the library, University of Saskatchewan, may make this thesis freely available for inspection. Moreover, the author has agreed that permission for extensive copying of this thesis for scholarly purposes may be granted by the professors who supervised the thesis work recorded herein or, in their absence, by the head of the Department or the Dean of the College in which the thesis work was done. It is understood that due recognition will be given to the author of this thesis and to the University of Saskatchewan in any use of the material in this thesis. Copying or publication or any other use of the thesis for financial gain without approval by the University of Saskatchewan and the author's written permission is prohibited.

Requests for permission to copy or to make any other use of material in this thesis in whole or part should be addresses to:

Head of the Department of Civil and Geological Engineering,
University of Saskatchewan,
57 Campus Drive,
Saskatoon, Saskatchewan,
Canada, S7N 5A9

ABSTRACT

Large-scale mining practices have disturbed many natural watersheds in northern Alberta, Canada. To restore disturbed landscapes and ecosystems' functions, reconstruction strategies have been adopted with the aim of establishing sustainable reclaimed lands. The success of the reconstruction process depends on the design of reconstruction strategies, which can be optimized by improving the understanding of the controlling hydrological processes in the reconstructed watersheds. Evapotranspiration is one of the important components of the hydrological cycle; its estimation and analysis are crucial for better assessment of the reconstructed landscape hydrology, and for more efficient design. The complexity of the evapotranspiration process and its variability in time and space has imposed some limitations on previously developed evapotranspiration estimation models. The vast majority of the available models estimate the rate of potential evapotranspiration, which occurs under unlimited water supply condition. However, the rate of actual evapotranspiration (AET) depends on the available soil moisture, which makes its physical modeling more complicated than the potential evapotranspiration. The main objective of this study is to estimate and analyze the AET process in a reconstructed landscape.

Data driven techniques can model the process without having a complete understanding of its physics. In this study, three data driven models; genetic programming (GP), artificial neural networks (ANNs), and multilinear regression (MLR), were developed and compared for estimating the hourly eddy covariance (EC)-measured AET using meteorological variables. The AET was modeled as a function of five meteorological variables: net radiation (R_n), ground temperature (T_g), air temperature (T_a), relative humidity (RH), and wind speed (W_s) in a reconstructed landscape located in northern Alberta, Canada. Several ANN models were evaluated using two training algorithms of Levenberg-Marquardt and Bayesian regularization. The GP technique was employed to generate mathematical equations correlating AET to the five meteorological variables. Furthermore, the available data were statistically analyzed to obtain MLR models and to identify the meteorological variables that have significant effect on the evapotranspiration process. The utility of the investigated data driven

models was also compared with that of HYDRUS-1D model, which is a physically based model that makes use of conventional Penman-Monteith (PM) method for the prediction of AET. HYDRUS-1D model was examined for estimating AET using meteorological variables, leaf area index, and soil moisture information. Furthermore, Wavelet analysis (WA), as a multiresolution signal processing tool, was examined to improve the understanding of the available time series temporal variations, through identifying the significant cyclic features, and to explore the possible correlation between AET and the meteorological signals. WA was used with the purpose of input determination of AET models, a priori.

The results of this study indicated that all three proposed data driven models were able to approximate the AET reasonably well; however, GP and MLR models had better generalization ability than the ANN model. GP models demonstrated that the complex process of hourly AET can be efficiently modeled as simple semi-linear functions of few meteorological variables. The results of HYDRUS-1D model exhibited that a physically based model, such as HYDRUS-1D, might perform on par or even inferior to the data driven models in terms of the overall prediction accuracy. The developed equation-based models; GP and MLR, revealed the larger contribution of net radiation and ground temperature, compared to other variables, to the estimation of AET. It was also found that the interaction effects of meteorological variables are important for the AET modeling. The results of wavelet analysis demonstrated the presence of both small-scale (2 to 8 hours) and larger-scale (e.g. diurnal) cyclic features in most of the investigated time series. Larger-scale cyclic features were found to be the dominant source of temporal variations in the AET and most of the meteorological variables. The results of cross wavelet analysis indicated that the cause and effect relationship between AET and the meteorological variables might vary based on the time-scale of variation under consideration. At small time-scales, significant linear correlations were observed between AET and R_n, RH, and W_s time series, while at larger time-scales significant linear correlations were observed between AET and R_n, RH, T_g, and T_a time series.

ACKNOWLEDGMENTS

It is a pleasure to take this chance to thank those who made this thesis possible. First and foremost I would like to show my deepest gratitude to God for giving me the opportunity to learn and for His presence and unspeakable generosity, patience, support, and love.

I am grateful to my supervisor, Dr. Amin Elshorbagy, for his guidance, support, and opportunities he provided in my graduate experience. His comments and advices during this research work are sincerely appreciated. I would like to express my gratitude to my advisory committee members, Dr. Bing C. Si and Dr. Gordon Putz for the valuable assistance, suggestions, and feedbacks they provided at all levels of my research project. I also thank Dr. Warren Helgason for taking time to serve as my external examiner.

This thesis would not have been possible without the financial support of the Natural Science and Engineering Research Council (NSERC) of Canada, Cumulative Environmental Management Association (CEMA), and Civil and Geological engineering, University of Saskatchewan with the scholarship program. Dr. Sean Carey and Syncrude Canada Ltd. are greatly acknowledged for providing the required data and cooperating throughout this research work.

I am profoundly indebted to my beloved parents for their unconditional love and support through my entire life. A special thank you to my dear brother, Mohammad, and my lovely sisters, Maryam and Zahra, for their support and advices during the hard times. Appreciation also goes to Dr. Mingbin Huang and Suhad Al Bakri for their kind assistance in this research.

TABLE OF CONTENTS

LIST OF TABLES

LIST OF FIGURES

LIST OF SYMBOLS AND ABBREVIATIONS

AET	actual evapotranspiration [mm/h]
b	bias [-]
c_p	specific heat of soil moisture [kJ kg^{-1} $^oC^{-1}$]
CWT(τ,s)	continuous wavelet transform at scale s and time location τ [-]
e_s	saturation vapour pressure [kPa],
e_s-e_a	vapour pressure deficit [kPa],
e_a	actual vapour pressure [kPa],
ET_o	potential evapotranspiration from reference crop [mm h^{-1}]
$f(\theta_{rel})$	soil wetness function [-]
G	soil heat flux [MJ m^{-2} h^{-1}]
g_k	gradient of the error function surface [mm/h]
J	maximum number of studied scales [-]
k	number of observations in AIC formula [-]
K_c	crop coefficient [-]
l	number of optimized parameters in AIC formula [-]
LAI	leaf area index [m^2/m^2]
LE	latent heat energy [MJ m^{-2}]
m	number of ANN weights [-]
MARE	mean absolute relative error [-]
$msereg$	modified error function [mm/h]
n	number of independent variables in MLR [-]
N	number of instances in the sub dataset under consideration [-]
O	observed AET [mm/hr]
$\bar{O}$	mean of observed AET [mm/hr]
P	predicted AET [mm/hr]
$\bar{P}$	mean of predicted AET [mm/hr]
P_q	Fourier transform of red noise signal [-]
q	frequency index
R	pearson's correlation coefficient [fraction]
r_a	aerodynamic resistance [s m^{-1}]

r_c	crop canopy resistance [s m^{-1}]
RH	relative humidity [fraction]
RH'	normalized relative humidity [-]
RMSE	root mean squared error [mm/h]
R_n	net radiation [MJ h^{-1}]
R'_n	normalized net radiation [-]
RSS	residual sum of squares [mm^2/h^2]
s	wavelet scale [hour]
s_0	smallest analyzed scale [hour]
SSE	summation of squared error [mm^2/h^2]
T	mean half-hour temperature [^oC],
T_a	air temperature [^oC]
T'_a	normalized air temperature [-]
T_g	ground temperature [^oC]
T'_g	normalized ground temperature [-]
w	ANN synaptic weight [-]
w_{ij}(k)	weight vector at neuron *j* of layer *i* of ANN at epoch k [-]
w_{ij}(k+1)	weight vector at neuron *j* of layer *i* of ANN at epoch k+1.[-]
w_v	vertical wind speed component [ms^{-1}]
W_s	wind speed [ms^{-1}]
W'_s	normalized wind speed [-]
$W^{XY}(\tau, s)$	cross wavelet between time series X and Y at scale *s* and time location τ [-]
x_i	discrete time series signal [dimension of the variable under consideration]
X	independent variable in MLR [dimension of considered meteorological variable]
x_n	red noise time series at time location n [dimension of the associated variable]
Y	dependent variable in MLR [mm/hr]
Y_i	observed AET [mm/hr]
Y_i'	MLR-predicted AET [mm/hr]
$Z(p)$	confidence level at probability *p* [-]
z_n	Gaussian white noise [dimension of the associated variable]
α	lag-1 autocorrelation coefficient [-]

α_k	learning rate [-]
β_0	intercept of MLR [-]
β_i	MLR coefficients [-]
γ	performance ratio [-]
γ'	psychrometric constant in Penman-Monteith equation [kPa $^oC^{-1}$]
Δ	slope of the vapour pressure curve [kPa $^oC^{-1}$]
δ_j	scale step size [-]
ε	random error in MLR [mm/hr]
η	time parameter in Morlet wavelet [-]
θ	water content [fraction]
θ_{fc}	water content at field-capacity of the soil [fraction]
θ_{pwp}	water content at permanent wilting point [fraction]
θ_{rel}	relative water content [-]
λ	latent heat of vaporization [MJ kg^{-1}]
$\lambda_{\omega t}$	Fourier period [hour]
ν	degrees of freedom [-]
ρ	air density [kg m^{-3}]
ρ_v	absolute humidity [$kg.m^{-3}$]
ρ_w	water density [$kg.m^{-3}$]
σ	standard deviation of time series [dimension of the variable under consideration]
σ^2	variance of the time series [square of considered variable dimension]
τ	time location.[hour]
χ^2	chi-square [-]
$\psi_o(\eta)$	mother wavelet function [-]
$\psi_{\tau,s}(t)$	normalized wavelet function at scale *s* and time location τ [-]
ω_0	frequency parameter in Morlet wavelet [-]

AET	actual evapotranspiration
AI	artificial intelligence
AIC	akaike's information criterion

ANNs	artificial neural networks
AR [1]	lag-1 auto regressive process
ASCE	American society of civil engineers
COI	cone of influence
CWT	continuous wavelet transformation
DWT	discrete wavelet transform
EBBR	Energy-balance-Bowen-ratio
EC	eddy-covariance
EPR	evolutionary polynomial regression
ET	evapotranspiration
ET_c	potential evapotranspiration from actual crop
ET_o	potential evapotranspiration from reference crop
FAO	Food and Agricultural Organization
FFNNs	feed forward neural networks
GA	genetic algorithms
GP	genetic programming
LE	latent heat flux
MARE	mean absolute relative error
MCDA	multi-criterion decision analysis
ML	machine learning
MLR	multilinear regression
P_c	crossover probability
Pdf	probability distribution function
PET	potential evapotranspiration
P_m	mutation probability
PM	Penman-Monteith
P_r	reproduction probability
PT	Priestley-Taylor
R	Pearson's correlation coefficient
RBF-ANN	radial-basis function neural network
RMSE	root mean squared error
RSS	residual sum of squares
SMNNs	spiking modular neural networks

SSE	summation of squared error
SWSS	south west sand storage
WA	wavelet analysis
WC	water content
WNN	wavelet neural network

CHAPTER 1. INTRODUCTION

1.1 Background

One of the major human activities that threaten the natural environment is large-scale surface mining, which put the original ecosystem and hydrology of a local region at high risk. As a result of these large-scale mining practices, which usually extend to hundreds of square kilometres of area and hundreds of meters of depth, millions of tonnes of solid waste are produced (O'Kane et al., 1998) and various functions of natural watersheds are destroyed. As a solution for this growing concern, many governments have forced mine operators to adopt reasonable reclamation strategies for the mined landscapes (Haigh, 2000). Land reclamation is described as the process of restoration of disturbed landscapes and establishment of sustainable soil-vegetation-water relationship to achieve land capabilities corresponding to the natural state (Gilley et al., 1977).

The oil sands industry has disturbed many natural watersheds in northern Alberta, Canada, where mining activities have been in operation for the extraction of oil from oil-bearing sands (Fig. 1.1). The oil sands mining practices at Mildred Lake area near Fort McMurray have affected approximately 1200 km^2 of natural environment with the expectation of expansion to 2000 km^2 by 2020 (Carey, 2008). During the mining process, soil and overburden are removed to gain access to oil bearing deposits. When the mining practices are over, large-scale open pits resulting from mining operation are filled and contoured with stockpiled tailing materials and overburden, and then covered with a topsoil layer to reconstruct the disturbed landscape (Boese, 2003; Elshorbagy et al., 2005).

The global aim of these reconstruction practices is to establish a sustainable reclaimed land, which can evolve over time by dynamic interactions between local flora and fauna and hopefully mimic the natural watershed in the future (Jutla et al., 2006). As a result, mining industries should adopt reclamation strategies based on sustainable reclamation principles.

Soil cover design is one of the major issues in a reclamation project, which directly affects the local hydrological processes of the reconstructed watershed, such as runoff, drainage, infiltration, and evapotranspiration. The decisions regarding the material, structure, layering, and depth of the soil cover should be taken with consideration of local climate conditions. Understanding the various processes controlling the reconstructed ecosystem, either as an integrated hydrological system or as individual processes, helps the mining industry to evaluate the hydrological performance of the reconstructed watersheds and to optimize the design of reclamation strategies that can potentially decrease financial expenses (Elshorbagy, 2006).

Figure 1.1. Large-scale oil sands mining operation at Mildred Lake Area, Fort McMurray, Alberta.

1.2 Area of Interest

Monitoring and simulation of various hydrological processes in the reconstructed watersheds have been the interest of many researchers (Elshorbagy et al., 2005, 2007; Parasuraman et al., 2006, 2007). Various hydrological processes driving the hydrology of the reclaimed watershed can be simulated as a unique system, which is complicated considering the interrelationships among the various processes. By monitoring and simulating these processes, one can understand the hydrology of the reconstructed landscape better and adopt more efficient strategies in watershed management and future reclamation designs. One of the important hydrological processes that needs to be monitored and modeled is evapotranspiration.

Evapotranspiration (ET) is a combined term including the transport of water to the atmosphere in the form of evaporation from the soil surfaces and from the plant tissues as a result of transpiration. Evapotranspiration plays an important role in the hydrological cycle and it is considered a major cause of water loss around the world. Almost 62% of precipitation falls on continents are returned back to the atmosphere through the evapotranspiration process (Dingman, 2002). In the sub-humid climate of northern Alberta, ET is the largest annual loss of water (Devito et al., 2005), showing its vital role in the hydrological system of the reconstructed watersheds.

Evapotranspiration can be conceptually expressed either in the form of potential or actual evapotranspiration. Potential evapotranspiration (PET) describes the maximum loss of water from a short green crop under specific climatic conditions when unlimited water is available. Reference evapotranspiration (ET_o), which is a commonly used concept in engineering and scientific practices, is defined as the rate of evapotranspiration from a well-defined reference environment (e.g. well-watered short grass). ET_o can be multiplied by a crop-specific coefficient for estimating the crop evapotranspiration (ET_c) (Irmak and Haman, 2003). The actual evapotranspiration (AET) is the rate at which water is actually removed to the atmosphere from a surface due to the evapotranspiration process. AET is the preferred form of evapotranspiration in hydrological analysis because in most cases limited water is available for evapotranspiration and the actual rate of water loss is of interest.

Accurate assessment of evapotranspiration is of vital importance from different points of view, such as reliable quantification of hydrological water balance, hydrological design, water resource planning and management, irrigation system design and management, and crop yield simulation. In this study actual evapotranspiration as an individual hydrological process is of interest to be modeled, estimated, and analyzed. The realization of the evapotranspiration process, which is obtained through understanding of the temporal variations of AET time series and the meteorological variables influencing the AET, can be considered as a step forward in the global aim of better understanding and management of reclaimed watersheds.

1.3 Problem Definition

Despite the importance of evapotranspiration in the water balance, it is one of the least measured components of the water cycle (Brutsaert 1982; Jackson 1985), probably because of the expensive and cumbersome requirements needed for its direct measurement methods. As a result, indirect methods varying from empirical relationships to complex combined equations are used for estimating ET.

Evapotranspiration is a complex phenomenon because several interacting meteorological factors, such as solar and terrestrial radiation, wind speed, temperature, relative humidity, and growth stage of the crop are driving the ET process. Based on available meteorological variables, several models including empirical solar radiation-based or temperature-based equations and physically based equations; e.g. Penman and Penman-Monteith equations, have been developed for the estimation of potential ET. Since potential ET depends on meteorological variables, many equations have been developed for its estimation in the past.

AET is dependent on the available soil moisture, and is, consequently, region-specific, which makes its modeling or estimation more complicated than the potential ET. AET is currently estimated indirectly and in relation to potential ET estimation models using approaches that require information on soil moisture for considering the water supply deficit in the estimation of the AET. However, soil moisture is not readily available information in many cases, which results in less applicability of this method. In addition, in order to use this method, users are required to make reasonable estimates for some of the parameters in the employed potential evapotranspiration models, which involve some uncertainties and might not result in reliable AET estimates. Considering the disadvantages and limitations of the current AET modeling methods, there is a vital need to develop some techniques that can accurately estimate AET values based on conventionally available meteorological variables, and are also easy to apply.

For some complex hydrological processes, such as AET, it is difficult to develop mechanistic models, since the underlying physics of the AET process can be too complicated to be accurately represented in a physically based manner. Consequently, an

inductive (data driven) modeling approach, which can provide a model to predict and investigate the process without having a complete understanding of it, can be a useful tool. Inductive modeling approach is also interesting because of its knowledge discovery property. Using data driven models, one can extract useful implicit information from a large collection of data and improve the understanding of the underlying process.

For reconstructed watersheds, it is suggested to perform, at least, five years of monitoring (Rick, 1995). However, Syncrude Canada Ltd. has changed some of the field measurement and data collection strategies at some of the reclaimed sites, which shows the possibility of facing an insufficient monitoring period for modeling purposes. Data driven models with high generalization abilities can be employed for AET prediction issues in the reclaimed sites where no AET measurement instrumentation can be made available.

Among the data driven modeling approaches, standard multilinear regression (MLR) is a known statistical modeling technique, which has been widely used in the past for data mining and function estimation problems. Despite the huge development in the area of data driven modeling, multilinear regression is still popular and being used for various modeling and model comparison issues. This technique can be examined as a benchmark modeling method in this study.

Machine learning (ML) techniques are modern data driven modeling methods that originated from the advances in computer technologies and mathematical algorithms. These techniques are usually employed for characterizing complicated systems, which cannot be easily understood, analyzed, and modeled. Artificial neural networks (ANNs) and genetic programming (GP) are two robust ML techniques, which apply artificial intelligence for the modeling of complex systems. ANNs are computational models that can be used for the modeling of complex relationships by simulating the functional aspects of biological neural networks. GP is an evolutionary-based technique inspired by the biological evolution to generate computer programs (e.g. models) for solving a user-defined problem. ANNs and MLR techniques have been commonly used for modeling of the potential ET process (Kumar et al., 2002; Trajkovic, 2005; Bhakar et al., 2006; Zanetti et al., 2007; Landeras et al., 2008; Chauhan and

Shrivastava, 2009), but not considerably for the estimation of AET (Sudheer et al., 2003; Parasuraman et al., 2006; 2007). GP has been infrequently employed in the characterization of the ET process, whether AET or potential ET, (Parasuraman et al., 2007; Parasuraman and Elshorbagy, 2008).

Understanding of AET as well as its correlation with the interacting meteorological variables can be improved by exploiting the available time series data and some data mining tools. A new digital signal processing tool, namely wavelet analysis (WA), has a robust property for providing multiresolution representation of hydrological time series. Representation of the time series data into time and scale domains makes it possible to extract useful information about temporal cyclic events existing in the underlying signal. In addition, the correlation structure of time series data, in terms of temporal cyclic variations, can be investigated using extensions of wavelet analysis such as cross wavelet analysis. Temporal variations of AET and meteorological variables, as well as their correlations, can be examined using wavelet analysis.

1.4 Objectives

This study aims to develop some data driven models and compare their performances for the estimation of the AET process. It is also of interest to investigate if data driven models can reveal some information about the AET function and its most influential variables. Contribution of the meteorological variables to the AET temporal variations is also of interest and will be examined using wavelet analysis as an approach to modeling input determination.

The broad aim of this study is to model and analyze the hydrological process of AET using the data driven techniques and WA. The specific objectives of this study are:

1) To predict actual evapotranspiration using meteorological variables by developing three different models using ANNs, GP, and statistical multilinear regression techniques;

2) To compare the developed models in terms of predictive accuracy, generalization ability, structure, and complexity;

3) To identify the most important meteorological variables influencing the AET process; and

4) To examine the utility of the wavelet analysis in determination of the most important variables for estimation of AET, prior to the modeling.

1.5 Scope of the Research

The current study fulfills a part of a large research program that aims to develop a framework to improve understanding of the dynamics of various hydrological functions driving the hydrology in reconstructed watersheds. The presence of such a framework seems to be a vital need for efficient and desirable application of an extensive monitoring program conducted at the experimental reclaimed sites in northern Alberta, Canada (e.g. south bison hill (SBH) and south west sand storage (SWSS)). The overall findings of this research program will help the mining industry as well as reclamation scientists to have a better understanding of the hydrology of the reconstructed lands and to regulate optimum reclamation strategies that lead to self-sustainable watersheds. Figure 1.2 (Modified after Jutla, 2006 and Parasuraman, 2007) shows a diagram of the ongoing overall research program.

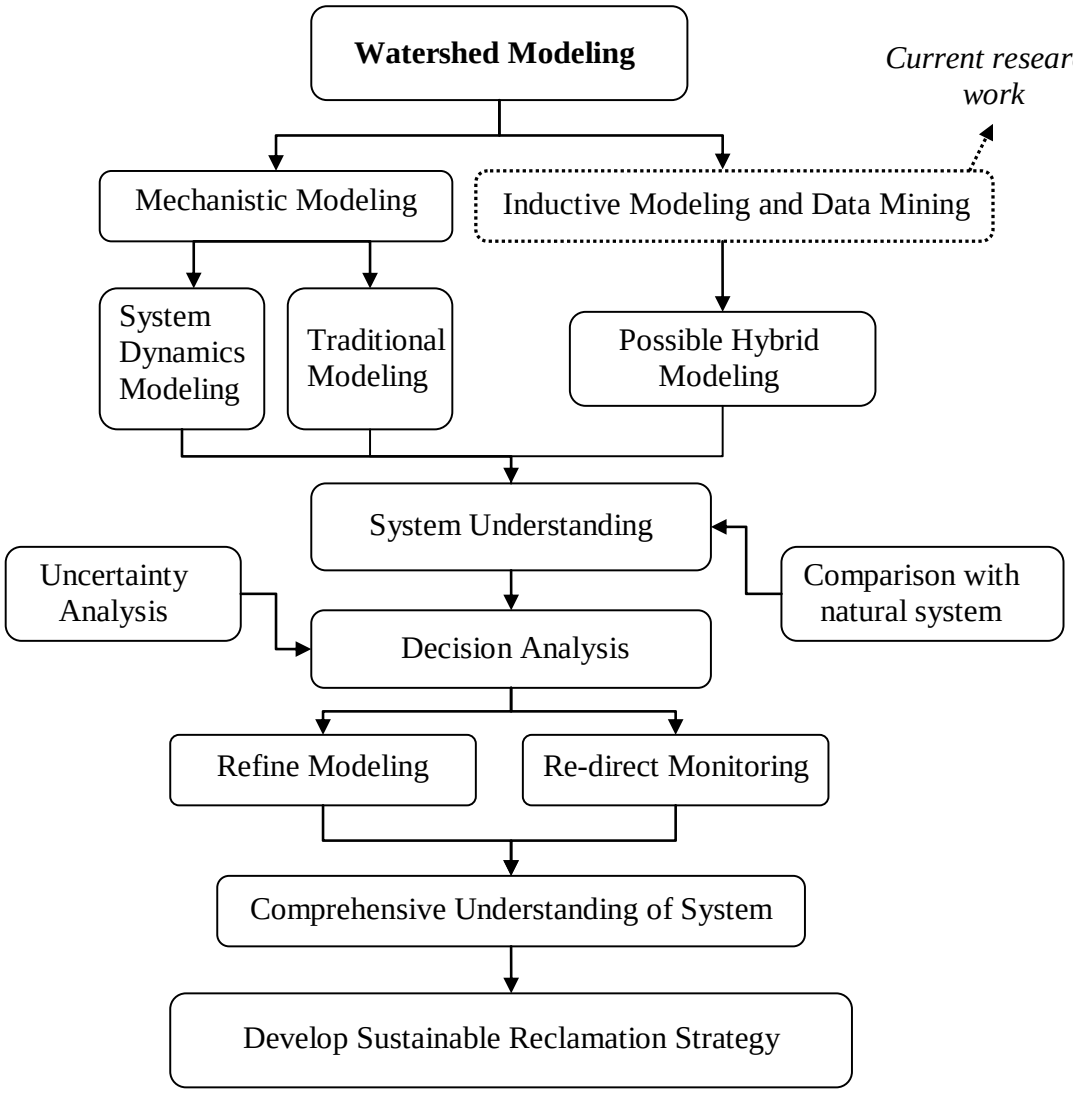

Figure 1.2. Research Program Framework for Developing a Sustainable Reclamation Strategy.

Initial understanding obtained from field data collected in the reconstructed watersheds is utilized in two parallel modeling approaches of inductive (data driven) and mechanistic modeling. The latter can be either traditional available models (using for example HSPF, SLURP) or system dynamics models. The partial understanding gained from both modeling approaches along with the knowledge obtained through comparison between natural and reconstructed systems can be encapsulated together to give an initial understanding of the system through a decision analysis approach, which requires comprehensive and detailed sensitivity and uncertainty analysis (Jutla et al., 2006).

Decision analysis provides some feedback on the already executed monitoring and modeling program and will be followed by re-directed monitoring and refined modeling processes to achieve a comprehensive understanding of the reconstructed watershed systems. Finally, the current reclamation practices can be modified based on the quantified system understanding to establish a sustainable reclamation strategy. The framework of the research program comprises the following specific tasks to be completed (After Jutla, 2006 and Parasuraman, 2007):

- Develop a system dynamics watershed simulation model that helps to improve the understanding of various hydrological functions associated with the reclaimed watersheds. This task is part of a study running in parallel to the current study (Keshta et al., 2009);

- Adapt some of the available watershed models (e.g. HSPF, SLURP) to the reconstructed watershed systems and compare the performances of the available models with the system dynamics model developed in the previous task. This is to identify the capability of different modeling approaches in capturing the dynamics of hydrological functions in reconstructed watersheds. A step in this direction has been recently taken (Keshta and Elshorbagy, 2009);

- Conduct inductive modeling and data mining approaches for modeling, estimation, and analysis of different hydrological processes, individually or as a system, without considering the physics of the investigated processes. The current research work attempts to complete this task for one of the important components of the hydrological cycle in reconstructed watersheds (Fig 1.2). This study complements earlier attempts by Parasuraman and Elshorbagy (2008); Parasuraman et al. (2007); and Parasuraman et al. (2006);

- Develop inductive and deductive models for natural watersheds and conduct a comparison between the performances of both watershed modeling approaches to identify the possible lack of knowledge in the system understanding. This task also helps to identify the required data for modeling and decision making;

- Investigate the possibility of combining the advantages of both mechanistic and inductive modeling approaches for developing the most suitable integrated or hybrid models for reconstructed watersheds;

- Develop a multi-criterion decision analysis (MCDA) tool comprising the knowledge obtained from different reclamation alternatives for identifying the most important components influencing the system understanding and reclamation strategies of reconstructed watersheds. The MCDA technique will be employed for determining the parameters and hydrological processes that are highly required to be measured and modeled, and also for identifying the most suitable modeling approach and the most sustainable reclamation strategies. A step forward was taken by Elshorbagy (2006); and

- Conduct comprehensive uncertainty analysis to determine various uncertainty components that influence the watershed modeling and decision making exercise; including the uncertainties associated with the measured variables, model structures and parameters, and scale and representation of various hydrological functions.

The current research study is restricted to the inductive modeling and data mining analysis of actual evapotranspiration function as an individual hydrological process in reconstructed watersheds, as highlighted in Fig. 1.2. The study is more focused on the assessment of different data driven modeling techniques and also the extraction of knowledge from the monitored processes of AET and the meteorological variables. The current modeling and analysis of the AET process is restricted to an experimental reconstructed site called south west sand storage (SWSS). The available data, in this site, are limited to the years of 2005 and 2006, which are used for the modeling and analysis purposes in this study. The small scale resolution of the data (hourly) is of interest in this study to be modelled and analyzed. As a result, the applicability and performance of the proposed models on larger time resolutions are not discussed here. Since the current study is restricted to one site only, the influence of vegetation (species and age) and soil structure on the evapotranspiration mechanism are

not studied in this thesis. Uncertainty analysis of the modeling exercise will also not be covered in the present study.

1.6 Synopsis of the Thesis

The rest of this thesis is organized in the following chapters. Chapter 2 provides the literature review on evapotranspiration modeling methods, development history and hydrological application of the data driven modeling techniques; ANNs and GP, and WA. Chapter 3 presents a description of the study area and the experimental data that were used for modeling and analysis purposes. This chapter also provides a description of the data driven modeling techniques; ANNs, GP, and MLR, and the WA along with the associated methodologies for developing the AET prediction models and analysis of the time series data, respectively. Chapter 4 presents the results and discussions of the AET modeling, comparative analysis among the various models, and the WA of the AET and the meteorological time series. In the last chapter, chapter 5, the summary of the study, conclusions of the results and analysis, research contributions, possible extensions of the research, and study limitations are provided.

CHAPTER 2. LITERATURE REVIEW

Three main techniques, namely, artificial neural networks (ANNs), genetic programming (GP), and wavelet analysis (WA), were investigated in this study for modeling and analyzing the challenging process of evapotranspiration. ANNs and GP were employed as data driven modeling (sometimes called machine learning) techniques and the wavelet analysis was considered as a signal processing tool. This chapter provides a brief literature review of these three techniques and their relevant use in hydrology. In addition, a brief description of the evapotranspiration mechanism and a literature review on the currently available evapotranspiration models are also presented.

2.1 Evapotranspiration

Evapotranspiration (ET) is the process of returning water back to the atmosphere through evaporation from open water, soil, and plant surfaces, and transpiration from plants. Theoretically, evaporation is a diffusive process that follows Fick's first law and can be written as a function of vapour pressure deficit (at evaporating surface and overlying air) and wind speed. Evaporation is accompanied by heat loss from evaporating surface in the form of latent heat, which can be compensated by radiative or sensible-heat transfer or by heat transfer from within the evaporating body to the surface (Dingman, 2002). The rate of latent heat (LE) is related to the evaporation rate using the latent heat of vaporization and the mass density of water. Physically, the four basic factors involving the evaporation mechanism include energy availability, water availability, vapour pressure gradient, wind, and the atmospheric conductance. Any other parameters that influence the above factors also influence the evaporation process (McNamara, 2009).

Transpiration is the evaporation of water from the vascular system of the plants into the atmosphere as a consequence of the photosynthesis process. It involves the absorption of water from soil through roots and its translocation through the vascular system of the roots, stem, and branches to the leaves. The water is then moves from the

vascular system of the leaf to the walls of stomatals where evaporation takes place. Water vapour is then released to the atmosphere through the openings of the leaf, called stomata. Transpiration is limited by energy availability, water availability, humidity, temperature, ambient CO_2 concentration, and wind speed. Plant species come into play by influencing the leaf conductance and the plant adaptation to water availability (Dingman, 2002).

When unlimited water is available, the rate of ET is mostly controlled by the atmospheric conditions, and ET might be near the maximum rate. However, when the soil water becomes limited, the soil water content starts to control the rate of ET and may stop the process when the transport of water through the soil becomes critical (Dingman, 2002). Since in real situations the water is usually not unlimited, the rate of ET under the limited water supply conditions is said to be the actual rate of evapotranspiration (AET).

2.2 Modeling of Evapotranspiration

The importance of evapotranspiration (ET) in the water cycle and hydrological management, in addition to expensive and sensitive measuring equipment, led to extensive efforts for modeling the ET mechanism. Many methods have been developed, revised, and proposed for the estimation of ET in different climatic conditions using different predictor variables. Jensen and Allen (2000) reviewed the evolution of different types of ET estimation methods. Conventional ET models are basically categorized into physically based and empirical models. Some examples of the physically based ET models include the equations developed by Penman (1948), Monteith (1965, 1973), Shuttleworth and Wallace (1985), and Granger and Gray (1989).

Penman (1948) derived a sound physically based evaporation model by combining the energy-balance method with the mass-transfer method. The Penman evaporation model was later modified by Monteith (1965) to take into account the vegetation surface and the aerodynamic resistance terms, which resulted in the well-known Penman-Monteith (PM) equation for the estimation of ET. The PM method

proved to be superior to about 20 other methods based on the regression analysis of lysimeter measurements (Jensen et al., 1990). FAO-24 Penman (Doorenbos and Pruitt, 1977) and Kimberly Penman (Wright, 1982, 1996) methods were developed afterwards following Penman's theoretical method.

FAO-24 was shown, by different studies such as Jensen et al. (1990), Allen et al. (1998), and Walter et al. (2001), to lack global validity. The United Nation's Food and Agricultural Organization (FAO) recommended a PM-based approach, namely FAO-56 PM (Allen et al., 1998), as the standard method for the estimation of potential evapotranspiration from a reference surface (ET_o) (e.g. grass). The PM model basically estimates the rate of evapotranspiration from a wet and uniformly vegetated surface where unlimited water supply is available. The American Society of Civil Engineers (ASCE, 2004) recommended a Standardized Reference Evapotranspiration (ET_o) Equation on the basis of the ASCE-PM method (Jensen et al., 1990), which is now generally considered to be the standard technique for the estimation of ET_o.

Empirical models were developed with the aim of proposing simpler ET equations, which require fewer input variables that are also routinely available. Attempts for empirical modeling of evapotranspiration resulted in various methods: temperature-based (Thornthwaite, 1948; Blaney and Criddle, 1950; Hargreaves and Samani, 1985), radiation (and temperature)-based (Priestley and Taylor, 1972; Makkink, 1957; Jensen and Haise, 1963; Stephens and Stewart, 1963), water budget-based (Guitjens, 1982), and mass-transfer-based (Harbeck, 1962; Rohwer, 1931). The empirical models have the advantages of being simple and using a small number of meteorological variables; however, reasonable estimation of model parameters is required for local applications. This is considered to be a limitation for the empirical ET prediction models.

In the literature, the vast majority of the studies have been focused on modeling of the potential evapotranspiration process in which the evaporation occurs from soil and plant surfaces under no water stress. However, actual evapotranspiration (AET) occurs under actual conditions of water supply. Quantifying AET has been made possible by using time- and labour-consuming methods, such as water-balance, energy-balance-Bowen-ratio (EBBR), and eddy-covariance (EC). EBBR and EC methods are

micrometeorological estimation (observation) methods (Droogers, 2000). Since theoretical modeling of the AET mechanism is complicated, its values are currently estimated using the available ET_o models, crop coefficient (K_c) (as an indication of actual vegetation), and the information of soil moisture. This approach basically adjusts the estimated ET_o values for the actual investigated plant and soil water condition.

Compared to the ET_o, limited studies were observed in the literature, which investigated the modeling of AET mechanism. Some of these studies are briefly described here. A simplified method was developed by Slabbers (1980) to predict the AET based on ET_o, crop-dependent critical leaf water potential, and the fraction of available soil moisture. Poulovassilis et al. (2001) developed a simple semi-empirical approach for estimating AET using meteorological, crop, and soil data. AET was also estimated using the relationships developed between AET and pan evaporation (Bernatowicz et al., 1976; Linacre, 1976; Dolan et al., 1984; Koerselman and Bertman, 1988) and between AET and Penman's potential evaporation (Koerselman and Bertman, 1988). According to Slabbers (1980), the concept of AET is often limited to the semi-empirical models (Denmead and Shaw, 1962; Zahner, 1967; Grindley, 1969), which are subject to several limitations.

Some equation-based ET models have also been adapted for the estimation of AET, such as Penman-Monteith equation (Monteith, 1973) and the work conducted by Shuttleworth and Wallace (1985). In the PM method, the model parameters (e.g. aerodynamic resistance of leaf surface) should be specified for the estimation of AET in cases where the theoretical assumptions of PM method are not valid (e.g. low soil moisture conditions). Priestley-Taylor (PT) method (Priestley and Taylor, 1972) was also adapted for the estimation of AET using an empirical parameter (Pauwels and Samson, 2006). A strong dependence was found between the empirical parameter of PT method and the soil moisture condition by Gavin and Agnew (2004). The proposed AET models mainly require extensive predictor variables, such as meteorological parameters, soil moisture information, leaf area, and canopy aerodynamic characteristics. The most encountered problem in the application of the currently available models is the lack of the required information. According to Poulovassilis et al. (2001), determination of

critical parameters (e.g. threshold soil moisture and threshold leaf water potential) is also a serious obstacle in AET estimation using the available models.

2.3 Data driven modeling

2.3.1 Overview

Improving the predictive ability of hydrological models and the understanding of hydrological processes are the concern and focus of most hydrologists and modelers (Lange, 1999). Therefore, extensive studies have been conducted for developing more reliable and efficient hydrological models. Owing to the recent developments in computer technologies and new mathematical algorithms, data driven modeling techniques have been developed as a new approach for simulation and prediction of various natural and artificial phenomena. These new techniques are of particular interest in hydrological modeling, which is extensively used for modeling complex and not fully understood natural processes.

Among the available data driven techniques, which do not require comprehensive knowledge of the physics of the investigated processes, are ANNs and GP. ANNs and GP are the two machine learning techniques employed in this study for the modeling of the AET process. The utility of these techniques for modeling and predicting various complex processes has been investigated in the literature, and is briefly reviewed in the following two sections. Furthermore, in this literature review, a short history of the development of each technique is provided to highlight the long road each technique has passed through to become as readily applicable as it is today. These modeling techniques are becoming even more popular with the recent advances in software/hardware technologies and digital data acquisition (measuring) methods.

2.3.2 Artificial Neural Networks (ANNs)

- *Development history of ANNs*

The concept of Artificial Neural Networks (ANNs) was introduced more than 60 years ago in 1943 (McCulloch and Pitts, 1943) when efforts were concentrated on the understanding of the human brain and simulating its analytical functioning (Govindaraju, 2000). Since that time ANNs has experienced huge developments through a three stage evolvement history (Schalkoff, 1997). During the first stage, preliminary work was conducted on the development of the artificial neuron. This era ended by a 20-year lull in neural network research caused by the results of Minsky and Papert's (1969) work showing the limitations of the preliminary neuron theorem (Jain et al., 1996).

The second phase of ANNs development began with the Hopfield's (1982) effort in iterative autoassociable neural networks and the introduction of Hopfield networks (Govindaraju, 2000). The second era was followed by the discovery (Werbos, 1974) and the popularization (Rumelhart and McClelland, 1986) of a rigorous ANN training algorithm, namely back-propagation. Introduction of the back-propagation training algorithm made a giant forward step in the transition of ANN research into the applications in a variety of areas. The third stage involved studying the ANN limitations and generalizations, its combination with other computational techniques (e.g., genetic algorithm), and the role of hardware advances in the ANN implementations (Dawson and Wilby, 2001).

- *Hydrological modeling using ANNs*

Increasing numbers of published studies, especially during the last decade, on the employment and development of ANNs in various fields including hydrological modeling, indicates their popularity among researchers. ANNs have been increasingly used in a variety of fields, such as financial management, computer science, various branches of engineering, control systems, and environmental science (Dawson and Wilby, 2001). Taylor (1996) wrote a brief discussion on the general application of

ANNs, whereas Flood and Kartam (1994, 1997) discoursed on the ANNs application in solving different civil engineering problems. The hydrology-related literature is the focus of this section.

The potential of ANNs in environmental science was discussed by Schmuller (1990) and Maier and Dandy (2001). Some earlier instances of ANNs in the modeling of hydrological systems were proposed by Daniel (1991). ASCE (2000a, b) presented a detailed review on the various applications of ANNs in hydrology. Some examples of hydrological studies that investigated the potential of ANNs in the modeling of different hydrological processes include: rainfall-runoff modeling (Zhu et al.,1994; French et al., 1992; Minnes and Hall 1996; Tokar and Johnson 1999; Elshorbagy et al., 2000; Dawson and Wilby, 2001; Birikundavy et al., 2002; Campolo et al., 2003; Huang et al., 2004; Riad et al., 2004; Hettiarachchi et al., 2005; Senthil Kumar et al., 2005), stream flow modeling (Kang et al., 1993; Karunanithi et al.,1994; Poff et al., 1996; Muttiah et al., 1997; Elshorbagy et al., 2002), water quality modeling (Maier and Dandy 1996; Rogers 1992; Rogers and Dowla 1994; Starrett et al., 1996; Hutton et al., 1996), river stage forecasting (Lachtermacher and Fuller, 1994; Thirumalaian and Deo, 1998; Campolo et al., 1999), characterization of ground water (Aziz and Wong, 1992; Ranjithan et al., 1993; Rizzo and Dougherty, 1994; Yang et al., 1997), estimation of precipitation (French et al, 1992; Tohma and Igata, 1994; Hsu et al., 1996, 1997; Kuligowski and Barros, 1998), and estimation of soil moisture content (Elshorbagy and Parasuraman, 2008). In hydraulic engineering, ANNs have been employed for the prediction of sediment load (Abrahart and White, 2001; Nagy et al., 2002; Yitian and Gu, 2003; Bhattacharya et al., 2005) and studying flood wave propagation (Dartus et al., 1993).

Despite the large number of studies which have been conducted on different hydrological problems, few applications of ANNs can be found in the area of evapotranspiration, and especially, actual evapotranspiration. Kumar et al. (2002) developed an ANN model for the prediction of reference evapotranspiration (ET_o) and compared its performance with that of a conventional method (Penman-Monteith equation) to examine the capabilities of ANNs in ET_o prediction compared to the PM method. The results of the study showed that the ANN model can predict ET_o better than

the conventional method for the considered local case study. Jothiprakash et al. (2002) investigated the capability of ANNs for the estimation of ET_o using the daily meteorological variables. It was found that the results of ANN models were in good agreement with those of FAO-modified Penman method, and that four basic meteorological variables were sufficient for remarkably accurate estimation of ET_o using ANNs. Trajkovic et al. (2003) developed a radial-basis function type neural network (RBF-ANN) model for the prediction of ET_o. Trajkovic (2005) examined the reliability of RBF-ANNs as well as three other calibrated temperature-based approaches for the estimation of ET_o. The results confirmed the efficiency of the temperature-based RBF-ANN model for the prediction of ET_o. The utility of ANNs for the estimation of reference and crop evapotranspiration (ET_c) of wheat crop was examined by Bhakar et al. (2006) and it was revealed that the ANN model was suitable for the prediction of ET_o and ET_c. Zanetti et al. (2007) found that by using ANNs, it was possible to estimate ET_o just as a function of maximum and minimum air temperature. The results of a study conducted by Jain et al. (2008) indicated that ANNs can efficiently estimate ET_o from the limited meteorological variables of temperature and radiation only.

The degree of influence of each of the meteorological variables; wind speed, solar radiation, relative humidity, air and soil temperature, on the estimation of daily ET_o, and the performance of ANNs compared to those of Penman, Hargreaves, and multilinear regression (MLR) methods were investigated by Kisi (2006). The study concluded that the ANN model trained by Levenberg-Marquardt algorithm was superior to the MLR, Penman, and Hargreaves method. Also, the input combination of wind speed, solar radiation, relative humidity, and air temperature resulted in the best performance statistics.

Landeras et al. (2008) developed seven ANNs with different input combinations and then compared ANNs to locally calibrated empirical and semi-empirical equations of ET_o. Their proposed ANNs performed better than the locally calibrated equations particularly in situations where appropriate meteorological inputs were lacking. Wang et al. (2008) employed the capability of ANNs for the prediction of ET_o with a limited meteorological dataset of minimum and maximum air temperature. It was observed that

ANN predictions were more accurate than those of the local reference model, Hargreaves, and Blaney-Criddle method in a semiarid area. Kumar et al. (2008) developed several ANNs-based ET_o models, corresponding to the best ranking conventional ET_o estimation methods, and compared the results with FAO-56 PM ET_o estimation model. The ANN models were consistent with the non-ideal condition of data availability and predicted ET_o values with better closeness to the FAO-56 PM ET_o than the conventional methods.

Dai et al. (2009) investigated the predictive ability of ANNs for the prediction of ET_o in arid, semi-arid, and sub-humid areas of Mongolia, China, and conducted a comparison between the estimated ET_o values from ANNs and MLR. The results showed that regional ET_o can be satisfactorily estimated using ANN models and conventional meteorological variables. The study also demonstrated that ANNs modeled ET_o better than MLR. Chauhan and Shrivastava (2009) investigated the climatic based methods as well as ANNs to identify the approach that estimates the closest ET_o to the standard PM ET_o. It was found that ANN model can perform better than the climatic based models and is able to estimate ET_o by using only maximum and minimum temperatures.

In the majority of the conducted studies, researchers have focused on the modeling of potential and reference crop evapotranspiration but not actual evapotranspiration (AET). To the knowledge of the author, the only publications reporting the application of ANNs for the modeling of AET include the studies conducted by Sudheer et al. (2003) and Parasuraman et al. (2006; 2007). Sudheer et al. (2003) estimated the lysimeter-measured AET of rice crop using RBF-ANNs. The results demonstrated that ANNs can successfully estimate the AET.

Parasuraman et al. (2006) developed spiking modular neural networks (SMNNs) for modeling the dynamics of EC-measured hourly latent heat flux. The results demonstrated that although the SMNNs are computationally intensive, they can perform better than regular feed forward neural networks (FFNNs) in modeling evaporation flux. Parasuraman et al. (2007) developed a regular three-layered FFNN model for the estimation of EC-measured hourly AET as a function of net radiation, ground

temperature, air temperature, wind speed, and relative humidity. Their results indicated that the ANN model performed better than the currently used PM method in northern Alberta, Canada.

2.3.3 Genetic Programming (GP)

- *Development history of GP*

The origins of evolutionary computation traced back to the late 1950's (Box, 1957; Friedberg, 1958; Friedberg et al., 1959; Bremermann, 1962) when it was proposed for the first time and then remained unknown for almost three decades. Fundamental works (Holland, 1962; Fogel, 1962; Rechenberg, 1965; schwefel, 1968), conducted during the 1970's, started to change the face of this computational approach to an adaptable and well-suited problem solving tool in the scientific and economic fields (Back et al., 1997). Genetic algorithm (GA) was first introduced by Holland (1962; 1975; Holland and Reitman, 1978) and then studied and developed by several scientists (De Jong, 1975, 1987; Goldberg, 1985, 1989; Grefenstette, 1986; Koza, 1989; Davis, 1991; Goldberg et al., 1993; Forrest and Mitchell, 1993; Mitchell, 1996). Genetic programming (GP), as an extension of GA, was first recognized as a different and new development in the world of evolutionary algorithms in the seminal monograph of Koza (1992). In his book, problem solving using GP and evolving tree-like structure solutions were precisely described.

- *Hydrological modeling using GP*

Evolutionary algorithms, in general, and GP, in particular, have been successfully applied in many fields as diverse as engineering, natural science, economics, and business (Back et al., 1997). The use of GP in hydrological problems is still not as popular as some other ML techniques such as ANNs. However, an increasing number of publications shows the rapid growth of the GP acceptability among researchers as well as hydrologists.

In hydraulic engineering, GP has been employed for modeling of sediment transport (Babovic, 2000; Kizhisseri et al., 2005; Aytek and Kisi, 2008), estimation of vegetation and channel resistance coefficients (Giustolisi, 2004; Baptist et al., 2007), and estimation of circular pile scour (Guven et al., 2009). In the latter study, Guven et al. (2009) compared the developed linear GP model with an adaptive neuro-fuzzy model and the conventional regression analysis. It was found that the GP and hybrid ANN model performed better than the regression model. Furthermore, GP was judged as more flexible, practical, and robust than the hybrid ANN model. Aytek and Kisi (2008) also compared their proposed GP-based sediment estimation model with the MLR. It was observed that the results of GP model are better than those of MLR in the modeling of sediment load.

The efficiency of GP in hydrological modeling was shown by various studies. Some studies investigated the application of GP in rainfall-runoff modeling (Cousin and Savic, 1997; Savic et al., 1999; Whigham and Crapper, 1999, 2001; Khu et al., 2001; Liong et al., 2002; and Babovic and Keijzer, 2002). Savic et al. (1999) conducted a comparison among the results of the developed GP and ANN rainfall-runoff models. It was observed that the two employed data driven techniques are in good agreement with the best optimized conceptual model, however; GP provided more insight into the rainfall-runoff relationship than ANN. The results of the Whigham and Crapper (2001) study showed the potential of the evolutionary GP technique in capturing rainfall-runoff correlation especially when it is poorly understood.

Partially known dynamics of an urban fractured-rock aquifer was modeled using the GP technique by Hong and Rosen (2002). In this study, explicit representation of the GP model improved the understanding of the dynamic behaviour of the aquifer system, in addition to its efficiency in predicting the groundwater level fluctuations. Coulibaly (2004) employed the GP technique for spatial downscaling of large scale meteorological variables to local extreme temperatures, and then compared its results with the statistical downscaling model. It was shown that the GP technique was able to provide simpler and more efficient model than the available regression-based method. Hong et al. (2005) induced a rainfall recharge model using the GP technique and found that the evolved GP

models were more reliable than the soil water balance model at predicting the observed rainfall recharge. Makkeasorn et al. (2006) generated a soil moisture estimation model using the GP technique. The results indicated that the GP was a useful tool for modeling the highly nonlinear structure of soil moisture distribution with strong agreement between the model results and the observed values.

The capability of GP in flow forecasting was examined by Sivapragasam et al. (2007), Makkeasorn et al. (2008), and Wang et al. (2009). The results of Sivapragasam et al. (2007) demonstrated that by the use of the GP technique, the short lead prediction of river flow improved significantly, and the appropriate input variables could be efficiently identified for longer lead forecast. They also compared the evolved GP model with its ANNs counterpart, and it was observed that, except for the advantage of GP in identifying suitable inputs, there was no significant difference between the prediction accuracy of the GP and the ANN models. Makkeasorn et al. (2008) developed and compared GP- and ANNs-based long-term flow forecasting models and observed that the ANN models generally performed worse than the GP derived models. Wang et al. (2009) conducted a comparative study among various artificial intelligence (AI) techniques for forecasting river flow discharge. The results indicated that the hybrid ANN (neuro-fuzzy) and GP models were, in order, the most promising estimation models.

Among the various published studies on the application of GP in hydrological modeling, only a few studies examined the applicability and robustness of GP for modeling of the evapotranspiration process. To the best knowledge of the author, the only publications that investigated the application of GP for modeling the evapotranspiration mechanism are the studies conducted by Parasuraman et al. (2007), Parasuraman and Elshorbagy (2008), and El-Baroudy et al. (2009). Parasuraman et al. (2007) employed equation-based GP for modeling the hourly actual evapotranspiration process as a function of net radiation, ground temperature, air temperature, wind speed, and relative humidity. The performance of the evolved GP model was compared with that of ANN model and the traditional Penman Monteith (PM) method. It was noted that GP and ANN models had comparable performances and both predicted AET values with

better closeness to the measured AET than the PM method. Their analysis also indicated that the effect of net radiation and ground temperature on the AET dominated over other variables. Parasuraman and Elshorbagy (2008) investigated a GP-based modeling framework for quantifying and analyzing the model structure uncertainty on an AET case study. The results of the study demonstrated the capability of the ensemble-based GP in quantifying the uncertainty associated with the hourly AET model structure. In addition, it was observed that the uncertainty of the model increased with higher level of the model's structural complexity, which was also accompanied by better prediction accuracy. El-Baroudy et al. (2009) did not develop a new GP model for AET, but rather developed models using a technique called evolutionary polynomial regression (EPR), and then compared its performance to the ANN and GP models developed by Parasuraman et al. (2007). With the exception of Parasuraman et al. (2007), Parasuraman and Elshorbagy (2008), and El-Baroudy et al. (2009), no other publication was observed that reports an explicit equation for the prediction of AET.

2.4 Wavelet Analysis (WA)

2.4.1 Overview

Hydrological processes are widely known with their property of being highly variable in time and space, which makes them physically challenging with regard to understanding and modeling. Temporal and spatial variability of hydrological systems can be attributed to the variability of different processes having interactions with the target mechanism. Wavelet analysis (WA) makes it possible to decompose any signal into location (time/space) and scale (or frequency) domains and subsequently, to detect and describe the periodic patterns that exist in the signal.

Wavelet analysis, as a relatively new signal processing tool, has been used for investigating the fluctuations in physical processes. Using this WA tool, it is also possible to clarify the presence of relationships among the variability of different signals involving a mechanism. WA was used in this study as multiresolution signal processing tool for gaining more insight into the temporal variability of the complex AET process

and also for exploring the signals that are more correlated and have more contribution to the temporal fluctuations of the AET. WA has the potential to be employed either for signal analysis or to be coupled with other modeling approaches for various prediction (estimation) issues. This literature review mainly covers the signal processing application of WA.

2.4.2 Development History of Wavelet Analysis

Underpinnings mathematics of WA was placed by Joseph Fourier in the 19th century with his theories of frequency analysis by which one was able to present a periodic function as the sum of its Fourier series. The first mention of the WA, as what it is known today, appeared in the thesis of Alfred Haar in 1909. In 1980, wavelet was conceptually defined based on physical intuition by Jean Morlet and the team working under Alex Grossman at the Marseille Theoretical Physics in France. In 1985, the main algorithm was proposed in the Stephane Mallat work in digital signal processing (Mallat, 1989). Afterward, the methods of wavelet analysis have been mainly developed by Yves Meyer and his colleagues. Meyer constructed the first non-trivial wavelets, which sped the dissemination of the method (Meyer, 1993). Ingrid Daubechies (1988) constructed a set of wavelet basis functions, using the Mallat's work, which have become the cornerstone of the current applications of wavelets (Graps, 1995). The wavelet analysis method became practically popular after the work conducted by Torrence and Compo (1998).

2.4.3 Applications of Wavelet Analysis

Wavelet analysis (WA) has become an attractive tool for researchers, in different fields, who are interested in analyzing the non-stationary signals of data both in frequency and temporal/spatial domains. WA covers a wide range of applications in diverse fields of sciences, such as mathematics, engineering, image processing, optic, turbulence, quantum mechanics, medical, and biomedical research (Lau and Weng, 1995). A collection of papers on the application of wavelet in different fields of

geosciences (e.g. fluid mechanics, meteorology, oceanography, climatology, and geophysics) can be found in Labat (2005) and Foufoula-Georgiou and Kumar (1994). Some examples of WA in geophysics include the studies conducted by Gamage and Blumen (1993), Gu and Philander (1995), Kumar and Foufoula-Georgiou (1997), Baliunas et al. (1997), Yokoyama and Yamazaki (2000), Guyodo et al., (2000), and Lui (2002).

In the field of hydrology, wavelet has been increasingly used for the analysis of spatial-temporal variability of hydrological processes and systems as well as their interactions with climatic variations. Earlier application of wavelets in hydrology was presented in Foufoula-Georgiou and Kumar (1994). WA has been frequently applied for feature extraction of discharge time series data in hydrology (Smith et al, 1998; Compagnucci et al., 2000; Labat et al., 2000; Saco and Kumar, 2000; Kirkup et al., 2001; Gaucherel, 2002; Cahill, 2002; Lafreniere and Sharp, 2003; Anctil and Coulibaly, 2004; Coulibaly and Burn, 2004; Labat et al., 2004; Labat, 2006; Schaefli et al., 2007; Gang et al., 2008; Labat, 2008; Zanchettin et al., 2008). In the above-mentioned studies, the utility of WA was mainly employed for detecting and analyzing different periodic events existing in the discharge and correlated meteorological signals. Schaefli et al. (2007) employed wavelet and cross wavelet analysis for detecting potentially flood producing meteorological situations and identifying the prevailing hydrometeorological conditions associated with different types of flood events. It was noted by Schaefli et al. that the WA has the potential to be a powerful tool in understanding and modeling of hydrological processes. The results of the WA conducted by Labat (2008) revealed the non-stationary long-term fluctuations of the world's largest river and their connections to climatic variability and trends. Coulibaly and Burn (2004) investigated the temporal and spatial variability of Canadian streamflows. The results exhibited different period bands of significant activities in the streamflow time series, which were found to be correlated to the considered climatic patterns at some spatial locations.

Multiresolution analysis of wavelet has been also applied for characterization of temporal variability of rainfall (Waymire et al., 1984; Gupta and Waymire, 1990; Kumar and Foufoula-Georgiou, 1993a, b; Kirkup et al., 2001; Coulibaly, 2006; Westra and

Sharma, 2006, Xiaomei et al., 2006; Miao et al., 2007; Chen and Liu, 2008). Coulibaly (2006) employed wavelet and cross wavelet analysis to investigate both spatial and temporal variability in seasonal precipitation and its relationship with climatic modes in the Northern Hemisphere. The results revealed striking climatic-related cyclic features in the precipitation time series and, in the temporal-spatial variability of the relationship between precipitation and climate throughout Canada. Westra and Sharma (2006) used wavelets for analyzing the modes of variability in three rainfall characteristics. The results exhibited significant periodicities in Australian rainfall and highlighted the role of not-conventionally considered phenomena in rainfall variations. Using WA, Xiaomei et al. (2006) discovered spatial structures and periodic oscillations exist in Yellow River Basin rainfall.

Lau and Weng (1995) applied wavelet transformation to two well-known climate time series, and the results provided new information on the nonlinear basis of the earth's climate variations. Multiresolution analysis has also been used for understanding the behaviour of karst environments in river flow components, and for improving the performance of the surface hydrological modeling (Salerno and Tartari, 2009). In the Salerno and Tartari study, contribution of groundwater to the river discharge was examined by comparing correlation spectra (cross wavelet and wavelet coherency) of error-precipitation, error-groundwater, and precipitation-groundwater time series. The error signal was obtained from the difference between measured and physically simulated river discharge.

In addition to the application of WA in the feature extraction of time/spatial series signals, it has been effectively employed for various modeling approaches. As an example, wavelets have been successfully coupled with ANNs. In the literature, conjugate wavelet-ANN modeling approach has been developed for drought forecasting (Kim and Valdes, 2003), streamflow simulation (Ju et al., 2008), and sediment load estimation (Partal and Cigizoglu, 2008). Kim and Valdes (2003) adopted an ANN model to forecast the wavelet-decomposed subsignals of regional drought and reconstruct the predicted response signal. The study indicated that the conjugate approach significantly improved the ability of ANNs in forecasting the drought index. Ju et al. (2008)

developed a wavelet neural network (WNN) model for simulation of daily streamflow and compared its performance with that of back propagation neural network model. It was observed that the results of WNN model were more accurate than those of the traditional ANN model.

There are very limited case studies in the literature that investigated the application and capability of WA in analyzing the variability of the evapotranspiration process. Kaheil et al. (2008) used discrete wavelet transform (DWT) for decomposing and reconstructing processes involving the AET phenomenon at various spatial scales, and to find the relationship between the inputs and outputs using support vector machines technique. The spatial scaling behaviour of evapotranspiration (latent heat) was also investigated by Brunsell et al. (2008) using a combination method of wavelet multiresolution analysis and information theory metrics. Furthermore, the relationship between spatial variability of remotely sensed latent heat flux and vegetation, temperature, and elevation was examined using WA. It was shown that the spatial variability of latent heat flux was most closely controlled by the radiometric temperature (a proxy for soil moisture).

Wang and Luo (2007) combined the wavelet transformation and neural network techniques for developing a forecasting model for reference crop evapotranspiration (ET_o). In the Wang and Luo study, WA was used to decompose the time series data of ET_o into different frequency components and then ANNs were adopted for forecasting (modeling) the obtained frequency components. The effectiveness of WNN model was verified and it was shown that simulation error of new proposed hybrid model was smaller than that of the traditional ANN models. To the best knowledge of the author, no effort has been made, in the literature, which benefited from the capability of WA in the temporal scaling of AET variations. Time-scale analysis of the AET signal seems to be an effective approach in improving the understanding of the AET process as well as the efficiency and predictive ability of AET prediction models.

CHAPTER 3. MATERIALS AND METHODS

3.1 Overview

This chapter provides a description of the study area and the experimental data that were used for modeling and analysis purposes. The analysis and modeling work constitute of two main parts: data driven modeling of actual evapotranspiration (AET) process and time-scale (multiresolution) analysis of the AET and the meteorological time series. Artificial neural networks (ANNs) and genetic programming (GP) are the main data driven (machine learning) techniques adopted in this study and are explained in this chapter. Statistical multilinear regression (MLR) was used as a common standard modeling technique. In addition, a physically based model, namely HYDRUS-1D, which employs the standard Penman Monteith model and additional soil information, was used for estimation of AET. The MLR and HYDRUS 1-D methods were investigated as possible alternatives to the proposed data driven techniques with which their prediction abilities were compared. A brief description of MLR and HYDRUS 1-D is also presented in this chapter. The last part includes a description of the wavelet and cross wavelet transforms that were carried out for multiresolution analysis of time series variability.

3.2 Site description

The experimental data, which were used in this study, were collected from the South West Sand Storage (SWSS) site, located at Mildred Lake mine approximately 40 km north of Fort McMurray, Alberta, Canada (Fig. 3.1). The SWSS facility is an active tailing disposal facility (dam), which covers an area of about 23 km^2, holding approximately 435×10^6 m^3 of materials, with 40 m relief higher than the surrounding landscape and an overall side slope of 5% (Parasuraman et al., 2007). The construction of the SWSS facility began in 1990 and was later covered between 1995 and 1998 with a layer of reclamation material (45 cm topsoil) (Chaikowsky, 2003) followed by vegetation seeding in 2001.

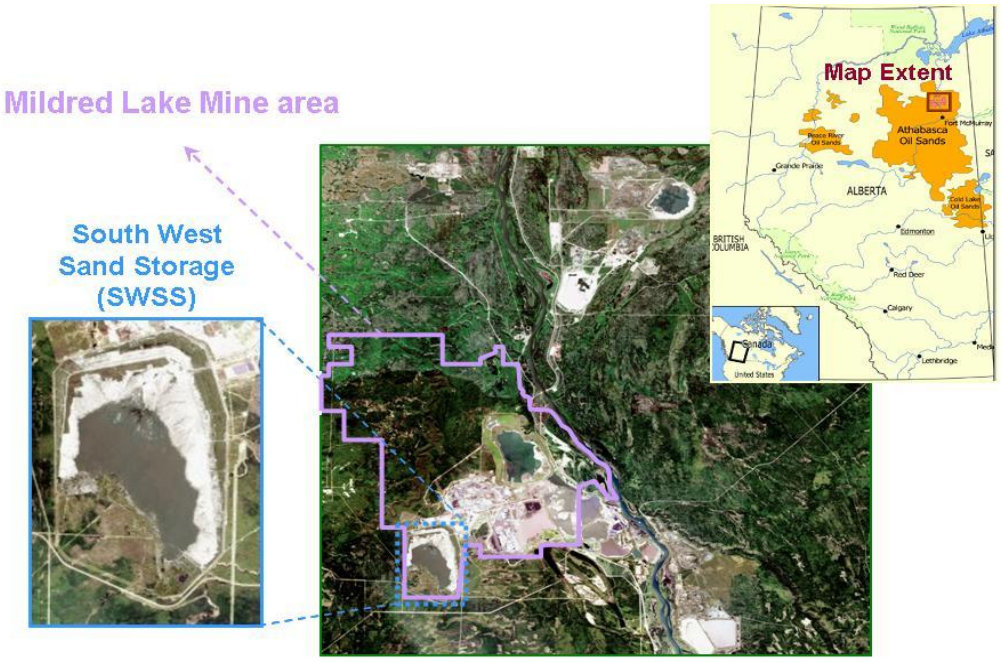

Figure 3.1. Location of the reconstructed study area (SWSS).

The soil cover system within the SWSS consists of a 45 cm thick peat/secondary mineral soil mix with a clay loam texture overlying the tailing sand (Fig. 3.2). The vegetation cover system varies across the SWSS site; including the dominant groundcover of horsetail (*Equisetum arvense*), fireweed (*Epilobium angustifolia*), sow thistle (*Sonchus arvense*), white and yellow sweet clover (*Melilotus alba*, *Melilotus officinalis*), and tree and shrub species including Siberian larch (*Larix siberica*), hybrid poplar (*Populus* sp. hybrid), trembling aspen (*Populus tremuloides*), white spruce (*Picea glauca*), and willow (*Salix* sp.) (Parasuraman et. al., 2007).

Figure 3.2. Soil cover system of the SWSS site.

3.3 Experimental data

The latent heat flux technique was originally applied on a continuous basis (Baldocchi et al., 1988) using the micrometeorological method of eddy covariance (EC). EC is considered as the most promising method of measuring patch-scale (e.g. on the order of 100s of meters) dynamics of the water cycle (Baldocchi, 2003; Baldocchi et al., 1988). The EC technique makes use of sensitive and expensive instruments to measure high-frequency changes of the vertical component of the wind velocity, humidity, and temperature simultaneously. In the EC technique, the covariance of the vertical wind speed with temperature and water vapour are used to estimate the sensible heat and latent heat (LE) flux (Drexler et al., 2004). For estimating the LE flux, high frequency-measured absolute humidity (ρ_v) and vertical wind speed component (w_v) are expressed as the summation of fluctuations and time-averaged components; $\rho_v = \overline{\rho_v} + \rho_v'$ and $w_v = \overline{w_v} + w_v'$, where overbar signifies a time average over a specified interval of time and the prime indicates fluctuation from the mean. The averaging period must be larger than the duration of the largest eddy in the turbulent transport process for which 10-30 minutes periods are usually used. The time averaging period of 30 minutes applied for

the LE data were used in this study. The LE flux is then estimated as $= \lambda \overline{w_v' \rho_v'}$, which is equal to the mean covariance of the fluctuations of the vertical wind and absolute humidity from their means (Drexler et al., 2004). λ is the latent heat of vaporization. Using EC technique it is possible to do the calculations in real time as fast as the readings are taken (Strangeways, 2003). "The accuracy of the EC technique ranges from ±15% to ±20% of the actual evapotranspiration for hourly values" (Strangeways, 2003). In addition to the high level precision and high degree of temporal and spatial resolution of the EC technique in direct measurement of LE, it has an exceptional property of self-verification, in case when other components of the energy balance closure can be computed at the same time. Drexler et al. (2004) stated that no other methods have this self-verification property.

The latent heat (LE) flux measurement system on the SWSS site consisted of a triaxial sonic anemometer (CSAT3, Campbell Scientific, USA), for capturing the high-frequency wind vector, an open-path infrared gas analyser (LI-7500, Li-Cor, USA) as a humidity sensor and a fine-wire thermocouple, for recording the temperature fluctuations, located in the approximate center of the sonic head about 2.9 m above the ground surface. All measurements and their fluctuations were obtained at a frequency of 10 Hz and the mean fluxes were recorded every 30 minutes on a CR23X datalogger (Campbell Scientific, USA) (Carey, 2008). The quantities are measured at high frequency to record the most rapid fluctuations that are important to the process (Drexler et al., 2004).

The EC tower was equipped with instrumentation to measure supplemental data including long- and short-wave radiation (CNR1 net radiometer, Kipp and Zonen, Netherlands) and wind speed (015A MetOne, USA) at 3.1 m above the ground, air temperature and relative humidity (HMP45C, Vaisala Oyj, Finland) at 3 m, and ground temperature (TCAV-L thermopile, Campbell Scientific, USA) at 0.03 m below the soil surface. The supplemental data were sampled at 1 minute intervals and recorded every half hour on a CR23X datalogger (Carey, 2008). Figure 3.3 shows the EC tower on the SWSS site.

The LE and net radiation (R_n) fluxes were originally recorded in $W.m^{-2}$ on a half hourly basis. For convenient interpretation, the latent heat flux [$W.m^{-2}$] was converted to the equivalent depth of water [$mm.m^{-2}$]. This was implemented using the following equations (Dingman, 2002):

$$AET = \frac{1000(LE)}{\rho_w \lambda} \quad [3.1]$$

$$\lambda = 2.5 - 2.36(10^{-3})(T) \quad [3.2]$$

where, AET is the rate of actual evapotranspiration [mm/ 0.5hr], LE is the latent heat energy [$MJm^{-2}0.5hr^{-1}$], T is the mean half-hour temperature [^oC], λ is the latent heat of vaporization [$MJkg^{-1}$] and ρ_w is the water density [$kg.m^{-3}$]. Air temperature (T_a; ^oC), ground temperature (T_g; ^oC), relative humidity (RH), and wind speed (W_s; $m.s^{-1}$) constituted the rest of the meteorological data used for this study. Since the hourly time scale of the data was the subject of study, conversion of the recorded half-hourly data to hourly data was also implemented in the pre-processing step.

In data driven modeling, it is important to have large enough collection of data, which contain several different instances for appropriately capturing the investigated function. Using short time intervals, e.g. hourly, large number of instances can be used for modeling, especially when the available measured data are associated with limited time period. For instance, for the current case study, only two years of data are available from which 1207 hourly instances can be obtained for modeling the ET process. However, if daily time step is used, only 102 instances would be available. Consequently, the hourly time scale of the data was selected for the current modeling study. AET variations at small time-scales are also important because this type of variation is more challenging than the larger scales and is important to be modeled and analyzed. There are many water related functions (e.g. water quality) in engineering that needs to be estimated at small-scales for which the rate of evapotranspiration at the same time-scale is required. Small time-scale models can always be used for estimation of larger-scale variations, by aggregating the small-scale predicted values. However, the other way round might not be easily possible. For consistency in the data driven

modeling and time series analysis, the same time scale (hourly) was used for the wavelet signal analysis in this study.

Figure 3.3. Eddy covariance tower at the SWSS site.

For modeling purposes, the day-time data, associated with the period of 8:00 AM to 8:00 PM, from May 3 to September 21, 2005 and from May 27 to September 8, 2006, were used. In the first step, the data of the year 2006 were used for modeling purposes with the three proposed techniques (ANNs, GP, and statistical models). Disregarding the missing data, the total number of available instances for modeling in year 2006 is 1207, which were randomly divided into three data subsets consisting of 604 instances (50%), 201 instances (17%), and 402 instances (33%) of the data, for training, cross-validation, and testing purposes, respectively. To obtain three statistically consistent subsets, a population of 100 groups of three data subsets was randomly generated by sampling from the entire dataset. The statistical characteristics of the data, i.e. mean and standard deviation, were determined for every subset of each group. Then, the group possessing three subsets with relatively similar statistical characteristics was selected for this study. Aside from the described modeling procedure, a rigorous test was also implemented in

the second step, using the data of 2005, to assess the generalization ability of the developed models in a more realistic way. Disregarding the missing data in 2005, 1600 instances are available. The 2005 dataset has different statistical properties from the data of 2006, which are discussed later in this study.

Multiresolution analysis of the AET and meteorological signals (wavelet analysis) was conducted using the data of the year 2006. Since wavelet analysis (WA) cannot be applied to a non-continuous time series, which contains a gap or missing data, gap filling was performed to obtain a continuous time series. In the dataset of the year 2006, only AET time series contained missed values, which were filled using the most fitted AET model developed in this study using the 2006 data (statistical multilinear regression). The total number of instances that were available for wavelet analysis of the 2006 data is 2520, which constitute the hourly data from May 27 to September 9. All of the observed time series data were pre-treated before performing the WA. The time series data were standardized, following Grinsted et al. (2004), by subtracting the mean value and then dividing by the standard deviation (zero mean and unit standard deviation) for convenience when the results were compared.

The air temperature during the growing season of the year 2006 varied between 7 to 34 ^{o}C with an average value of 21 ^{o}C. The average day-time net radiation flux and relative humidity were about 230.11 W/m^2 and 0.51, respectively. The total rainfall received during the growing season of 2006 was approximately 226.2 mm. During the growing season of 2005, the air temperature ranged between -4 to 29 ^{o}C, with the average of 17 ^{o}C. The average day-time net radiation flux and relative humidity values were 215.36 W/m^2 and 0.53, respectively. The total received rainfall during the growing season of 2005 was 279.2 mm. The normal rainfall in the Fort McMurray is about 307.9 mm for the period of May to September. The average soil water content in the top 45 cm of the soil during the studied periods of years 2005 and 2006 were 0.296 and 0.264 cm^3/cm^3, respectively

3.4 Data driven modeling

3.4.1 Artificial Neural Networks (ANNs)

ANNs (Swingler, 1996) are massive networks of parallel information processing systems resembling (simulating) the human brain's analytical function, and they have an inherent ability to learn and recognize highly nonlinear and complex relationships by experience. ANNs learn from empirical examples, which make them a non-rule-based technique, like statistical methods (Maier and Dandy, 2000). ANNs use mathematical transfer functions to relate target variables to predictor (input) variables (Dawson and Wilby, 2001).

Each neuron (information-processing unit) in ANNs consists of input connection links, a central processing unit, and output connection links (Fig. 3.4). Input signals are received through the connection links from the outside environment or other neurons. Each connection link is assigned a synaptic weight (w) representing the strength of the connection between two nodes in characterizing input-output relationship (ASCE, 2000a). Received information is processed in the central processing unit (neuron body), by adding up the weighted inputs and bias (Eq. 3.3), and passed through the activation function (Eq. 3.4). Bias (b) is the threshold value, which must be exceeded before the node (neuron) can be activated (ASCE, 2000a). Activation function forms the output of the node and enables the nonlinear transformation of inputs to outputs. The type of activation function, which can be sigmoid, linear, threshold, Gaussian, or hyperbolic tangent function (Dawson and Wilby, 2001), depends on the network's type and associated training algorithm. The log-sigmoid activation function is one of the two most commonly used activation functions in the literature because it is continuous, relatively easy to compute, its derivatives are simple (during the training process), maps the outputs away from extremes, and provide nonlinear response (ASCE, 2000a).

$$t = \sum_{i=1}^{n} w_i x_i + b \qquad [3.3]$$

$$f(t) = \frac{1}{1 + e^{-t}} \qquad [3.4]$$

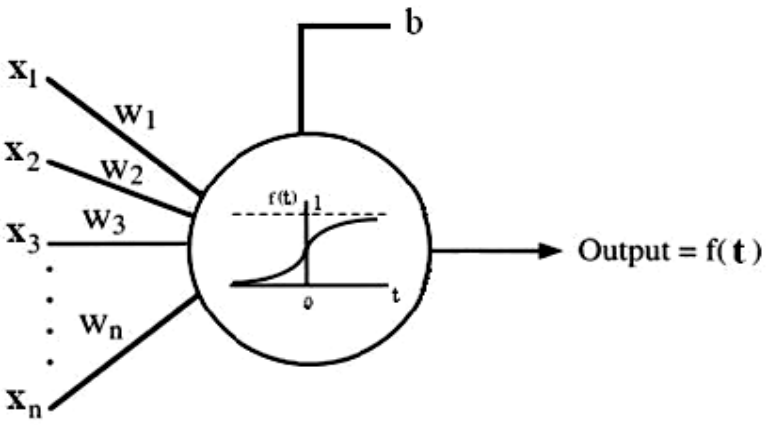

Figure 3.4. Schematic diagram of an artificial neuron.

A typical ANN consists of a number of neurons organized following special arrangement (ASCE, 2000a), which represents the pattern of connections among network nodes (Fausett, 1994). One of the popular types of ANNs, in water resource problems, is the feed forward neural networks (FFNNs) in which the neurons are arranged in layers; input layer, one or more hidden layers, and output layer. The information in FFNNs flows and is processed in one direction from input layer, through hidden layer(s), to the output layer. In FFNNs, neurons of each layer are operating in parallel and are fully connected to those of the next layer (Fig. 3.5). Each of the neurons in the hidden layer receives the input signals from the input layer through the weighted connection links. Received information is processed individually in each of the hidden layer neurons and the outputs (processed information) are passed to the output layer neuron(s) to release the final response of the network. A simple configuration of a three-layer feed forward ANNs is shown in Fig. 3.5.

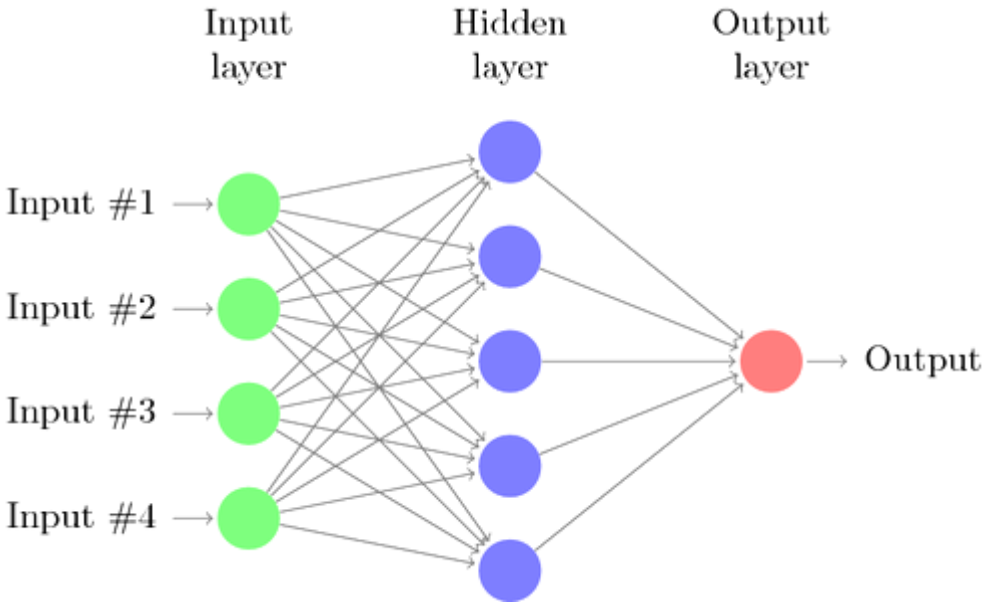

Figure 3.5. Simple configuration of three-layer feed forward ANN (from Fauske, 2006).

An ANN model can consist of several hidden layers; however, it was observed in the literature that a single hidden layer has been usually sufficient for the approximation of conventional hydrological processes (Maier and Dandy, 2000), and it was noted also, in particular, for the process of evapotranspiration (Kumar et al., 2002; Parasuraman et al., 2007). As a result, three-layer FFNNs were adopted in this study for the modeling of AET process. Input and output layers may contain one or more neurons depending on the problem at hand (number of predictors and predictands, respectively). For this study, the input layer contained five nodes providing the information of predictor variables; R_n, T_g, T_a, RH, and W_s, to the network and the output layer consisted of a single neuron representing the model output (predicted AET values).

The number of hidden layers and hidden neurons is specified, based on the complexity of the problem, using different methods (usually trial-and-error procedure (ASCE, 2000a)). In this study, trial-and-error procedure was used and different number of hidden neurons ranging from 1 to 14 was investigated for finding the optimum number of hidden neurons. Activation functions adopted here include the log-sigmoid and linear functions for the hidden layer and output layer neurons, respectively. ANNs with single hidden sigmoid layer and linear output layer are the most popular network architectures in the field of water resources (Cybenko, 1989; Hornik et al., 1989).

In addition to the type of ANNs, geometry of the network (number of hidden layers and neurons), and activation functions, ANNs are characterized by the method of determining the optimum connection weights, namely training algorithm (Fausett, 1994). ANNs learn the pattern of the investigated process (or trained) by adjusting the connection weights and bias values using the provided examples of input-output relationship (namely, training samples). A training algorithm is employed to optimize the weight matrices and bias vectors, which minimize the value of a predetermined error function. Minimum error function results in an ANN model that can generate the most similar output vector to the target vector.

The Back propagation algorithm is the most common type of training algorithm in the FFNNs in water related problems (Maier and Dandy, 2000). Basically, back propagation algorithm is a gradient descent technique that adjusts weights and biases in the direction of the most rapid decrease in the network error function. The network starts with random weight and bias values and generates the output of the network using the given input data; this step is called the forward step (ASCE, 2000a). The network output is compared with the desired target output, and the associated error value is computed. The error is propagated backward through the network and the connection weights are adjusted accordingly using the following equation:

$$w_{ij}(k) = w_{ij}(k+1) - \alpha_k g_k \qquad [3.5]$$

where w_{ij}(k) and w_{ij}(k+1) are the weight vectors of neuron *j* of the layer *i* at two sequent paths (epochs). The parameters g_k and α_k are the gradient of the error function surface and the learning rate, respectively. Learning rate is the step-size parameter affecting the speed of arriving at the minimum error value. The forward and backward steps, together called an epoch, are implemented repeatedly for several times until the error function reaches its minimum value and the optimum weight and bias values are achieved.

One of the problems that threaten the learning process is over-fitting. It usually occurs when the network has memorized the training examples, but it has not learned to generalize to new situations. Various techniques can be employed to, avoid over training and, improve network generalization ability such as; regularization and early stopping

(Neural Network Toolbox User's Guide, 2009). Regularization attempts to smooth the network response by keeping the size of the network weights adequately small (MacKay, 1992) using the modified form of the error function, which considers network weights and biases (Neural Network Toolbox User's Guide, 2009). Benefiting from the regularization method, the modified error function (*msereg*) that was employed in the training process of ANNs in this study is given as:

$$msereg = \frac{\gamma}{N}\sum_{i=1}^{N}(O_i - P_i)^2 + \frac{(1-\gamma)}{N}\sum_{j=1}^{m} w_j^{\,2} \qquad [3.6]$$

where O_i, P_i, N, γ, and w_j are the target output, ANN predicted output, number of training samples, performance ratio, and network weights, respectively.

Through the early stopping approach, an independent test set, namely cross-validation, can be used to monitor the performance of the model on a set of not-yet-encountered examples at some stages of the training process. Training is stopped when error on the cross-validation dataset begins to rise to prevent the model from being over-trained (Neural Network Toolbox User's Guide, 2009). In this study, both regularization and early stopping approaches were employed with the examined training algorithms; Levenberg-Marquardt (Levenberg, 1944; Marquardt, 1963) and Bayesian-regularization (MacKay, 1992). Levenberg-Marquardt is one of the high-performance algorithms that appear to be the fastest method for training moderate-sized FFNNs (Neural Network Toolbox User's Guide, 2009). Bayesian-regularization algorithm is an automated regularization algorithm, which uses Bayesian framework to automatically determine the optimal regularization parameter, performance ratio (γ), in the modified performance function. This algorithm also provides a measure of network parameters (weight and biases) that are being effectively used by the network. This ensures that the network will not use a larger number of parameters than the identified effective ones in estimating network output values. In other words, it keeps the network size as small as possible (Neural Network Toolbox User's Guide, 2009).

Neural Network Toolbox in MATLAB (MATLAB® Software, 2003) was used to develop the ANN models to predict AET based on five inputs of meteorological

variables, R_n, T_g, T_a, W_s, and RH. The data pool of 2006 was randomly divided into three subsets of training, cross validation, and testing using the approach explained earlier. The employed approach for splitting the data pool ensured that all three sub datasets were fairly representing the population to be modeled. The training subset was used for optimizing the connection weight matrices and bias vectors of the network. The cross-validation subset was used to stop the training process when the network starts to over-fit the training subset (early stopping). Once the network was trained, the generalization and predictive ability of the network was evaluated using a completely unseen subset of 2006 called testing subset.

The data subsets were normalized so that data fell between 0 and 1. Such scaling of data smoothes the solution space and averages out some of the noise effects (ASCE, 2000a). Based on the training subset, different ANN models were trained using Levenberg-Marquardt and Bayesian-regularization training algorithms, using different number of hidden neurons ranging from 1 to 14. For each examined network architecture, the training process was repeated several times, each time started with different random initial weight matrices, until satisfactory optimal network (with minimum errors) was obtained. The ANN model with the best performance measures associated with the cross-validation subset was selected as the optimal predictive network. The performance and generalization ability of the trained model was evaluated on the testing subset. This model validation determines how well the ANN model performs on the dataset that have not been seen during the training process (Cheng and Titterington, 1994).

ANNs, as a data driven technique, have the ability to determine the critical model inputs (Maier and Dandy, 2000). In this study, the ANN modeling technique was used to identify the important meteorological variables affecting the AET process. In this approach, no prior knowledge was assumed about the physics of AET mechanism and the relationships among variables. All possible combinations of input variables, 26 combinations, were considered to be examined as ANN model input sets. Separate optimal ANN models were developed and trained for each input combination set using the model development approach explained earlier. The developed ANN models were

compared based on their prediction accuracy in order to identify the most appropriate and efficient combinations of inputs for the estimation of AET. This approach is commonly referred to as trial-and-error procedure, which is under the category of heuristic approaches. The possible combination sets of five available input variables include; five-input combination, "R_n, T_g, T_a, RH, W_s", four-input combinations, "R_n, T_g, RH, W_s"; "R_n, T_g, T_a, RH"; "R_n, T_g, T_a, W_s"; "R_n, T_a, RH, W_s"; "T_g, T_a, RH, W_s"; three-input combinations, "R_n, T_g, RH"; "R_n, T_g, W_s"; "R_n, T_g, T_a"; "R_n, RH, W_s"; "R_n, T_a, RH"; "R_n, T_a, W_s"; "T_g, RH, W_s"; "T_g, T_a, W_s"; "T_g, T_a, RH"; "T_a, RH, W_s"; and two-input combinations, "R_n, T_g" ; "R_n, RH" ; "R_n, W_s" "R_n, T_a" ; "T_g, RH" ; "T_g, W_s" ; "T_g, T_a" ; "T_a, RH" ; "T_a, W_s" ; "RH, W_s".

3.4.2 Genetic programming (GP)

Genetic algorithms (GA) belong to the family of evolutionary algorithms, and are generally considered as an optimization method for searching global optimum of a function using natural genetic operators. Genetic programming (GP), which was introduced by Koza (1992), is an extension of GA for inducing computer programs, as solutions for problems at hand, using an intelligent and adaptive search. This type of search uses the information gained from the performance (fitness) of individual computer programs, in the search space, for modifying and improving the current programs. Depending on the particular problem, computer programs of the GP search space may be different, e.g. Boolean-valued models and symbolic mathematical models (Koza, 1992). Symbolic regression GP evolves computer programs in the form of mathematical expressions in which both functional form and numerical coefficients of the regression symbolic model are optimized through the evolutionary process of GP. This application of GP was adopted in this study for obtaining explicit mathematical AET models.

In the first step of GP implementation, a population of computer programs are randomly generated using no primary knowledge about the optimum solution (e.g. structure of the underlying relationship model) and possible relationships among

variables. This initial population is called initial random generation (or first generation). Symbolic regression models are represented by structured parse trees (Fig.3.6), which are composed of functional and terminal sets appropriate to the problem. A functional set can be a set of mathematical arithmetic operators such as {+, -, *, /}, mathematical functions, Boolean and conditional operators, and any other user-defined functions where the number of arguments of each function is specified. The terminal set, which is associated with the nodes that terminate a branch of a tree in tree-based GP (Banzhaf et al., 1998), is defined as independent variables; i.e. the terminal set $z=\{x,y\}$ where x and y are independent variables (Sette and Boullart, 2001).

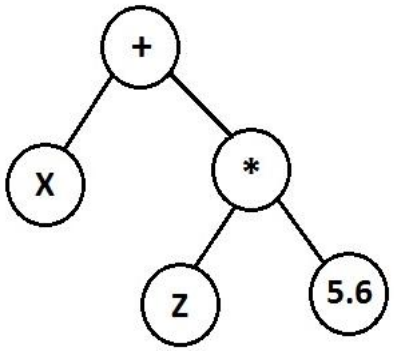

$$Y = X + Z \times 5.6$$

Figure 3.6. Tree structure symbolic regression GP model for estimation of predictant Y.

GP begins to search in the search space of randomly generated models of initial generation. The fitness measure is used to evaluate how well each individual in the population performs. Fitness is usually measured by the errors produced by individual models (error-based fitness measure). Each model in the population is run using a number of provided data instances (training dataset) to measure the performance of each individual over a variety of representative different situations (Koza, 1992). A scalar fitness value is assigned to each individual using the defined fitness evaluation function. Base on the assigned fitness values, some individuals in the population perform better than others with smaller error values, which means that they have higher chance to be selected for the next step of GP.

In the second step, genetic operators, based on the Darwinian principles of reproduction and survival, are used to create the next generation. Individuals with better performance are allowed to survive and be reproduced in the next population, called mating pool, using the *fitness-proportionate reproduction* operator. This operation improves the average of fitness of the population (Koza, 1992). Mating pool is an intermediate stage in transforming from current generation to the next generation. In the mating pool, two other operations are performed on the reproduced individuals, namely crossover and mutation. Crossover acts on specific percentage of the mating pool population, *crossover probability* (P_c), and results in the creation of new individuals in the population. Crossover exploits two individuals (parents), selected based on their fitness, and splits each parent at the crossover point into two fragments (sub trees), which are swapped between the parents to create two new offspring (Fig. 3.7). The offspring (new models) are improved individuals, compared to their parents, which carry some genetic properties from each of them.

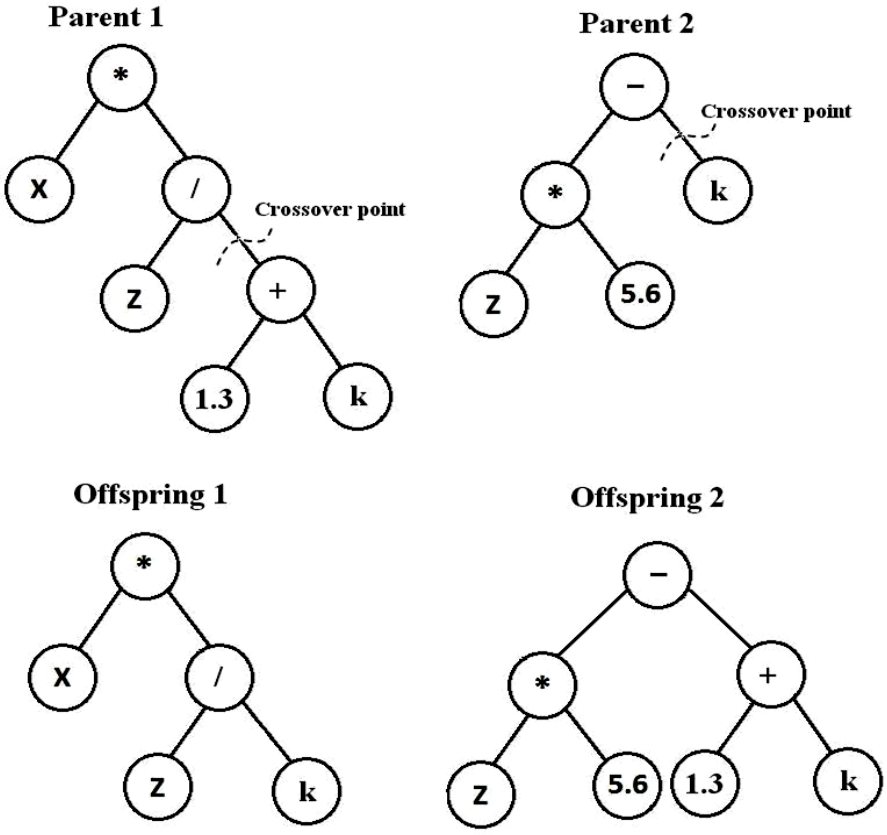

Figure 3.7. Crossover operation on two selected individuals.

Mutation operates on the population individuals in proportion to the *mutation probability* (P_m). A string is randomly selected from the mating pool and it undergoes some changes at the randomly selected mutation point (Fig. 3.8). The mutation operation also results in new individuals, which increases the genetic diversity of the population (Koza, 1992). The remaining percentage of the population participates in the reproduction operation corresponding to *reproduction probability* (P_r), which simply reproduces individuals from the mating pool to the next generation. Reproduced and newly created individuals resulted from genetic operations of reproduction, crossover, and mutation form the next generation of GP search space.

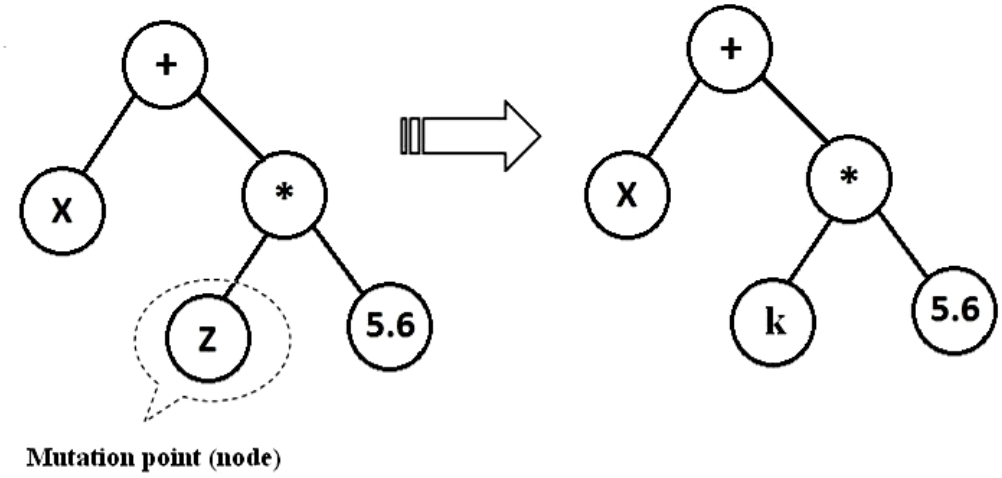

Figure 3.8. mutation operation on a selected individual.

The described evolutionary process is performed iteratively over several generations until some *termination criterion* is satisfied. The termination criterion might be a maximum number of generations or some measure of the goodness of the generated solution and stop the algorithm once the solution is found (Koza, 1992). The result of the GP algorithm, which is a GP-evolved model for the investigated problem, based on the termination criterion, is either the best found model or the best individual of the last GP generation.

Major steps in the implementation of GP to solve a problem, e.g. evolution of AET models in the current study, include determination of functional and terminal sets, fitness measure, initializing method, selection method, levels of GP parameters over the

run (crossover and mutation probabilities, population size), and the termination criterion. The functional set, which was introduced to GP, included {+, -,*, /}. The terminal set was defined as *{R_n, T_g, T_a, W_s, RH}*. Root mean squared error (RMSE) was selected as the fitness function for evaluating individual performance and further fitness-based selection. Ramped-half-and-half method was adopted for initializing the first generation tree structures. This initializing method increases the diversity of the tree structures using various shapes and sizes by mixing two common methods of tree initializing, namely, full method and grow method. Further descriptions of initializing methods can be found in Koza (1992) and Banzhaf et al. (1998).

The next important issue in the implementation of GP is the fitness-based selection method. Selection method determines the manner by which the individuals are selected based on the assigned fitness values for further GP operations (e.g. crossover, mutation). Roulette wheel selection method was employed for implementing selection operation in the GP runs. Roulette wheel method is the simplest selection scheme that follows a stochastic algorithm. In this method, individuals are attached to contiguous slices of a roulette wheel; each slice is proportional in size to the fitness value of the attached individual. A random number is generated and the individual whose slice spans the random number is selected. Following this method, individuals with better fitness values were given larger chance to be selected and passed into the next generation. Several different levels of GP parameters; crossover and mutation probabilities, number of evaluated generations, and the size of population, were executed for obtaining symbolic regression AET models using the training subset. The termination criterion for each GP run was the identified maximum number of generations. The performances of the generated symbolic equations were assessed using the cross-validation subset to select the best equation (model). The selected symbolic equation was then tested using the unseen testing subset to evaluate the predictive accuracy and generalization ability of the proposed model.

Data subsets that were used with the GP technique were exactly the same as those used with the ANNs. The data were normalized by dividing the values of variables by their corresponding maximum values. In this way, all variables could have

dimensional consistency during the GP implementation (Parasuraman et al., 2007). In this study, GPLAB (Silva, 2005), GP toolbox for MATLAB, was used for the implementing of the GP technique and generating mathematical models based on the datasets where AET is a dependent variable as a function of the five independent variables: R_n, T_g, T_a, W_s, and RH.

3.4.3 Multilinear regression (MLR)

Linear regression is a conventional approach in the statistical modeling of the relationship between variables in which the unknown parameters of the regression model are estimated using the data instances. Multilinear regression (MLR) is a statistical model that contains more than one predictor variable. The general form of the first order MLR model is:

$$Y = \beta_0 + \beta_1 X_1 + \beta_2 X_2 + ... + \beta_n X_n + \varepsilon \qquad [3.7]$$

where Y is the dependent variable (predictant) that is represented as a function of n independent variables (predictors), X. β_0 is the unknown intercept, β_1, ... , β_n are the unknown coefficients (also called partial regression coefficients) of the function, and ε is the random error term with assumed normal distribution.

Since the statistical regression is the simplest and most straight forward form of a model, it is usually the first modeling approach that is adopted and investigated for modeling of a relationship (Laverty, 2009) and might be considered as a benchmark modeling approach. Many nonlinear models can be represented in the form of linear models by appropriately transforming any or all of the independent variables. In this way, nonlinear models are linearized and the unknown parameters are estimated (specified) using the simple method of linear regression. Equation (3.7) is the standard form of the MLR, which includes only the first order of the independent variables. Two other forms of the MLR, which were employed for the statistical modeling of AET process in this study, are given below:

$$Y = \beta_0 + \beta_1 X_1 + \beta_2 X_2 + ... + \beta_n X_n + \beta_{n+1} X_1 X_2 + \beta_{n+2} X_1 X_3 + ... + \beta_{n+k} X_n X_{n-1} + \varepsilon \quad [3.8]$$

$$Y = \beta_0 + \beta_1 X_1 + ... + \beta_n X_n + \beta_{n+1} X_1 X_2 + \beta_{n+2} X_1 X_3 + ... + \beta_{n+k} X_n X_{n-1} + \beta_{n+k+1} X_1^{\,2} + ... + \beta_m X_n^{\,2} + \varepsilon \quad [3.9]$$

Equation (3.8) includes the linear terms and the cross-product terms of the two predictor variables, which are referred to as interaction effect. Interaction refers to the effect that a change in a predictor variable can have on the predictand depends on the level of the other predictor variable(s) (ReliaSof's DOE++ software User's Guide, 2008). In Eq. (3.9), in addition to the already defined terms of linear and interaction, the higher order terms (second order here) of the predictor variables are considered. Both given regression functions, Eq. (3.8) and (3.9), are still linear because the models are linear in parameters (ReliaSof's DOE++ software User's Guide, 2008). Consequently, they can be expressed in the general form of Eq. (3.7), using the appropriate transformations such as $x_1=X_1.X_2$ and $x_2=X_1^2$, and then the unknown parameters are specified using the data samples. This approach was used in this study for fitting the statistical regression models for the estimation of AET.

The experimental data of AET including the first and second orders of five independent variables and all their two-factor interactions were statistically analyzed using a statistical analysis software (SAS/STAT® software, 2003). All data subsets employed in the statistical analysis were exactly the same as those used with ANNs and GP techniques. Using the training subset, two different MLR equations were developed by following the functional forms of the Eq. (3.8) and (3.9). In addition, as a baseline comparison, a simple first order regression equation (Eq. 3.7) was fitted to the data using the linear factors of the meteorological variables; R_n, T_g, T_a, W_s, and RH. The best equation was selected based on the error statistics associated with the cross-validation dataset.

In the first developed statistical model, the input variables introduced to the SAS/STAT® software included the linear factors of the meteorological variables, R_n, T_g, T_a, W_s, and RH, and all of their two-factor interactions, T_aT_g, T_aRH, T_aR_n, T_aW_s, T_gRH,

T_gR_n, T_gW_s, RHR_n, RHW_s, and R_nW_s. For the second statistical model, in addition to the already defined input variables, the second orders of the meteorological variables, R_n^2, T_g^2, T_a^2, W_s^2 and RH^2, were also considered. The stepwise selection method was performed to fit the multilinear regression equations and to assess the significance of the introduced variables on the AET process. The stepwise method uses both forward and backward selection techniques for finding the best model that is also adequately simple (containing all important variables). The least squares method was employed for identifying the unknown parameters of the MLR models. In this method, the regression parameters of β_0, β_1, β_2,…, β_m are estimated to minimize the residual sum of squares (RSS) (Eq. 3.10) between observed and predicted values provided by the model over fitness cases (training subset). RSS fitness function is defined as:

$$\text{RSS}= \sum_{i=1}^{N} (Y_i - Y_i')^2 \qquad [3.10]$$

where Y_i, Y_i', and N are observed value, predicted value, and number of training samples, respectively. To identify the terms having significant effects on AET, the tests of hypothesis was conducted at 95% confidence level.

3.5 HYDRUS-1D model

The main idea behind the use of the HYDRUS model was to compare a currently available AET estimation model with the proposed data driven models. The predictive abilities of some data driven models, e.g. ANNs and GP, have already been compared with that of the widely used standard FAO Penman-Monteith (PM) method (Parasuraman, et al., 2007). However, the standard PM method estimates the potential evapotranspiration, since it assumes that the soil moisture is not a limiting factor. Therefore, this comparison with the data driven AET models may not seem appropriate. In order to perform such comparison more reasonably, one of the available methods for estimation of AET was employed, through using HYDRUS-1D software modeling package (Version 4.0; Šimunek et al., 2006), and its performance was compared with those of the developed data driven models.

One of the most widely used methods for the estimation of AET is to make use of meteorological data and the commonly available reference evapotranspiration (ET_o) models and compute the AET using the soil wetness function ($f(\theta_{rel})$), Eq. (3.11), (Dingman, 2002). Soil wetness function describes the relationship between AET/ET_o and relative water content, θ_{rel}.

$$AET = f(\theta_{rel}).\mathrm{ET_o} \qquad [3.11]$$

where θ_{rel} is defined as:

$$\theta_{rel} = \frac{\theta - \theta_{pwp}}{\theta_{fc} - \theta_{pwp}} \qquad [3.12]$$

where θ, θ_{pwp}, and θ_{fc} are the current water content, permanent wilting point, and field-capacity of the soil. HYDRUS-1D is a physically based software package simulating the water, heat, and solute movement in one-dimensional variably-saturated media. HYDRUS-1D model can simulate the rate of actual evapotranspiration based on the described method incorporated with some numerical methods. In this model, ET_o is estimated with the FAO recommended PM equation (Monteith, 1981; Monteith and Unsworth, 1990; FAO, 1990), which is the widely adopted physically based model for the modeling of ET. Then, the rate of AET is estimated using the PM-predicted ET_o, simulated soil moisture profile, and evaporation rate, which is described below.

For this type of AET modeling, in addition to the meteorological data of R_n, T_a, RH, and W_s, the data of leaf area index (LAI) and rainfall were also required. The data of LAI were available on an approximately weekly basis, which were disaggregated to hourly basis using linear interpolation for consistency with temporal resolution of other meteorological data. Rainfall data were also available in event-based records for which some aggregation procedure was performed to obtain hourly rainfall data. Hydraulic conductivities of the soil layers were optimized through an inverse simulation procedure in HYDRUS-1D model. Other required physical and hydraulic parameters of the soil were selected based on the previously conducted research on the same soil type

(Shurniak, 2003). Using HYDRUS-1D software, ET_o was determined with the FAO recommended PM combination equation (FAO, 1990):

$$ET_o = \frac{1}{\lambda}\left[\frac{\Delta(R_n - G)}{\Delta + \gamma\prime(1 + r_c/r_a)} + \frac{\rho c_p(e_s - e_a)/r_a}{\Delta + \gamma\prime(1 + r_c/r_a)}\right] \quad [3.13]$$

where ET_o is the rate of potential evapotranspiration from reference crop [mm h^{-1}], λ is the latent heat of vaporization [MJ kg^{-1}], R_n is net radiation at surface [MJ m^{-2} h^{-1}], G is the soil heat flux [MJ m^{-2} h^{-1}], ρ is the air density [kg m^{-3}], c_p is the specific heat of soil moisture [kJ kg^{-1} $^oC^{-1}$], $(e_s\text{-}e_a)$ is the vapour pressure deficit [kPa], e_s is the saturation vapour pressure at temperature T [kPa], e_a is the actual vapour pressure [kPa], r_c is the crop canopy resistance [s m^{-1}], r_a is the aerodynamic resistance [s m^{-1}], γ' is the psychrometric constant [kPa $^oC^{-1}$], and Δ is the slope of the vapour pressure curve [kPa $^oC^{-1}$] (HYDRUS-1D Software Package User's Manual, 2008).

Estimated ET_o was partitioned into potential soil evaporation and potential plant transpiration using the *LAI* information. Actual transpiration was then calculated from the obtained potential transpiration and the plant water stress function proposed by Van Genuchten (1978). The gradient of simulated water pressure head in the soil profile along with the soil hydraulic conductivity were used for the simulation of actual evaporation rate from the soil surface. Simulated evaporation was compared with the calculated potential evaporation to give the actual rate of soil evaporation. This comparison is performed because the PM model sometimes overestimates the rate of evaporation. If the PM-estimated evaporation is larger than the simulated evaporation, the simulated value is given as the actual rate of evaporation. Estimated values of actual evaporation and transpiration were aggregated to estimate the actual rate of evapotranspiration (AET). Because the HYDRUS model was not within the main scope of this thesis, the detailed methodology associated with this type of modeling is not provided here. Detailed description of AET simulation using HYDRUS-1D can be found in HYDRUS-1D Software Package User's Manual (2008). HYDRUS model was used for estimation of AET in years 2005 and 2006 out of which the model comparison was performed only based on the 2005 dataset. The reason for using 2005 data was that the data driven models were trained using a large portion of 2006 data on which they

expectedly perform well. As a result, a fair model comparison can be performed using the dataset of the year 2005.

3.6 Evaluation of models' Performance

The performances of the data driven models; ANNs, GP, and multilinear regression models, as well as the HYDRUS-1D model were evaluated to compare their predictive accuracies based on three statistical criteria: Pearson's correlation coefficient (R), root mean squared error (RMSE), and mean absolute relative error (MARE), which were calculated as follows:

$$R = \frac{\sum_{i=1}^{N}\left(O_i - \overline{O}\right)\left(P_i - \overline{P}\right)}{\left[\sum_{i=1}^{N}\left(O_i - \overline{O}\right)^2\right]^{0.5}\left[\sum_{i=1}^{N}\left(P_i - \overline{P}\right)^2\right]^{0.5}} \quad [3.14]$$

$$MARE = \frac{1}{N}\sum_{i=1}^{N}\frac{\left|O_i - P_i\right|}{\left|O_i\right|} \quad [3.15]$$

$$RMSE = \sqrt{\frac{\sum_{i=1}^{N}\left(O_i - P_i\right)^2}{N}} \quad [3.16]$$

where O_i, P_i, $\overline{P}$, and $\overline{O}$ are observed values, simulated values, mean of simulated, and mean of observed values, respectively. N is the number of instances in the dataset. In addition to the above mentioned statistics, akaike's information criterion (AIC) was used for characterizing and comparing the goodness of fit of the obtained data driven models. The AIC provides a measure of model quality, which rewards a model for goodness of fit, but also penalizes it for unnecessary parameters. AIC is widely used for model selection and is defined as (Akaike, 1974; Russo et al., 1991):

$$AIC = k\left[\ln(2\pi) + \ln\left(\frac{SSE}{k-l}\right) + 1\right] + l \quad [3.17]$$

where SSE, *k*, and *l* are summation of squared error, number of observations and number of parameters to be optimized during modeling. Smaller AIC value indicates more approprite model.

3.7 Wavelet Analysis

Natural functions, e.g. meteorological and hydrological processes, operate over a wide range of spatial and temporal scales leading to spatial/temporal variability of interacting mechanisms. AET is a hydrometeorological signal (variable) interacting with several temporally/spatially variable meteorological signals. Evaluation of dominant cyclic variations in the AET and correlated meteorological signals improves the understanding of the mechanism as well as its modeling. In this study, only temporal scaling of the variables time series was investigated whereas the spatial variability of the AET and meteorological signals was not considered.

Temporal cyclic variations of natural processes are not usually stationary and contain several localized and transient frequency events. Therefore, conventional frequency domain analysis such as Fourier transform can not reveal the localized natural cyclic events, because in this kind of transformations the temporal variations of the signal is separated at different scales only (Si, 2008). Wavelet analysis (WA) provides a tool for decomposing the variations of a time series signal into time and scale (frequency) domains; allowing the identification and analysis of dominant temporal cyclic events. Theoretical description and a complete introduction of WA can be found in Daubechies (1992) and Lau and Weng (1995). Torrence and Compo (1998) developed an easy-to-use wavelet analysis toolkit, which includes statistical significance testing for improving the qualitative nature of the WA. The same approach as Torrence and Compo (1998) was employed in this study for WA of AET and meteorological time series.

The basic component of WA is the wavelet transformation in which the studied function is represented by wave-like oscillating functions. The choice of the wavelet function is of high importance within the wavelet transformation. Wavelet function is a small finite-length oscillating mathematical function (small wave) (Polikar, 1996),

which represents the data in terms of frequency component (Graps, 1995). Wavelet functions are defined in different forms, namely mother wavelets, to have specific properties for information extraction of different types of signals. Figure 3.9 shows some examples of mother wavelets.

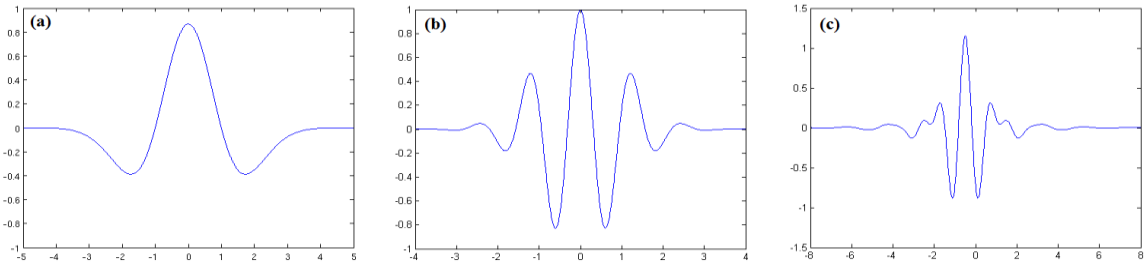

Figure 3.9. Examples of mother wavelet functions; (a) Mexican Hat, (b) Morlet, and (c) Meyer.

The term wavelet function generally refers to two types of wavelet functions, namely orthogonal and non orthogonal (Torrence and Compo, 1998). Orthogonality stems from the mathematical properties of the wavelet function. If the inner product of the basis functions (modulated versions of a mother wavelet) equals zero, the wavelet is said to be orthogonal. It means that a set of scaled wavelet functions, associated with different scales, do not have any similar (mutual) components (Polikar, 1996). Otherwise, the wavelet function is said to be non-orthogonal. Orthogonal wavelets are mainly used for decomposition of a signal into specific (preferably minimum) frequency bands, which reduces the computation time and provides properties for easier reconstruction of the original signal (Polikar, 1996). This type of wavelet analysis is usually referred to as discrete wavelet transformation, which may not provide a physically meaningful analysis all the time (Si, 2008).

Non-orthogonal wavelets are usually used for continuous wavelet transformation (CWT) of time series signals in which a continuous set of frequencies are examined. CWT results in a highly redundant time-scale resolution of the signal, which on one hand induces some uncertainties in the reconstruction of the signal and, on the other hand, provides better scale analysis of the time series (Si, 2003; He et al., 2007). Because of the wide range of possible dominant frequencies that can be obtained using

CWT, Coulibaly and Burn (2004) indicated that the CWT is more appropriate for analysis of geophysical and hydrological time series. For the current study, scale analysis of the time series data were of interest, so the CWT was employed and is described here.

3.7.1 Continuous wavelet analysis

As it was mentioned earlier, the choice of wavelet function is an important component in the wavelet transformation. Wavelet function can be a real or complex function. Complex wavelet functions make it possible to extract the information of both amplitude and phase, which is more suitable for analyzing the signal's oscillatory behaviour (Torrence and Compo, 1998). Morlet, Mexican Hat, and Haar are some of the mother wavelets usually employed in the CWT out of which the Morlet is a complex function. Depending on specific information one might be interested in, different wavelet functions can be selected. The selected mother wavelet must satisfy some non-restrict requirements, which assure the success of reconstruction procedure. This mathematical condition is called the "admissibility condition" at which the wavelet function should have zero mean and quickly decay in both time and scale space (Farge, 1992). The latter condition represents the localization quality of the function in time and space scale.

Morlet is a complex and non-orthogonal wavelet that provides sufficient resolution (localization) in time and scale domains (Grinsted et al., 2004; Si, 2008). Morlet function, with non-dimensional frequency parameter (ω_0) equal to 6, has been shown to successfully work for the analysis of observed time series in different hydrological applications (Lafreniere and Sharp, 2003; Anctil and Tape, 2004; Coulibaly and Burn, 2004; Labat et al., 2005; Si and Zelek, 2005; Coulibaly, 2006). This Morlet wavelet was used for the current wavelet transformation, which is an exponential oscillatory function defined as (Torrence and Compo, 1998):

$$\psi_o(\eta) = \pi^{-1/4} e^{i\omega_o \eta} e^{-\eta^2/2} \qquad [3.18]$$

where η and ω_0 are non-dimensional time and frequency parameters. The Morlet wavelet with $\omega_0 = 6$ was adopted to satisfy the admissibility condition (Farge, 1992).

The CWT of a discrete time series data of x_i (i=1,2,…,N) is defined as the inner product (convolution) of time series signal with the scaled and translated version of mother wavelet function, $\psi_o(\eta)$, according to a specific scale (s) and time location (τ), which is given as:

$$CWT(\tau, s) = \sum_{i=1}^{N} x_i(t).\psi^*_{\tau,s}(t) \qquad [3.19]$$

where $\psi_{\tau,s}(t)$ is the normalized wavelet function and (*) represents the complex conjugate. Wavelet function is normalized to ensure that the wavelet transform at each scale is not weighted by the magnitude of the scale, which makes a direct comparison of wavelet coefficients at different scales possible (Torrence and Compo, 1998). Normalized wavelet function is defined as:

$$\psi_{\tau,s}(t) = \frac{1}{\sqrt{s}}\psi_{o\tau,s}(t) \qquad [3.20]$$

where τ and s are associated with the time location (translation) and scale resolution at which the wavelet transformation is performed. Localization of the time series signal into time and scale domains (multiresolution representation of signal) is implemented, first, by modulating the mother wavelet, corresponding to the current scale, and shifting the scaled wavelet (also called daughter wavelet) through the signal to the end and performing the convolution at each discrete time location. This results in the time localization of the signal. The procedure is repeated, in the second step, for each scaled wavelet, corresponding to different values of scale, to localize the signal in the scale domain. Wavelet coefficients are computed for all time and scale steps (τ,s) to give the multiresolution representation (or CWT) of the signal. Scaled and translated wavelet at scale s and time location τ is computed by:

$$\psi_{\tau,s}(t) = \psi(\frac{t-\tau}{s}) \qquad [3.21]$$

According to the mathematical definition of CWT, WA investigates the resemblance of the wavelet function with the in hand signal in the sense of frequency content (Polikar, 1996). In other words, "if the signal has a major component of the frequency corresponding to the current scale, then the wavelet at the current scale will be similar or close to the signal at the particular location where this frequency component occurs. Therefore, the CWT coefficient at this point in the time-scale plane will be a relatively large number" (Polikar, 1996) and will spike in the contour plot of CWT spectrum. Computation of CWT using Eq. (3.19) can become considerably faster if it is implemented in the Fourier space (Torrence and Compo, 1998). Briefly, through this method, the product of Fourier transform of the signal and wavelet function is computed and then the inverse Fourier is performed on the result to give the signal's CWT. Further explanation on this approach can be found in Torrence and Compo (1998). The same methodology was employed in the current study for performing the CWT.

For implementing CWT, it is required to identify the set of analyzed scales a priori. In continuous wavelet analysis, the investigated scales must be incremented continuously to create a complete picture of the wavelet transform. Theses set of scales (s) can be generated using fractional powers of two (Torrence and Compo, 1998):

$$s_j = s_0 2^{j\delta j} \qquad j = 0, 1, 2, ..., J \qquad [3.22]$$

where s_0 is the smallest scale and J determines the maximum number of scales to be investigated. δ_j is the scale step size whose value depends on the selected wavelet function. For Morlet wavelet, δ_j value of 0.5 is the largest value that can also provide adequate scale sampling (Torrence and Comp, 1998). For the current analysis, the scale step size of $\delta_j = 0.083$ and the maximum examined scales of $S_J = 16$ and 48 hours were selected for performing the transformation. The smallest scale (S_0) was selected as approximately equal to $2\delta t$, where δt is the time step of the measured time series data.

The time step of the AET and meteorological variables is an hour ($\delta t = 1$) and subsequently $S_0 = 2$ hours.

Complex wavelet function, e.g. Morlet, results in complex wavelet coefficients constitute of real and imaginary parts or amplitude, $|CWT(\tau, s)|$, and phase, $\tan^{-1}[Im\{CWT(\tau, s)\}/Re\{CWT(\tau, s)\}]$, respectively. For convenient description of time series cyclic variations, it is common to use wavelet power spectrum, defined as, $|CWT(\tau, s)|^2$, instead of continuous wavelet spectrum. The obtained wavelet power spectrum was also normalized for easier comparison with different wavelet spectra. In this normalization, the wavelet power spectrum was divided by the variance of the time series (σ^2), $|CWT(\tau, s)|^2/\sigma^2$ (Torrence and Compo, 1998).

The cone of Influence (COI) has been defined in the wavelet spectrum to clarify the areas that are considerably affected by the zero paddings at the ends of the time series signal. Time series data are padded by zeros at both edges to overcome the problem caused by their finite lengths. These zero values decrease the magnitude of wavelet power at the areas close to the edge from which the COI distinguishes regions that are not or negligibly influenced. Length of COI (or e-folding time (Torrence and Compo, 1998)), is estimated for each examined scale using a mathematical expression, which is defined as a function of scale. Structural form of this function depends on the type of selected mother wavelet. For Morlet wavelet, the length of COI at each scale (s) was defined as $\sqrt{2}\,s$.

In WA, the wavelet scale is not necessarily equal to the inverse of Fourier frequency (Fourier period ($\lambda_{\omega t}$)) but they are usually related to each other by analytical relationship. For the Morlet wavelet with $\omega_0 = 6$, the wavelet scale almost equals the Fourier period ($\lambda_{\omega t}$=1.03 s) (Torrence and Compo, 1998). Therefore, either scale or period terms can be used for the representation of frequency modes.

3.7.2 Statistical significance test

Most of the natural processes (e.g. geophysical and hydrological) are affected with background color noise (white or red noise). The effect of noise is reflected on the signal's wavelet power spectrum. It is essential to identify the powers caused by the background noise and distinguish them from the actual wavelet power peaks (significant time series cyclic features). Torrence and Compo (1998) developed a statistical significance test for wavelet power spectra to establish significant levels. Following Torrence and Compo (1998), a statistical significance test was implemented by modeling the appropriate background noise (either white or red) and then testing the significance of the power spectrum peaks against the modeled background noise at certain statistical significance level. In this approach, a null hypothesis was established to examine if the wavelet peaks were significantly different from the noise spectrum generated by a stationary noise process. In other words, by significance test, it was investigated if the peaks of the wavelet spectrum represented some true cyclic features or they were just caused by noise.

White noise is a random signal with equal power at all frequencies, which appears as a flat power spectrum in time-scale domain. Red noise refers to the temporal fluctuations that have higher amplitude at lower frequencies and lose the magnitude as the frequency increases. Most of the geophysical time series are contaminated with red noise background signals (Grinsted et al., 2004). If the time series data are completely random, white noise is assumed as the background noise; however, most of the hydrometeorological time series data are auto-correlated for which the red noise is more appropriate to describe the background noise (Si, 2009). According to Hasselmann (1976), lag-1 auto regressive process (AR [1]) is a suitable background noise for many climatological applications. Following Torrence and Compo (1998) calculations, a simple theoretical AR [1] red noise model was employed in this study for modeling the background time series red noise (x_n) given by:

$$x_n = \alpha\, x_{n-1} + z_n \qquad [3.23]$$

where $x_0 = 0$, z_n is the Gaussian white noise, and α is the lag-1 autocorrelation coefficient that can be estimated from observed time series (Allen and Smith, 1996).

It was shown by Torrence and Compo (1998) that the local wavelet power spectrum of the theoretical red noise, at every randomly selected time location, is on average identical to the Fourier transform of the noise time series. Consequently, the wavelet power spectrum of the red noise process can be estimated by the Fourier power spectrum given as (Grinsted et al., 2004):

$$P_q = \frac{1-\alpha^2}{\left|1-\alpha e^{2i\pi q}\right|^2} \qquad [3.24]$$

where P_q is Fourier transform of red noise signal and q is the frequency index.

In the described statistical significance test, it is assumed that the time series variables have random normal distribution. Most natural time series data do not follow the Gaussian (normal) probability distribution function (pdf), but can be transformed to make them as close as possible to normal distribution. Most of the studied time series in this study do not have normal distribution. As a result, following Grinsted et al. (2004), the probability distribution of the time series data were converted to rectangular distribution (uniform distribution) to make them close to normal distribution. Fourier power spectrum of the theoretical noise, which is the square of the normally distributed spectrum, has chi-square (χ^2) distribution with two degrees of freedom, χ_2^2, corresponding to the real and imaginary parts. Statistical significance test was performed at 95% confidence level. To perform the test, the 95% line was developed by multiplying the red noise spectrum by the 95th percentile value of χ_2^2. Wavelet peaks were compared with this 95% line and the peaks that were above this confidence line were identified as cyclic features that are significantly different from background red noise at 95% confidence level.

3.7.3 Cross wavelet analysis

Cross wavelet analysis is an extension to WA, which examines the linear correlation between two time series. Cross wavelet analysis identifies the high common power of two time series signal in the time–scale domain. Cross wavelet spectrum between two processes, X and Y, is estimated by (Torrence and Compo, 1998):

$$W^{XY}(\tau, s) = CWT^{X}(\tau, s)CWT^{Y*}(\tau, s) \quad [3.25]$$

where $CWT^{X}(\tau, s)$ and $CWT^{Y}(\tau, s)$ are the continuous wavelet transforms of the investigated time series, X and Y, and (*) indicates the complex conjugate. Cross wavelet spectrum is complex and can be decomposed into amplitude and phase. Local relative phase between X and Y is estimated by the complex argument (phase), $\tan^{-1}[Im\{W^{XY}(\tau, s)\}/Re\{W^{XY}(\tau, s)\}]$ and the cross wavelet power is also defined as$|W^{XY}(\tau, s)|$. The phase information in the cross wavelet spectrum gives the phase angle difference between the components of the two time series.

Using cross wavelet spectrum, cyclic features at which the underlying time series are covarying can be detected. The covariations of two signals demonstrate the existence of a link, in some way, between the underlying processes and also the fact that the information of one process is capable of predicting the other process. This information is very useful when it is of interest to find out the processes that have correlation (or strong correlation) with a target time series, e.g. AET here. The signals, which are showing to have high common power with the target signal in the cross wavelet spectrum, can be used as predictors in the estimation of temporal variations of the target time series. This is important information in the modeling of complex processes, e.g. hydrometeorological processes, in which determination of important predictors (input variables) is essential and a challenging task.

Physical understanding of the AET mechanism indicates possible causality between the meteorological variables and the AET signal. The strength of the relationship between AET and each of the available meteorological variables can be investigated using cross wavelet transformation. The meteorological variables, whose

covariations with the AET time series were investigated in this study, include R_n, T_g, T_a, RH, and W_s.

Statistical significance test of the cross wavelet power spectrum against the background red noise was conducted at 95% confidence level using the theoretical Fourier spectra of the two underlying time series, P_q^X and P_q^Y, following the Torrence and Compo (1998) suggested testing approach. The distribution of the cross wavelet power of two time series is given as:

$$\frac{|CWT^X(\tau,s)CWT^{Y*}(\tau,s)|}{\sigma_X\sigma_Y} \Rightarrow \frac{Z_\nu(p)}{\nu}\sqrt{P_q^X P_q^Y} \qquad [3.26]$$

where σ_x and σ_y are standard deviations of the two time series, X and Y, $Z_v(p)$ is the confidence level at the probability p, 95% here, for the pdf of the cross wavelet spectrum, which can be derived from the square root of the product of two chi-square distributions (Jenkins and Watts, 1968). For the complex wavelet used in this study, v, degrees of freedom, equals to 2 and $Z_2(95\%) = 3.999$. More description on the development of cross wavelet significance test can be found in Torrence and Comp (1998).

One of the important issues in the cross wavelet analysis is the misconception of the peaks in the cross wavelet spectrum. Since the cross wavelet spectrum is obtained using the univariate power spectra, some of the seemingly high power features might be caused by strong powers of one variable power spectrum only, while the other variable power at the same time-scale location is average. Therefore, every large cross wavelet power does not necessarily indicate high powers in univariate spectra of both variables nor strong correlation between them (Schaefli et al, 2007; Si, 2008). Consequently, significant peaks in the cross wavelet spectrum should be interpreted (or strong correlation between two variables should be identified) based on the detected high powers in the univariate power spectrum (Si, 2008). In addition, consistency of phase information in the significant areas of cross wavelet spectrum can help in differentiating between true covarying features and false high powers.

The cross wavelet technique- is capable of investigating the covariation of only two signals at a time. So, interaction effects that multiple different underlying time series may have on each other cannot be considered in this type of analysis. The interaction among different meteorological processes, whose correlations with AET were studied here, is expected based on the physical understanding of the investigated system. In the current study, cross wavelet transformation was also employed for extracting the significant common features between the target time series of AET and the time series induced by the GP-evolved models. This analysis was implemented to investigate the correlation between a modeled AET signal, obtained from different composition of meteorological signals, and the observed AET time series in terms of cyclic temporal variations. In this analysis, it was important to investigate the influence of multiple meteorological variables together on the estimation of AET cyclic variations.

In this approach, 35 GP models were generated at different levels of GP parameters using the continuous time series data (night-time and day-time data) of the year 2006 as the training dataset. The data that were used for evolving the GP models were exactly the same as those used for the wavelet analysis. Four optimum GP models, which constituted of different predictor variables and functional forms, were selected and employed for estimating the AET time series. Cross wavelet analysis was then used to investigate covariations between predicted and observed AET signals in the time-scale domain.

Both continuous and cross wavelet analysis were implemented using the software package developed for MATLAB and provided on-line by Grinsted et al. (2004) (http://www.pol.ac.uk/home/research/waveletcoherence/). Wavelet and cross wavelet analysis were basically of interest to examine the temporal cyclic variations occurring during day-time (8:00 AM to 8:00 PM) of the AET and meteorological time series. However, wavelet transformation can only be performed on complete (continuous) time series but not non-continuous time series such as day-time data. To obtain accurate wavelet analysis, which were also associated only with the day-time variations, wavelet and cross wavelet analysis were performed using the complete time series data (day-time and night-time data). Then, the wavelet coefficients (spectrum

segments), which were associated with night-time data were cut out to give the spectrum of the day-time only time series data. Wavelet spectra provided in the next chapter are all associated with the day-time only time series.

CHAPTER 4. RESULTS AND DISCUSSION

The results of data driven modeling and digital signal processing (wavelet analysis) of time series are provided in this chapter. The actual evapotranspiration (AET) models developed using neural networks (ANNs), genetic programming (GP), and multilinear regression (MLR) are presented, analyzed, and compared in the data driven modeling section. The utility of the data driven AET models is also compared with that of HYDRUS-1D model, which makes use of conventional Penman-Monteith (PM) model for the prediction of AET. Continuous wavelet analysis and cross wavelet analysis were carried out for the analysis of intermittent variations in the AET and the time series of the meteorological variables in order to explore common covariances existing between AET and each of the meteorological signals. The wavelet analysis (WA) was examined as a possible pre-modeling tool for determination of appropriate AET model inputs (predictors).

4.1 Data driven modeling

4.1.1 Overview

Using three data driven techniques: ANNs, GP, and traditional statistical regression, different AET estimation models were developed. The models were analyzed and compared in terms of prediction accuracy, generalization ability, complexity/simplicity of the modeling approach, and model usage. The comparison was conducted to identify the most efficient technique, out of the studied three data driven techniques, for the prediction of the AET process. The results of the data driven models were compared with those of the HYDRUS-1D model in order to identify the possible advantages of the proposed models over one of the available methods for the estimation of actual evapotranspiration.

4.1.2 Data driven modeling data

The three different data subsets, namely, training, testing, and cross-validation, which were employed for the modeling purposes, were selected from a randomly generated population of 100 groups of data subsets. The selection procedure was conducted based on the statistical characteristics, e.g. mean and standard deviation, of the AET data. The group of data subsets with relatively similar statistical properties was selected for the current modeling task. The statistical characteristics of the selected data subsets are tabulated in Table 4.1. The similarities among the statistical characteristics of the three subsets indicate that the instances used at different stages of the modeling process are representing the same population to be modeled.

Table 4.1. Statistical Characteristics of data subsets employed for data driven modeling.

Dataset	Minimum (mm/h)	Maximum (mm/h)	Mean (mm/h)	SD[1] (mm/h)	CV[2]	Skew	Length of dataset
Training	-0.06	0.67	0.24	0.13	0.55	0.27	604
Testing	0.01	0.62	0.24	0.13	0.55	0.37	402
Cross-validation	-0.01	0.60	0.24	0.13	0.54	0.35	201

[1] Standard deviation
[2] Coefficient of Variation

4.1.3 Artificial Neural Network (ANN) model

- *Development of optimum ANN model*

In order to adopt the most appropriate training algorithm and network geometry, the influence of number of hidden neurons on the performance measures of two training algorithms; Levenberg-Marquardt and Bayesian-regularization, was examined and the results are illustrated in Figure 4.1. It appears that Levenberg-Marquardt training algorithm is more sensitive to the number of hidden neurons; represented by larger fluctuations in the error measures with respect to the number of hidden neurons than the Bayesian-regularization algorithm. Figure 4.1a indicates that the Levenberg-Marquardt algorithm leads to lower values of correlation coefficient (R) for all numbers of hidden neurons compared to the Bayesian-regularization algorithm. Figs. 4.1b and 4.1c show that Levenberg-Marquardt algorithm results in higher values of RMSE and MARE than

Bayesian-regularization for all numbers of hidden neurons. This finding indicates that the Bayesian-regularization training algorithm performs more efficiently than the Levenberg-Marquardt algorithm on the subset under consideration. This might be attributed to some hindrance caused by the use of redundant network parameters (weights and biases) in the output estimation of the network trained by Levenberg-Marquardt algorithm, while the networks trained by Bayesian-regularization training algorithm use only the effective network parameters for computing the output (Izadifar and Elshorbagy. 2010). Among the 28 assessed ANN models, the ANN model with eight hidden neurons trained by Bayesian-regularization algorithm resulted in relatively better statistical measures; R of 0.89, RMSE of 0.06 mm/h, and MARE of 0.28 when evaluated using the cross-validation subset. Therefore, eight hidden neurons were adopted for the ANN model for the rest of the modeling process.

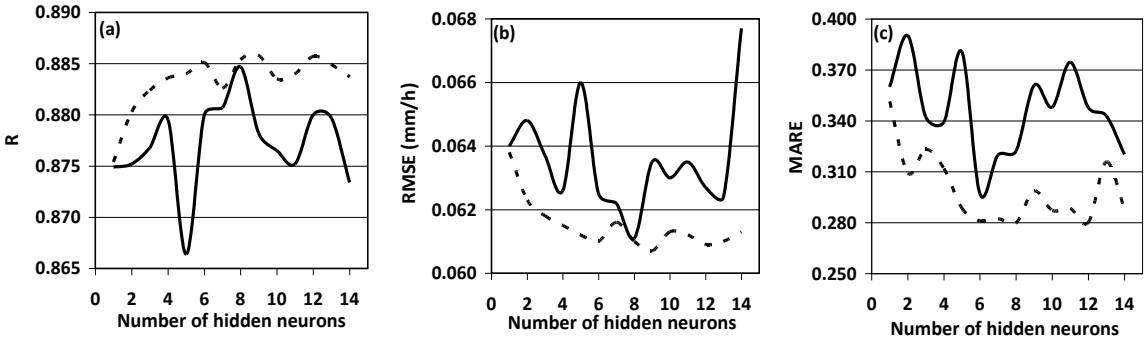

Figure 4.1. The influence of number of hidden neurons on the network performance for two training algorithms using the cross-validation subset: −, Levenberg-Marquardt; ---, Bayesian-regularization.

- *Testing the developed ANN model*

The predictive ability of the developed ANN model on completely unseen subset was examined using the testing subset. The ANN model with eight hidden neurons was applied to the testing subset, and the error measures were computed. Table 4.2 presents the performance statistics of the ANN model on the testing subset as well as the training and the cross-validation subsets. Low values of RMSE and MARE, and high values of correlation coefficient on the testing subset indicate the good generalization ability of the developed ANN model in the estimation of hourly AET values.

Table 4.2. Performance statistics of ANN model with 8 hidden neurons for three subsets.

Statistics	Training	Cross validation	Testing
RMSE	0.06	0.06	0.07
MARE	0.40	0.28	0.31
R	0.89	0.89	0.86

The statistical performance measures (Table 4.2) basically examine the prediction accuracy of the developed ANN model from an overall point of view using the mean of errors and the general correlation between observed and predicted AET values. In order to evaluate the performance of the ANN model more precisely, the observed and the predicted values of AET were visually compared for a typical data range of 100 data points from the testing subset (Figure 4.2). The visual comparison of predicted and observed AET values indicates that the ANN model was able to properly capture the variation of AET. However, some of the large AET values have been underestimated by the ANN model showing its relative weakness in the estimation of AET values with larger magnitude. However, considering the complexity of the hourly AET values, the ANN model performs well with regard to matching the pattern and the trend of the observed values.

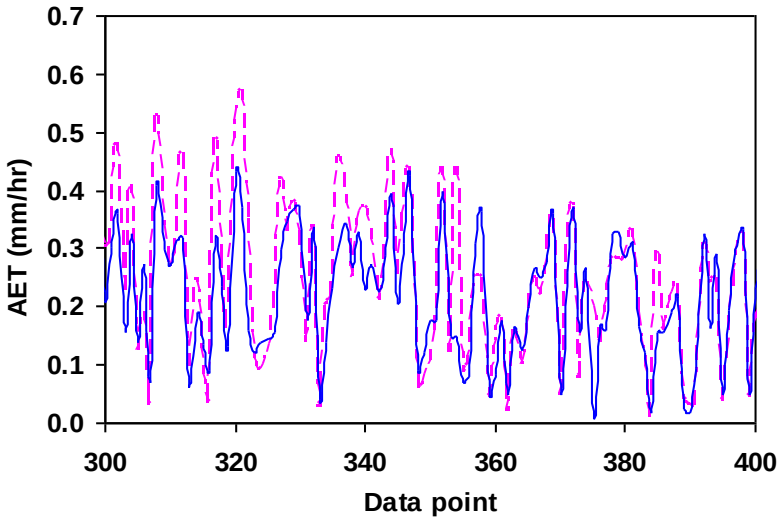

Figure 4.2. Visual comparison between the ANN predicted and the observed testing data of AET: --, observed values; —, predicted values.

- *Important (significant) input variables for AET modeling*

For the five available meteorological variables, R_n, T_g, T_a, RH, and W_s, 26 different input combinations could be assessed, which were already described in the previous chapter. In order to examine the importance of each input combination, the associated optimum ANN model, with optimized architecture and training algorithm, was developed using the training and the cross-validation subsets, and the network performance was evaluated using the testing subset. The primary results indicated that net radiation (R_n) is a crucial factor in the estimation of AET; its exclusion from the input set causes serious deterioration of the performance of the ANN models. For instance, ANN model with the predictors set of T_g, T_a, RH, and W_s (excluding R_n) resulted in the performance measures of 0.11 mm/h, 0.69, and 0.54 for the RMSE, MARE, and R, respectively, when applied to the testing subset (Table 4.3). The significant role of net radiation, as the main source of energy, in the AET mechanism is expected based on the physics of the AET process. As a result, the rest of the analysis was performed only for the input subsets, which include R_n as one of the predictors. Consequently, the total number of investigated input combinations decreased from 26 to 16. Table 4.3 shows the performance statistics of ANN models trained using 16 different combinations of inputs.

The best performance of ANNs was obtained when all five meteorological variables were used for the modeling of AET; however, ANN models, which employed the predictor combinations of "R_n, T_g, RH, W_s"; "R_n, T_g, T_a, RH"; "R_n T_g, T_a, W_s"; "R_n, T_a, RH, W_s"; "R_n, T_g, RH"; and "R_n, T_g, W_s", also resulted in comparable performances. Among the input combinations of two factors only, the ANN model with predictor set of R_n and T_g performed fairly well, which shows the possibility of using fewer number of predictors for estimating AET in an efficient and parsimonious way.

Obtaining acceptable prediction accuracies from different combinations of inputs demonstrates the difficulty of determining the significant input variables for modeling the AET process. Thus, the trial-and-error procedure using the ANN technique might not be the best approach for identifying the important AET predictors. This difficulty can also be associated with the complexity of the AET process itself. The interaction among

multiple processes and variables involving the AET makes it possible, for ANN model, to sufficiently capture the variations of AET by using different combinations of variables. It is understood from the results that determination of a unique set of meteorological variables might not be necessary for the estimation of AET. Instead, the effort can be concentrated on the determination of the most efficient and parsimonious set of predictor variables.

Table 4.3. Performance statistics of ANN models with different combinations of inputs.

Input combination	Training			Cross-validation			Testing		
	RMSE*	MARE	R	RMSE	MARE	R	RMSE	MARE	R
R_n,T_g,T_a,RH,W_s	0.06	0.40	0.89	0.06	0.28	0.89	0.07	0.31	0.86
R_n,T_g,RH,W_s	0.06	0.43	0.88	0.06	0.28	0.88	0.07	0.33	0.86
R_n,T_g,T_a,RH	0.06	0.43	0.88	0.06	0.31	0.88	0.07	0.32	0.86
R_n T_g,T_a,W_s	0.07	0.44	0.87	0.07	0.29	0.87	0.07	0.33	0.85
R_n,T_a,RH,W_s	0.07	0.49	0.85	0.07	0.30	0.87	0.07	0.36	0.83
T_g,T_a,RH,W_s	0.12	0.87	0.61	0.10	0.71	0.62	0.11	0.69	0.54
R_n, T_g,RH	0.06	0.44	0.88	0.06	0.30	0.88	0.07	0.34	0.86
R_n,T_g,W_s	0.07	0.42	0.87	0.07	0.29	0.86	0.07	0.32	0.85
R_n,T_g,T_a	0.07	0.48	0.85	0.07	0.31	0.87	0.07	0.35	0.84
R_n,RH,W_s	0.07	0.47	0.85	0.07	0.29	0.86	0.07	0.37	0.83
R_n,T_a,RH	0.07	0.54	0.84	0.07	0.35	0.86	0.07	0.40	0.83
R_n,T_a,W_s	0.07	0.54	0.83	0.07	0.32	0.86	0.07	0.37	0.83
R_n,T_g	0.07	0.57	0.85	0.06	0.34	0.87	0.07	0.42	0.84
R_n,RH	0.07	0.53	0.82	0.07	0.36	0.87	0.07	0.49	0.82
R_n,W_s	0.08	0.53	0.79	0.08	0.35	0.82	0.09	0.45	0.77
R_n,T_a	0.08	0.51	0.83	0.07	0.34	0.85	0.08	0.43	0.82

*RMSE in mm/h

4.1.4 Genetic Programming (GP) model

Using GPLAB (Silva, 2005) several equation-based GP models were generated at 42 different levels of GP parameters including crossover probability, mutation probability, number of generations, and population size. Table 4.4 presents the values of RMSE, MARE, and R along with the associated GP parameters obtained with the best eight models generated by GP. The optimum GP models that resulted in the best statistics associated with the cross-validation subset are given below (Equations 4.1-4.8):

$$AET = -0.013 + 0.148 R_n + 0.01 T_g - 0.104 RH \quad [4.1]$$

$$AET = -0.018 + 5.54 \times 10^{-3} T_g + 9.49 \times 10^{-3} R_n T_g \quad [4.2]$$

$$AET = 0.0784 + 9.2 \times 10^{-3} R_n T_g - 3.5 \times 10^{-3} R_n{}^2 T_g + 2.7 \times 10^{-4} R_n T_g T_a - 8.64 \times 10^{-7} T_a{}^2 \quad [4.3]$$

$$AET = 0.039 + 0.063 R_n + 1.88 \times 10^{-3} T_g + 7.37 \times 10^{-3} R_n T_g \quad [4.4]$$

$$AET = 0.0696 + 7.836 \times 10^{-3} R_n T_g + 2.569 \times 10^{-3} T_g \quad [4.5]$$

$$AET = 0.0633 + 3.1 \times 10^{-3} T_g + 0.011 \times R_n + 6.85 \times 10^{-3} T_g R_n \quad [4.6]$$

$$AET = 0.0775 + 2.23 \times 10^{-3} T_a + 6.35 \times 10^{-3} R_n T_a \quad [4.7]$$

$$AET = 0.129 R_n + 0.005 T_a \quad [4.8]$$

where, AET, R_n , T_g , T_a, and RH are the rate of actual evapotranspiration [mm h^{-1}], net radiation [MJ], ground temperature [^{o}C], air temperature [^{o}C], and relative humidity [fraction], respectively.

Table 4.4. The best generated GP-based models using various GP parameters for the cross-validation subset.

Model	Crossover prob.	Mutation prob.	No. of generation	Population size	RMSE (mm/h)	MARE	R
Eq. 4.1	0.6	0.2	50	60	0.06	0.37	0.88
Eq. 4.2	0.5	0.2	60	70	0.07	0.34	0.86
Eq. 4.3	0.6	0.3	60	60	0.07	0.37	0.86
Eq. 4.4	0.7	0.5	50	300	0.07	0.35	0.85
Eq. 4.5	0.5	0.2	200	100	0.07	0.43	0.86
Eq. 4.6	0.7	0.4	200	50	0.07	0.44	0.86
Eq. 4.7	0.8	0.3	100	40	0.07	0.46	0.85
Eq. 4.8	0.6	0.3	50	80	0.08	0.40	0.85

The optimum GP-evolved models are structurally simple, characterizing the variation of AET as semi-linear functions of meteorological variables, since the models are linear in parameters. Most (six out of eight) of the presented GP models contain R_n and T_g as AET predictors. The appearance of *RH* (one out of eight times) and T_a (three out of 8 times) was limited in the developed models. Interestingly, W_s never came up as an important predictor in the presented optimum AET models, which means that GP did not find wind speed to be an effective component in the estimation of hourly AET. The simplicity of the models seems to be interesting, especially when the error measures also indicate relatively good generalization ability of the models based on the testing subset (Table 4.5). It is perceived from the GP models that the AET mechanism can be characterized by structurally simple models, which are also not physically complex. This can be considered as a strong advantage of the GP technique that searches for any possible combination of predictors that can properly model the AET process. Thus, GP might generate some AET models with structures that might not be readily explainable in light of the intuitive understanding of the AET physics.

Table 4.5. Performance statistics of the GP-based models using testing subset.

Model	RMSE(mm/h)	MARE	R
Eq. 4.1	0.07	0.35	0.85
Eq. 4.2	0.08	0.32	0.83
Eq. 4.3	0.07	0.32	0.82
Eq. 4.4	0.08	0.32	0.82
Eq. 4.5	0.07	0.39	0.83
Eq. 4.6	0.07	0.40	0.83
Eq. 4.7	0.07	0.41	0.81
Eq. 4.8	0.09	0.36	0.79

Based on the equation-based GP models, the contribution of each meteorological variable in the estimation of AET can also be discussed. This is only possible by using the normalized form of the equations in which all input variables receive their values from a consistent range (e.g. less than 1). Then the contribution of each input variable or factor to the AET can be assessed based on the associated coefficient's magnitude. A selective set of models, which includes only GP models with different physical structures, was identified and the input variables were normalized for further analysis.

The selected models, Eq. (4.1), (4.2), (4.3), (4.4), and (4.7), are rewritten, in order, as follow:

$$AET = -0.013 + 0.385\,R_n' + 0.285\,T_g' - 0.095\,RH' \quad [4.9]$$

$$AET = -0.018 + 0.15\,T_g' + 0.53\,R_n' T_g' \quad [4.10]$$

$$AET = 0.0784 + 0.514\,R_n' T_g' - 0.49\,R_n'^2 T_g' + 0.424\,R_n' T_g' T_a' - 0.976 \times 10^{-3}\,T_a'^2 \quad [4.11]$$

$$AET = 0.039 + 0.164\,R_n' + 0.051\,T_g' + 0.412\,R_n' T_g' \quad [4.12]$$

$$AET = 0.0775 + 0.075\,T_a' + 0.396\,R_n' T_a' \quad [4.13]$$

In these normalized equations, input variables, which are associated with the models' linear coefficients (e.g. T'_g, $T'_g R'_n T'_a$, and $R'^2_n T'_g$), are normalized inputs by dividing each of them by its corresponding maximum values and AET is the rate of actual evapotranspiration [mm h^{-1}]. These normalized models were only developed and used for interpreting the contribution of different inputs to the estimation of AET.

Equation (4.9) indicates that AET can be estimated as a simple linear function of R'_n, T'_g, and RH', which is highly dominated by the net radiation and ground temperature variables. Equation (4.10) also has a simple structure describing the AET process as a nonlinear function, of only net radiation and ground temperature, which is dominated by the two-factor interaction of R'_n and T'_g. The average contribution of each input term to the estimation of AET can be computed and compared to obtain better insight into the influence of different inputs on the AET. This was implemented by applying the models to the data and computing the partial magnitudes of the AET values that each input term contributes. Then, the associated averages were taken over the available instances. The interaction factor of $R'_n T'_g$ has larger contribution to the estimation of AET than the T'_g, individually, with the average contribution magnitude of 0.15 and 0.10 mm/h for the terms $0.53 R'_n T'_g$ and $0.15 T'_g$, respectively. This indicates that when some factors are interacting, their interactions influence the individual contribution of each variable to the

AET mechanism. Consequently, the interaction term (factor) is more responsible for AET variations than the individual variables. In Eq. (4.11), the air temperature (T'_a) variable has been included in addition to the R'_n and T'_g. The air temperature has appeared both as an individual variable and as an interacting factor in the three-factor interaction term of $R'_nT'_gT'_a$. According to the coefficients associated with these variables in Eq. (4.11), T'_a can affect the rate of AET only through the influence it might have on the R'_n and T'_g (interacting coefficient of 0.424 compared to that of air temperature, 0.000976). The structure of Eq. (4.12) also confirms the importance of interaction effects of multiple variables rather than the individual processes. The combined component of $R'_nT'_g$ is more responsible for the variation of AET than the R'_n and T'_g individually. The average contribution magnitude of each of the terms $0.412R'_nT'_g$, $0.164R'_n$, and $0.051T'_g$ in the estimation of AET values are 0.12, 0.05, and 0.03 mm/h, respectively. Equation (4.13) demonstrates that the AET mechanism can even be characterized as a simple semi-linear function of R'_n and T'_a only, which are commonly available meteorological measurements. Again, the AET model is dominated by the interaction factor of the two variables. The interaction and individual terms of $0.396R'_nT'_a$ and $0.075T'_a$ are contributing to the estimation of AET by the average magnitude of 0.11 and 0.05 mm/h, respectively.

Although the generated models, based on error measures, are performing well and relatively similar, they are using different combinations of inputs with different mathematical structures. This demonstrates that precise identification of the meteorological variables driving the AET process is not an easy and straightforward task, where different combinations of inputs may result in relatively good AET estimation (Izadifar and Elshorbagy, 2010). The results obtained from the GP-evolved models indicate that the hourly AET process can be estimated by both linear and nonlinear relationships. The prediction accuracy of the AET models, using the GP technique, could vary within a possible range of 0.07 to 0.09 (mm/h), 0.32 to 0.41, and 0.79 to 0.85 for RMSE, MARE and R, respectively. Using the above-listed GP models, one may choose one of them for estimating the rate of AET based on the meteorological data that are available. Thus, the proposed GP models can suit different conditions of data availability.

The prediction accuracy of the GP-evolved models can also be investigated using the visual comparison between the observed and predicted AET. This was performed for the previously analyzed set of GP models, Eq. (4.1), (4.2), (4.3), (4.4), and (4.7), for a typical data range of 100 data points from the testing subset. Figure 4.3a to d shows that Eq. (4.1), (4.2), (4.3), and (4.4) are performing well in capturing the variation and the trend of the AET; however, they are slightly missing larger magnitude values of AET. Figure 4.3e, shows that the GP model, which estimates the AET only as a function of R_n and T_a (Eq.4.7), has the ability to predict the variation of AET but is performing slightly poorer with regard to the estimation of extreme AET values, compared to other investigated GP models (Equations 4.1-4.4).

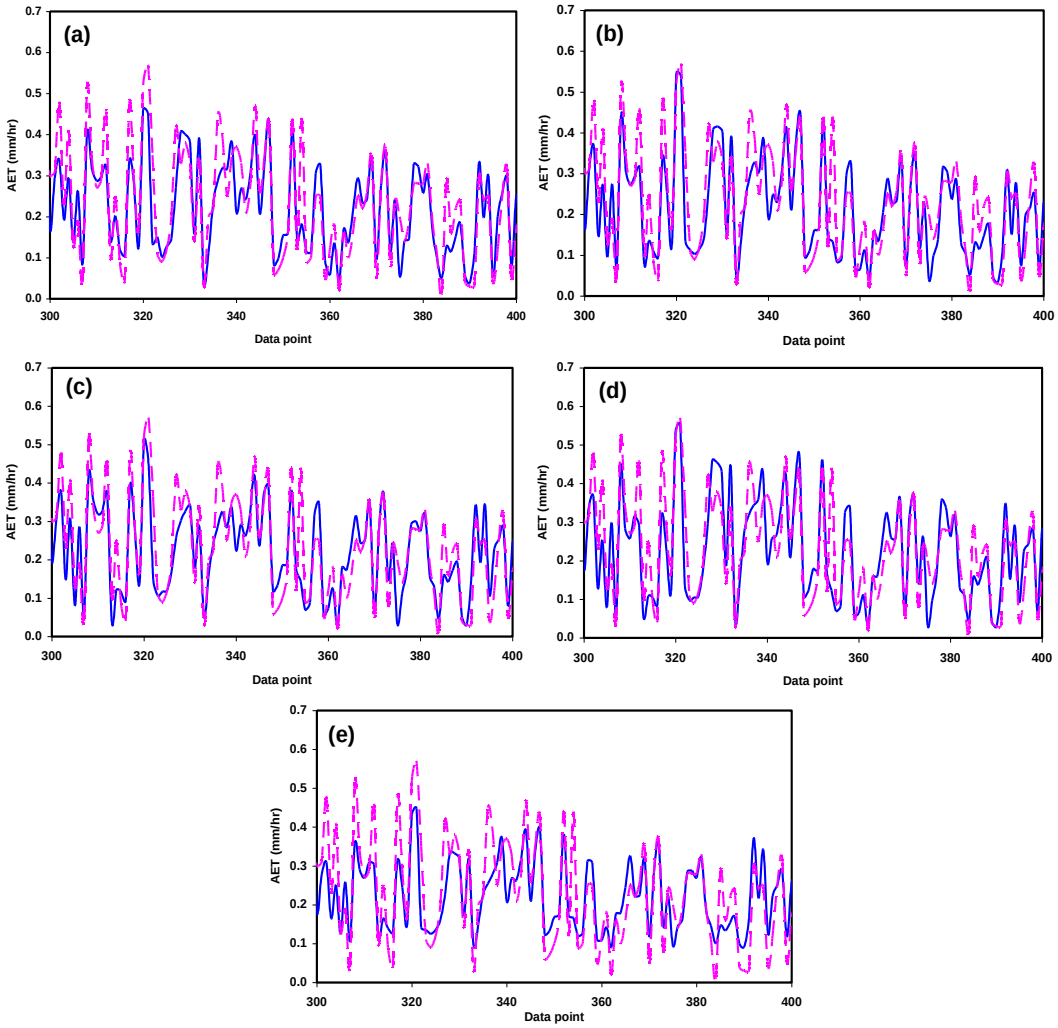

Figure 4.3. Visual comparison between the observed and the GP predicted AET values of testing data using (a) Eq. (4.1), (b) Eq. (4.2), (c) Eq. (4.3), (d) Eq. (4.4), and (e) Eq. (4.7): --, observed values; —, predicted values.

4.1.5 Statistical MultiLinear Regression (MLR) model

Equations (4.14) and (4.15) present the two multilinear regression (MLR) models resulting from the statistical analysis performed using SAS/STAT® software.

$$AET = -0.091 + 0.16R_n + 0.023T_g - 0.19RH - 0.012R_nW_s - 0.0004T_aT_g + 0.001T_aW_s \quad [4.14]$$

$$AET = -0.4086 + 0.1548R_n + 0.0546T_g - 0.0426R_n^2 - 0.0012T_g^2 - 0.0016W_s^2 + 0.0038R_nT_g - 0.0069R_nW_s + 0.0013T_gW_s - 0.010T_aRH \quad [4.15]$$

The summary of the statistical analysis conducted for determining the factors that have significant effects on AET is given in Table 4.6. In model 1 (Eq. 4.14), R_n, T_g, RH, and the two-factor interactions of T_aT_g, T_aW_s and R_nW_s were identified as the significant factors for the AET process at 95% confidence level. When the quadratic forms of input variables were also considered, in model 2 (Eq. 4.15), RH was no longer included in the equation; however, R_n and T_g were still identified as significant variables. The second orders of net radiation, R_n^2, ground temperature, T_g^2, and wind speed, W_s^2, also became significant as p-values are less than the significance level of 0.05. The effects of two-factor interactions also changed as the quadratic forms of input variables were included in the analysis. In model 2 (Table 4.6), the two-factor interactions of R_nT_g, R_nW_s, T_gW_s, and T_aRH demonstrate significant effect on AET. By the significant interaction effect, of R_nW_s for instance, it means that the wind speed contributes to the AET process but its contribution depends on the value of net radiation.

Model 1, Eq. (4.14), resulted in the Pearson's coefficient (R) of 0.87, RMSE of 0.06 mm/h and MARE of 0.34 based on the cross-validation subset. However, R improved up to 0.88, and MARE reduced to 0.32 when the second orders of variables were also taken into account (model 2, Eq. 4.15), as given in Table 4.7. Model 1 logically indicates that net radiation and ground temperature are positively correlated to AET and relative humidity is negatively correlated to the AET. The structure of model 2 (Eq. 4.15) demonstrates that the quadratic forms of R_n, T_g and W_s are negatively contributing to the AET process. Inverse influence of second order net radiation (R_n^2),

ground temperature (T_g^2), and wind speed (W_s^2) might not refer to any physical process and might be just included for numerical adjustments of model and for achieving better fitness. The effect of each interaction term on AET can be described based on the values taken by each component of the two-factor interaction term.

Table 4.6. Variables with significant effect on actual evapotranspiration.

Variable	*p-value<0.05*
Model 1:	
R_n	<0.0001
T_g	<0.0001
RH	<0.0001
R_nW_s	<0.0001
T_aT_g	<0.0001
T_aW_s	<0.0001
Model 2:	
R_n	<0.0001
T_g	<0.0001
R_n^2	<0.0001
T_g^2	<0.0001
W_s^2	0.0054
R_nT_g	0.0120
R_nW_s	0.0094
T_gW_s	<0.0001
T_aRH	<0.0001

Individual variables and two-factor interactions not given in this table were identified to be insignificant.

Table 4.7. Performance statistics of the MLR models for cross-validation subset.

Statistics	RMSE(mm/h)	MARE	R
Model 1	0.06	0.34	0.87
Model 2	0.06	0.32	0.88

Both statistical models can also be presented in a normalized form in which each contributing input variable (either linear, interaction, or quadratic) receives a value less than 1. This was implemented following the same approach used in the normalization of the equation-based GP models. The normalized models can be used for the identification

of variables having more contribution, to the estimation of AET, than others. The normalized form of the regression models (Eq. 4.14 and Eq. 4.15) are given, in order, as:

$$AET = -0.091 + 0.418R'_n + 0.623T'_g - 0.173RH' - 0.161R'_nW'_s - 0.35T'_aT'_g + 0.242T'_aW'_s \quad [4.16]$$

$$AET = -0.409 + 0.404R'_n + 1.48T'_g - 0.289R'^2_n - 0.881T'^2_g - 0.123W'^2_s + 0.212R'_nT'_g - 0.093R'_nW'_s + 0.263T'_gW'_s - 0.159T'_aRH' \quad [4.17]$$

In Eq. (4.16) the coefficient associated with the ground temperature is larger than the coefficients associated with other variables indicating that ground temperature has more contribution to the estimation of AET values than other variables. The magnitude of the average contribution of $0.623T'_g$ is equal to 0.42 mm/h, which is high compared to those of $0.418R'_n$ (0.13 mm/h), $0.35T'_aT'_g$ (0.16 mm/h), and $0.173RH'$ (0.10 mm/h). The T'_g variable was also given large coefficients in both forms of linear and quadratic in Eq. (4.17). Quantitative analysis of the variables' contribution to the estimation of AET indicated that, in model 2, the input terms of $1.48T'_g$ and $0.881T'^2_g$ have, in order, the average contribution of 1 and 0.42 mm/hr, which is high in comparison with that of $0.404R'_n$, 0.13 mm/h.

As a baseline comparison, a simple first order MLR model was also investigated for the estimation of hourly AET variations. For fitting the standard first order MLR, only the first orders of meteorological variables were statistically analyzed and the fitted model was obtained as:

$$AET = 0.018 + 0.133R_n + 0.015T_g - 0.0043T_a - 0.179RH + 0.0097W_s \quad [4.18]$$

where dependent and independent variables are exactly the same as the previously presented MLR models. The above linear regression model resulted in the Pearson's coefficient (R) of 0.87, RMSE of 0.06 mm/h and MARE of 0.38 when applied to the cross-validation subset. First order MLR (Eq. 4.18) performed relatively worse than model 1 and 2 (Eq. 4.14 and 4.15) in terms of MARE (Table 4.7). The normalized form of the given MLR model is:

$$AET = 0.018 + 0.347\,R_n' + 0.394\,T_g' - 0.145\,T_a' - 0.163\,RH' + 0.085\,W_s' \qquad [4.19]$$

The average contribution of the variable terms, in order of their presence in the model, are 0.11, 0.28, 0.09, 0.09, and 0.02 mm/h. Ground temperature and net radiation were given larger coefficient values than other variables indicating that they have more contribution to the AET values. This was also confirmed by the average contribution values. For the rest of the analysis, only the earlier proposed MLR models of 1 and 2 (Eq. 4.14 and 4.15) were considered.

Figure 4.4 illustrates the scatter plots of the predicted values by the MLR models versus the observed data. A slight improvement can be observed when model 2 is used, which has also the quadratic form of factors. However, some statistical analysis is needed to identify if the difference between the two models is significant. Comparing the general statistical characteristics of residuals resulted from model 1 and model 2 shows that the two proposed regression models are not performing substantially different. The mean and variance of residuals from model 1 are –0.002 and 0.005, respectively, which are very close to those of model 2; -0.001 and 0.004. The difference between the mean and the variance of the errors from the two models is only 0.001. The probability distribution, which was fitted to the errors of model 1, is the same as that of model 2, and it is LogLogistic distribution with relatively similar shape and scale parameters (Fig. 4.5).

In order to select one MLR model out of the two developed ones, the akaike information criterion (AIC) was computed for both models. The AIC values for model 1 and 2 are equal to -1597.7 and -1648.9, respectively, showing that model 2 is better than model 1. As a result, model 2 is considered as the MLR equation for the prediction of AET as a function of meteorological variables. Figure 4.6 illustrates the visual comparison between the observed and the predicted values of AET estimated by MLR models 1 and 2 for a typical data range of 100 data points from the testing subset.

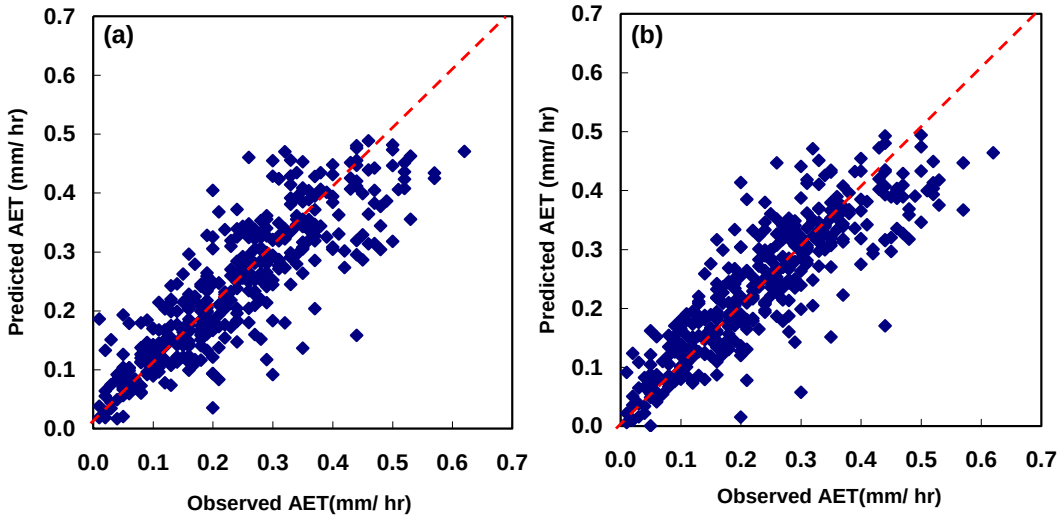

Figure 4.4. Scatter plots of predicted values resulted from (a) MLR model 1 and (b) MLR model 2 versus measured data using testing subset.

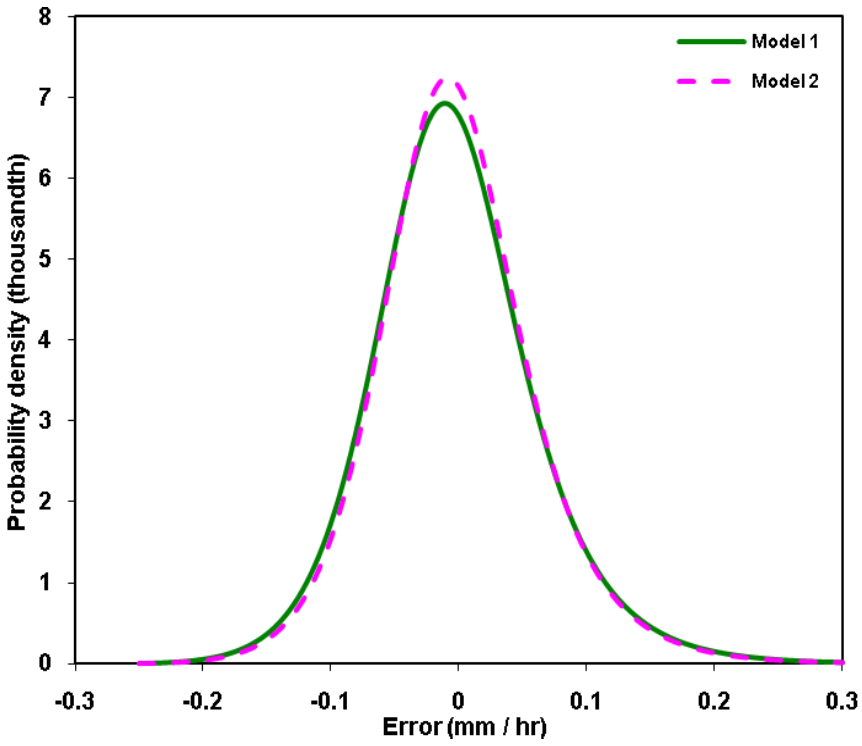

Figure 4.5. Probability distribution of the MLR models errors.

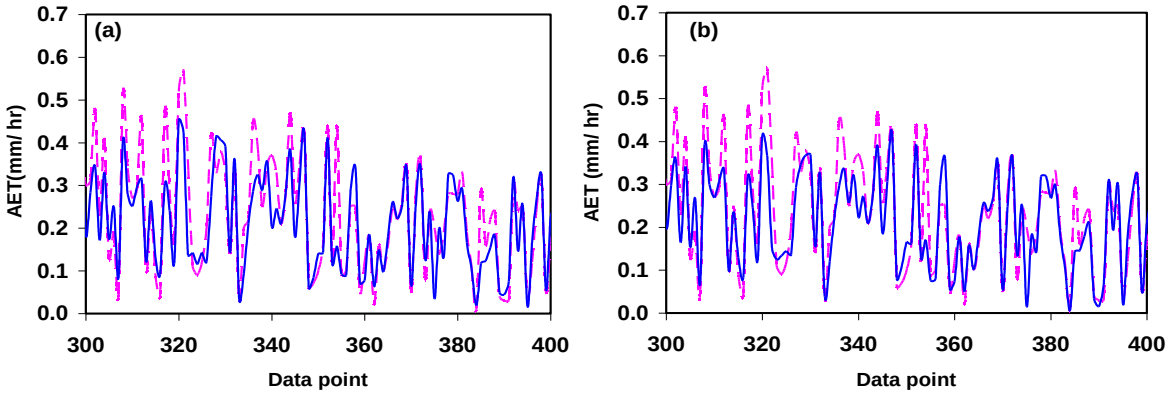

Figure 4.6. Visual comparison between the predicted values by (a) model 1 and (b) model 2 and the observed testing data of AET: --, observed values; —, predicted values.

4.2 Comparison among AET estimation models

4.2.1 Conventional model comparison approach

The performances of the models from the three proposed techniques; ANNs, GP, and the MLR, were compared based on the testing subset. It can be seen (Table 4.8) that ANN and regression models demonstrate relatively close performances based on the RMSE and R statistics; however, the MARE of the regression model is slightly better than that of the ANN model. The equation evolved by GP resulted in slightly larger MARE value compared to those of ANN and the MLR models. Despite discrepancies among the statistics, the differences are small, which implies that the models have comparable performances for estimating AET based on the meteorological variables. Test of hypothesis was performed using SAS/STAT® software to compare the general statistical characteristics of the residuals of the various models (Table 4.9). P-values associated with each pair of models are given in Table 4.10. Large P-values imply that there is no significant difference between the means and variances of the errors at 95% confidence level. Consequently, no substantial difference can be perceived among the predictive abilities of the proposed models. Furthermore, the errors produced by all three models follow the same probability distribution of LogLogistic (Figure 4.7).

Table 4.8. Performance statistics of different models using testing subset.

Model	RMSE(mm/h)	MARE	R
ANN	0.07	0.31	0.86
GP (Eq. 4.1)	0.07	0.35	0.85
MLR	0.07	0.29	0.86

Table 4.9. General statistical characteristics of errors obtained from different models.

Model	Mean	Variance
ANN	-0.003	0.004
GP (Eq. 4.1)	-0.002	0.005
MLR	-0.001	0.004

Table 4.10. A comparison among the statistical characteristics of errors obtained from different models at 0.05 significant level.

	Means of errors	Variances of errors
Groups	P-value	P-value
ANN & GP	0.75	0.60
MLR & GP	0.84	0.47
MLR & ANN	0.60	0.84

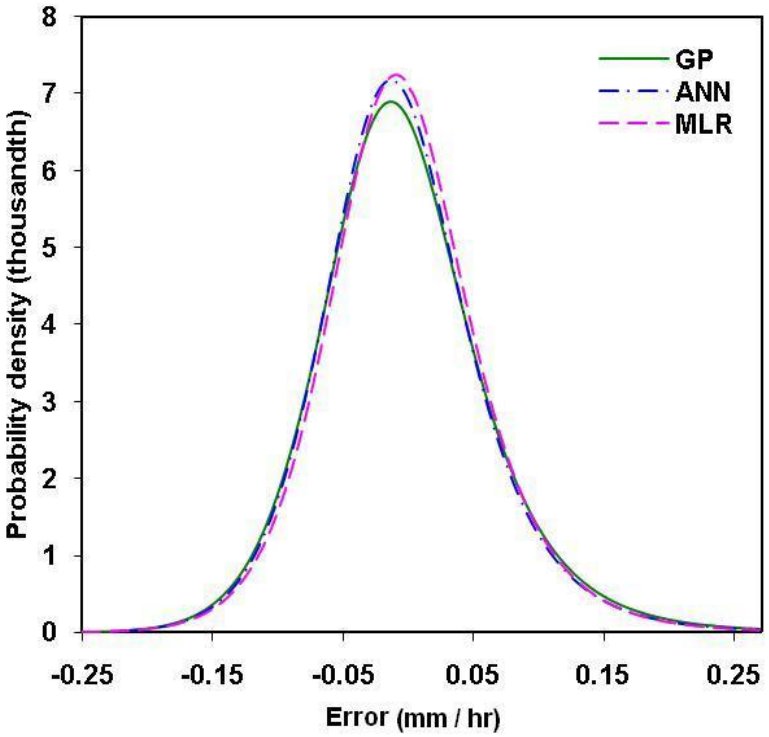

Figure 4.7. Probability distribution of the data driven models errors.

Figure 4.8 illustrates the scatter plots of the predicted AET values by ANNs, GP, and the MLR model (model 2), respectively, versus observed data, using the testing subset. Based on the visual comparison, no substantial difference can be observed among the predictive abilities of the proposed models, except that the variability in the scatter plot of the MLR model (Fig. 4.8c) is slightly less than those of ANN and GP models.

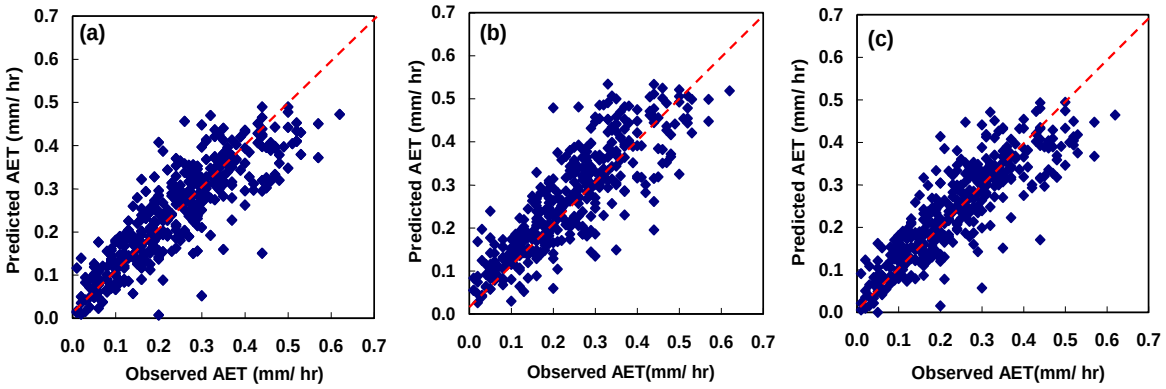

Figure 4.8. Scatter plots of predicted actual evapotranspiration (AET) versus observed AET by (a) ANN, (b) GP (Eq. 4.1), and (c) MLR model using testing subset.

4.2.2 Rigorous model evaluation approach

In order to evaluate the generalization ability of the developed models in a more realistic and rigorous way, all of the optimum models obtained from the ANNs, GP, and the regression techniques, using the 2006 data, were employed for the prediction of actual evapotranspiration of a different year (2005). This assessment was also conducted to identify the possible superiority of any of the proposed models for future prediction applications. The 2005 dataset, which was used for implementing the rigorous generalization test, has different statistical properties from the year 2006 dataset, which was employed for training and testing during model development (Table 4.11). Applying the developed models to a statistically different dataset helps to evaluate and compare the models' predictive abilities on instances from a statistically different population. The hourly meteorological variables of R_n, T_g, T_a, W_s, and RH of the year 2005 were used as the inputs of the optimum models, including ANN, GP (Eq. 4.1 and Eq. 4.2) and the MLR model 2 (Eq. 4.15) to estimate the AET.

In addition to the developed data driven models, the rate of AET in the 2005 was estimated using the physically-based HYDRUS-1D model. The meteorological variables, including R_n, T_a, W_s, *RH*, precipitation, vegetation factor, *LAI*, and physical/hydraulic parameters of soil were used as inputs for estimation of AET by means of HYDRUS-1D software package. The performance of the HYDRUS model was compared with those of the developed data driven models.

Table 4.11. Statistical characteristics of AET data of the years 2005 and 2006.

Year	Minimum (mm/h)	Maximum (mm/h)	Average (mm/h)	Median (mm/h)	SD* (mm/h)	Coefficient of variation
2005	-0.05	0.68	0.18	0.16	0.12	0.65
2006	-0.06	0.67	0.24	0.23	0.13	0.55

*Standard deviation

- *Comparative generalization abilities*

A comparison among the performance statistics of the data driven models, used for the prediction of AET in 2005, is given in Table 4.12. It is apparent that GP and regression models are performing better than the ANN model with lower error measure values and higher correlation coefficients. However, in terms of MARE, the GP model performed better than the regression model. GP and the regression techniques were able to capture the semi-linearity of the AET process and to characterize it by simple equations. However, the ANN model, because of its structure, tried to fit a complex non-linear model to the AET process, which was unnecessary and resulted in its poor performance in generalization. Based on the RMSE and correlation coefficient (R) metrics, GP and regression models have comparable generalization abilities.

Table 4.12. Performance statistics of different models using 2005 data.

Model	RMSE(mm/h)	MARE	R
ANN	0.10	0.91	0.78
GP			
- Equation (4.1)	0.07	0.55	0.82
- Equation (4.2)	0.06	0.47	0.85
MLR			
- Model 2	0.07	0.57	0.85
HYDRUS-1D	0.08	0.48	0.79

For better interpretation of models' performances, further analysis was conducted. Scatter plots of the predicted AET values by data driven models versus observed values, using the 2005 dataset, are illustrated in Fig. 4.9. It can be seen in Fig.4.9a that the ANN model is overestimating most of the AET values in 2005, which was expected from the large value of MARE. Figure 4.9b and c indicate that the GP and MLR (model 2) models are performing well and relatively similar on the estimation of AET in 2005. This demonstrates the superiority of GP and regression models over the ANN with regard to the generalization ability. The performances of the proposed data driven models can also be compared with regard to large AET values for the cases when high AET values are of interest to be predicted. A comparison was conducted among the performance statistics of the ANN, GP, and MLR models on the AET values, which are above a specified threshold value of 0.30 mm/hr (84^{th} percentile threshold, which is mean plus standard deviation of normally distributed dataset). The results are presented in Table 4.13 and indicate that the models have relatively similar performances on the estimation of large AET values although, in terms of overall prediction ability, GP and MLR models performed better than the ANN.

Table 4.13. Performance statistics of different models on the AET values above the 84^{th} percentile threshold using 2005 data.

Model	RMSE(mm/h)	MARE	R
ANN	0.08	0.15	0.80
GP (Eq. 4.2)	0.10	0.20	0.83
MLR	0.08	0.15	0.82

The two different types of comparison discussed above highlight the importance and also the reliability of the approach one may use for comparison purposes in the modeling process. In the first approach, the unseen testing subset, which was coming from the same year (statistical population) that was used for developing (training) the models, was employed for testing the generalization ability of the models. Based on this comparison, no considerable difference was observed among the three proposed data driven models in terms of models' generalization ability. However, using the second approach; testing the developed models using data from a different year, led to a more realistic assessment of the predictive accuracy, which revealed the discrepancies among

the data driven models much better. Consequently, the choice of the testing dataset on which the generalization ability of the models is evaluated is important, and in the case of inappropriate and/or insufficient testing data, incorrect conclusions might be made.

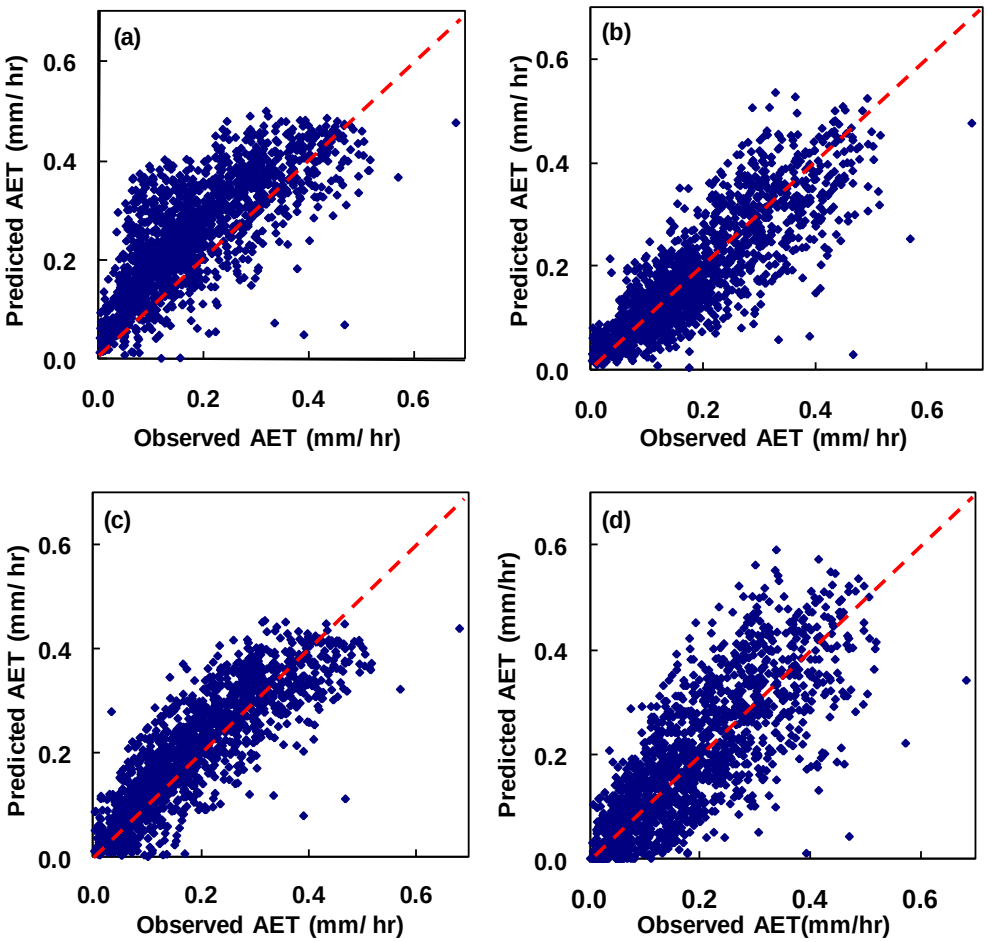

Figure 4.9. Scatter plots of predicted actual evapotranspiration (AET) versus observed AET by (a) ANN, (b) GP (Eq. 4.2), (c) MLR, and (d) HYDRUS model using 2005 data.

Another point of interest, which was observed in this analysis, is the issue of representation of a set of optimum GP equations instead of representing only the best GP equation. Out of the best GP-evolved models, Eq. (4.1), as an example, performed better than Eq. (4.2) when they were applied to the testing dataset of 2006. However, Eq. (4.2) had better performance than that of Eq. (4.1) when 2005 data were tested. This indicates that no single GP equation can be adopted as the best GP model, and thus, representation

of a set of GP equations as the optimum GP models is necessary (Parasuraman and Elshorbagy, 2008).

- *Comparison with the HYDRUS-1D model*

The HYDRUS-1D model uses the PM method along with the information about vegetation and soil moisture condition for estimating the rate of AET. The results indicated that the HYDRUS model is performing similar to the GP and better than the regression model on 2005 dataset in terms of MARE (Table 4.12). Based on the performance statistics of RMSE and correlation coefficient (R), HYDRUS model is performing better than ANN but not as good as GP and regression models. The scatter plot of HYDRUS-predicted AET values, Fig. 4.9d, shows that HYDRUS model is generally performing well in the prediction of AET in 2005, compared to the ANN. In comparison to the scatter plots of the GP and regression models (Fig. 4.9b and c), HYDRUS-predicted AET values are scattered more widely around the 1:1 line than those of GP and MLR, especially for large AET values.

The results of applying HYDRUS-1D model, along with the other proposed models, for the prediction of AET in 2006 (Table 4.14) indicated that the employed HYDRUS model might not necessarily perform better than or comparable to the ANN, GP, and MLR models at all times. Consequently, a physically-based model, such as HYDRUS-1D, which exploits the widely used PM method and considers soil moisture, might be inferior to the data driven models for the prediction of AET in terms of prediction accuracy. The currently used HYDRUS-1D model was not calibrated for the specific vegetation cover in the studied site, which might influence the performance of the model.

Table 4.14. Performance statistics of different models using 2006 data.

Model	RMSE(mm/h)	MARE	R
ANN	0.06	0.45	0.88
GP			
- Equation (4.1)	0.07	0.52	0.86
- Equation (4.2)	0.07	0.46	0.84
MLR			
- Model 2	0.06	0.41	0.88
HYDRUS-1D	0.13	0.61	0.71

- *General comparison of the proposed AET models*

The proposed AET estimation models can also be compared in terms of their complexity and efficiency. The AIC can be used as an index for assessing the complexity and the fitness of the models. The number and the data availability of the various inputs and the simplicity/complexity of the model usage can also be investigated for better comparison of the proposed models. Table 4.15 provides the AIC values associated with the proposed data driven models as well as their sum squared error (SSE) values. The AIC values were computed based on the training dataset because data driven models were trained and developed using this subset of data. Based on the AIC values, the ANN and MLR (model 2) models have better fitness to the data than the GP models although they are more complex based on the number of input variables and optimized parameters. This is mainly because of their smaller SSE values compared to those of GP models (Table 4.15). The GP model (Eq. 4.1) also has a comparable AIC value, which indicates its goodness of fit though it is simple in terms of the number of inputs and estimated parameters.

Table 4.15. Akiak information criterion and sum squared error of the data driven models and their required inputs.

Model	AIC	SSE*	No. of required input variables	No. of optimized parameters
ANN	-1640.31	2.16	5	24
GP				
- Equation (4.1)	-1516.44	2.83	3	4
- Equation (4.2)	-1391.04	3.50	2	3
MLR				
- Model 2	-1648.92	2.23	5	10

* Sum squared error

The ANN technique provides an implicit model from which no explicit information about the AET process can be easily obtained. As a result, ANN models might be used when prediction of AET is the only concern of the modeling process. In other words, accurate estimation of AET is more important than the understanding of AET mechanism itself. Furthermore, the significant input variables that are employed for AET estimation in the ANN model cannot be explicitly/easily identified, since the associated information is stored in the network connection weights and cannot be easily

interpreted. For the end user, application of ANN models is also not as easy as the equation-based models. The GP and MLR models are both equation-based models and are of interest for hydrologists and modellers because of their transparency and simplicity in application and usage. Explicit form of equation-based models, such as GP and MLR, makes it possible to extract some information about the physics of the process. The GP model has the advantage of using fewer input variables (Table 4.15) and also has simpler and more realistic structure than the regression model. Consequently, the GP model becomes more applicable when a limited number of meteorological variables is available or can be measured. From this point of view, GP is more efficient than the MLR for the prediction of AET. In addition, the simple structure of the GP models makes it easy for the users to understand how input variables are contributing to the AET process. This can also be achieved from the MLR equation; however, it is not as easy as the GP model because of the structural complexity of the MLR models.

The HYDRUS model that was employed for the estimation of AET required the rainfall and *LAI* information, in addition to the meteorological variables used in the data driven techniques. The information of *LAI* was measured in weekly basis and was disaggregated to the hourly basis for consistency with the time resolution of other variables. Disaggregation of data involves some uncertainty, which most probably has been propagated to the estimated AET values. Indirect estimation of AET using the HYDRUS model also introduces some uncertainty in the predictions. This is because the AET is calculated from its partitioned components (actual evaporation and transpiration), which are separately estimated using the standard PM model and simulated soil moisture profile where the latter is also a source of uncertainty in the model. These uncertainties, embedded in the estimated AET values, are considered as disadvantage in the modeling process. In addition, requirement of additional input variables, such as *LAI* and hourly rainfall, which are not readily available data for most case studies, is considered also a disadvantage of HYDRUS model compared to the proposed data driven models.

4.3 Wavelet analysis

4.3.1 Overview

Using the software package developed for MATLAB and provided on-line by Grinsted et al. (2004), continuous wavelet transform of the meteorological variables (predictors) and AET (predictand) time series was performed for identifying the dominant temporal cyclic events. In addition to continuous wavelet transform, the cross wavelet transform between each predictor variable and the AET signal was performed for identifying the possible covariances, which represent the influence of the predictor on the variations of AET. In general, the utility and applicability of WA were examined for identifying, prior to the modeling, the important variables that influence the hourly AET, and also to improve the understanding of the AET mechanism. In the following sections, the results and discussions will mainly focus on the small-scale variations (less than 16 hours), since these features are of interest in this study.

4.3.2 Continuous wavelet analysis

As it was described in the previous chapter, the length of cone of influence (COI) is defined as a function of scale (e.g. $\sqrt{2}\,s$ for Morlet wavelet) and increases with the scale. Since the studied range of scales mainly constitute of small scales (less than 16 hours), for all spectra shown hereafter, edge effects (COI) are negligible near both end regions of the wavelet transformation, and consequently, cannot be seen in the spectra. The thick black contour lines, seen in the wavelet spectra hereafter, enclose areas in which the values of wavelet powers are significantly greater than the background red noise at 95% confidence level. Black contour lines might be seen only as black areas in the spectra because the small-scale wavelet is narrow in time domain (high time resolution) and the peaks appear very sharp. The wavelet power spectra are represented by colors, whose scales are presented by color bars. The color scales in the hereafter wavelet spectra indicate the increase of the wavelet power from dark blue to red.

Daily variations are apparently the known cyclic pattern in the meteorological signals. Continuous wavelet transformation (CWT) conducted at scale range of 2 to 48 hours confirmed the presence of such diurnal cyclic variations. Figure 4.10 shows noticeably strong wavelet powers at the scale band of 16 to 32 hours, which is most likely due to the diurnal cyclic variations in the AET and R_n time series, as example. Similar spectra for other meteorological signals of T_g, T_a, RH, and W_s are provided in Appendix A. Strong wavelet powers at the band scale of 16 to 32 hours indicates that the larger-scale cyclic events are the dominant source of temporal variations in the studied time series. Consequently, small-scale cyclic events (e.g. less than 16 hours) may not play a considerable role in inducing the signals' temporal variations. In this study, the small-scale cyclic events were of interest to be investigated though they are not the main source of temporal variations. This is because the small-scale (hourly) variations and modeling of AET were the focus of this study, and the WA was examined for identifying the most important input variables in the estimation of small-scale AET values.

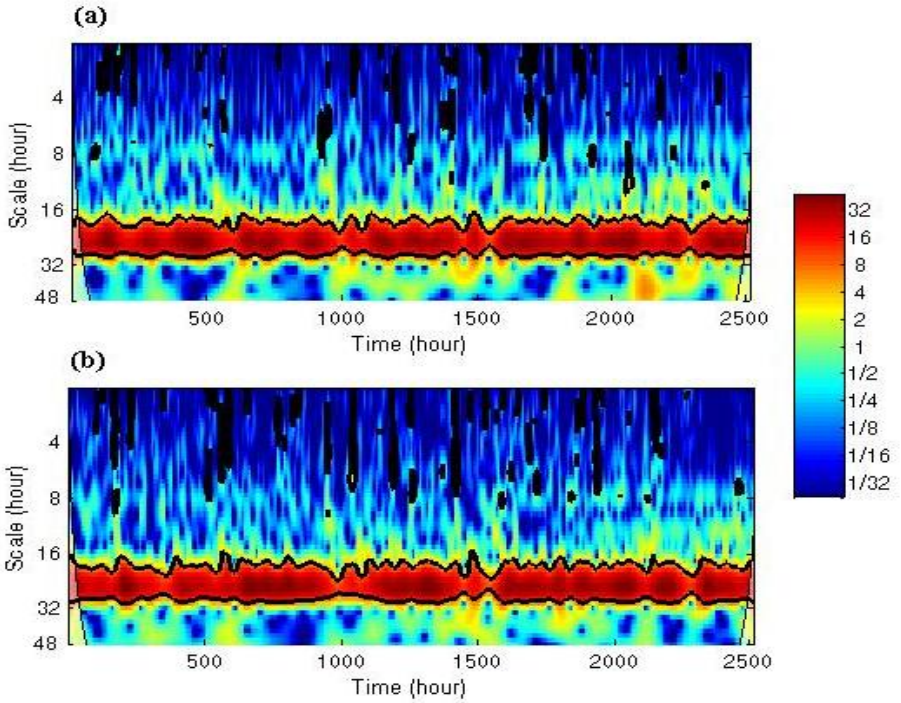

Figure 4.10. Continuous wavelet power spectrum of hourly time series for the scale range of 2 to 48 hours; (a) AET, (b) R_n. The thick black contours show the 95% confidence level against red noise.

Figure 4.11 shows continuous wavelet spectrum of the daytime hourly AET signal. Several wavelet peaks were found to be significantly different from the background red noise at scales of 2 to 8 hours, which were regularly observed along the studied period (growing season of 2006). The significant powers appeared at the scales of 2-4 hours are more frequent than those appeared at 4-8 hours showing that most of the short-time intermittent variations in the AET time series are probably produced by the 2-4 hours scale cyclic events.

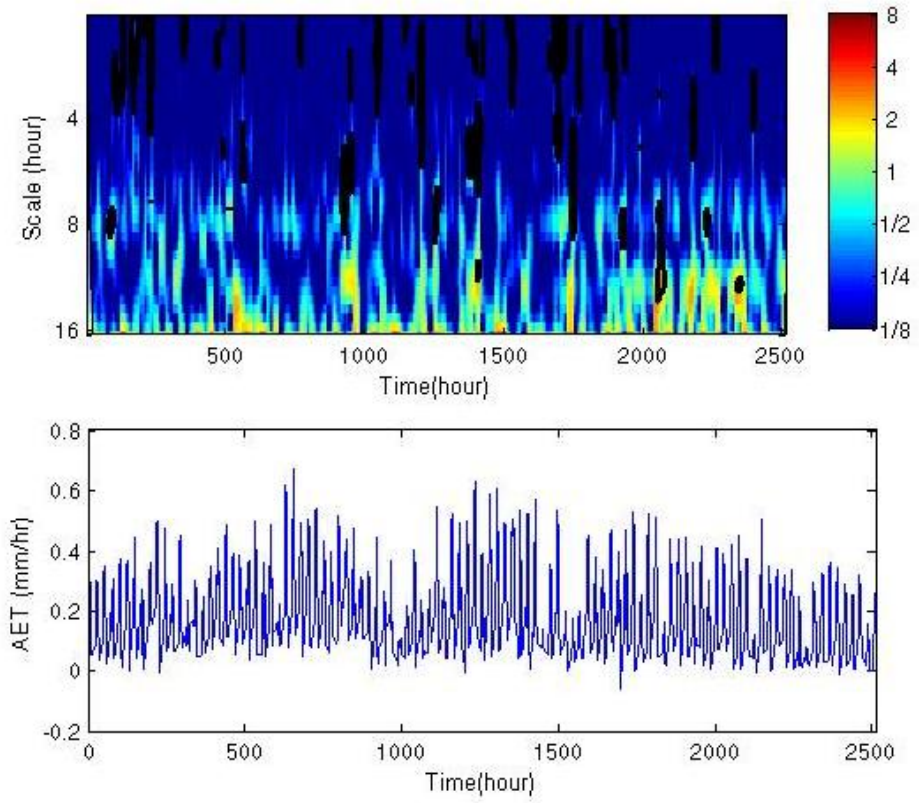

Figure 4.11. Continuous wavelet power spectrum (top) and time series of hourly AET (bottom). The thick black contours show the 95% confidence level against red noise.

Wavelet power spectrum of T_g signal is shown in Fig. 4.12 and exhibits no specific significant cyclic behaviour at scales less than 8 hour. The only cyclic features, which were identified to be significantly different from red noise, were at the scales of 8 to 16 hours. Detected features did not show high magnitude powers (mostly in green), which demonstrate the weak contribution of small-scale cyclic events in the temporal variations of T_g time series. This can also be observed in the zoomed time series of a typical 48-hour window of T_g signal (Figure 4.13). The time series of T_g does not exhibit

as much short-time cyclic variations, e.g., less than daily, compared to that of AET. This might be attributed to the physics of the T_g time series, which changes gradually over the short terms and is not immediately influenced by sudden fluctuations in the atmospheric condition. Similar comparison between AET and other meteorological time series for a typical time-window of 48 hours are provided in Appendix B.

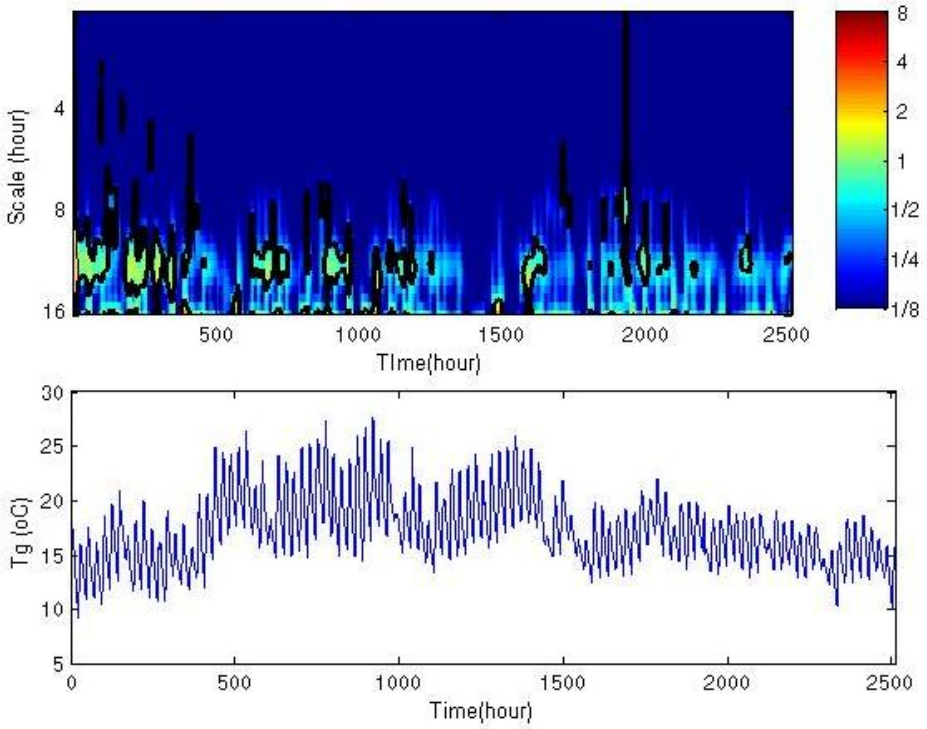

Figure 4.12. Continuous wavelet power spectrum (top) and time series of hourly T_g (bottom). The thick black contours show the 95% confidence level against red noise.

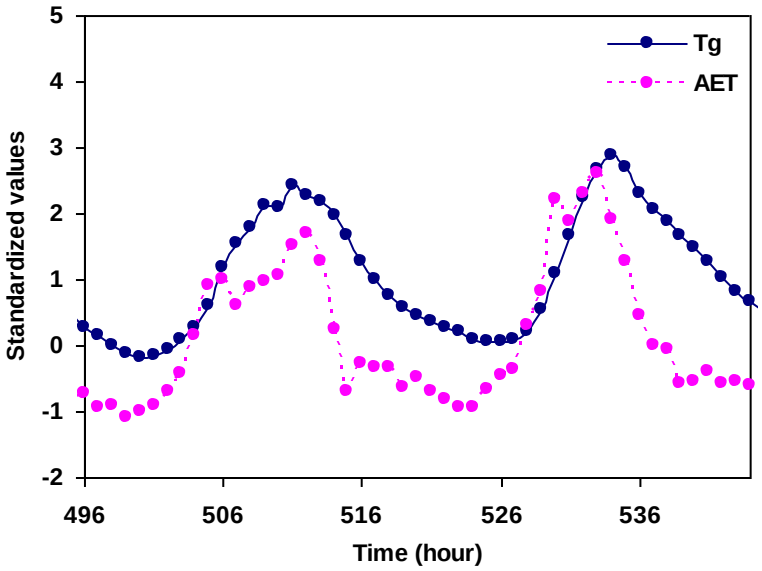

Figure 4.13. Time series of AET and T_g for a typical time-window of 48 hours.

Figure 4.14 demonstrates limited detected cyclic features in the wavelet power spectrum of T_a, which are different from the background red noise at scales of 2 to 8 hours. The significant wavelet peaks that were identified at scales 8 to 16 hours do not contain large magnitude powers. Consequently, T_a signal might not contain considerable small-scale cyclic variations. The wavelet power spectrum of *RH* (Fig. 4.15) shows significant peaks at scales of 2-8 hours at several time locations along the studied period. Wavelet powers of *RH* spectrum at very small scales (around 2 hours) are not significantly different from the background red noise.

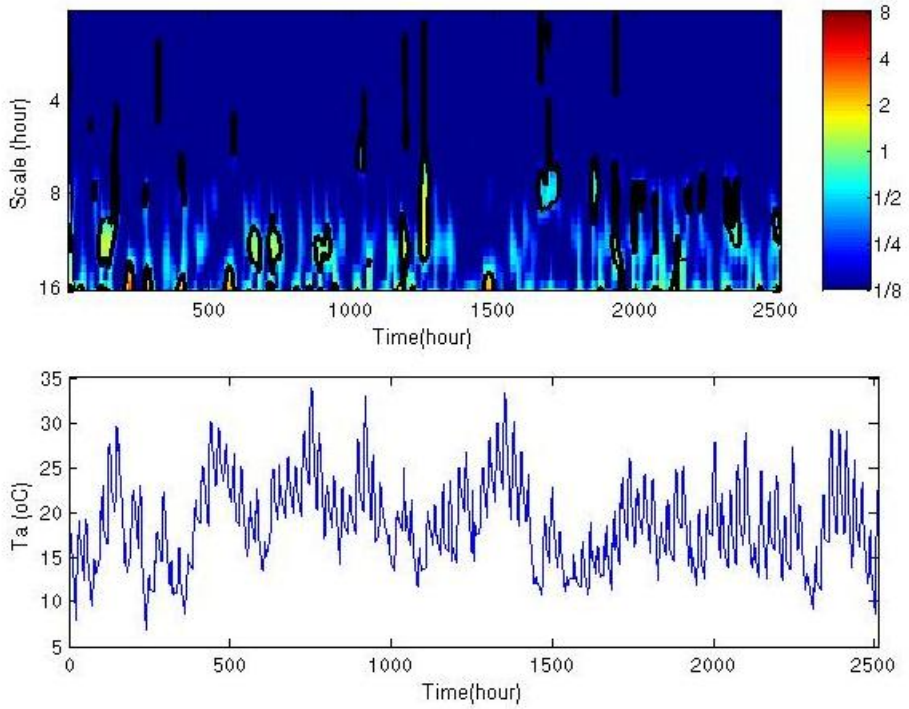

Figure 4.14. Continuous wavelet power spectrum (top) and time series of hourly T_a (bottom). The thick black contours show the 95% confidence level against red noise.

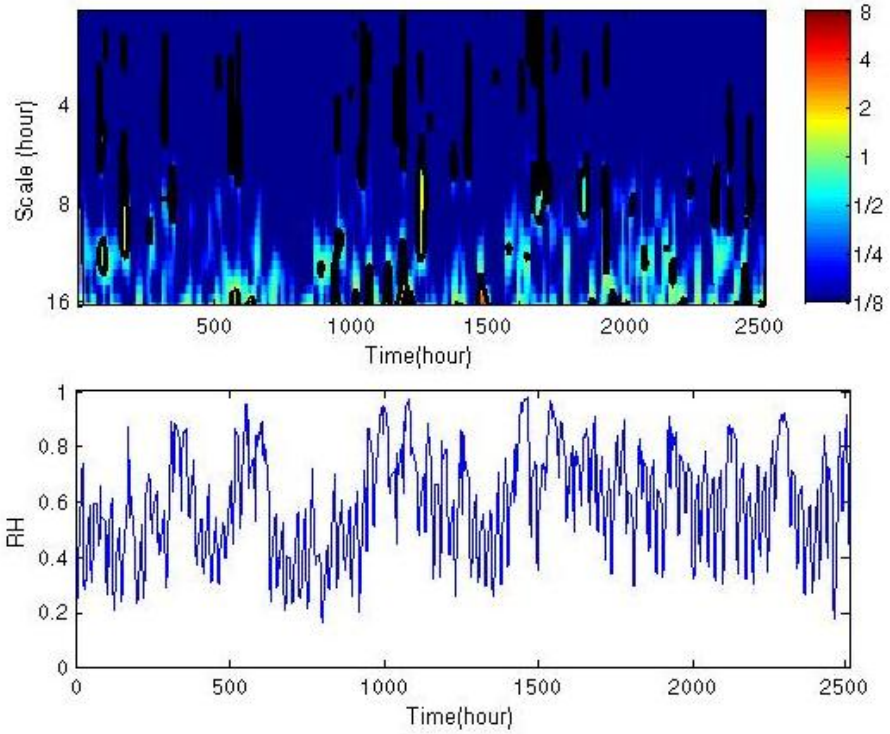

Figure 4.15. Continuous wavelet power spectrum (top) and time series of hourly *RH* (bottom). The thick black contours show the 95% confidence level against red noise.

Cyclic temporal variations of R_n were identified to be significantly different from the red noise at small-scale band of 2 to 8 hours (Fig. 4.16). These significant cyclic features appeared quite frequently along the studied time duration especially at scales of 2-4 hours. Wavelet analysis of the W_s signal exhibited significant cyclic features at scales of 2 to almost 7 hours and 8 to 16 hours (Fig. 4.17). Small-scale cyclic features (2-4 hours) appeared more frequently than the larger-scale features (8-16 hours).

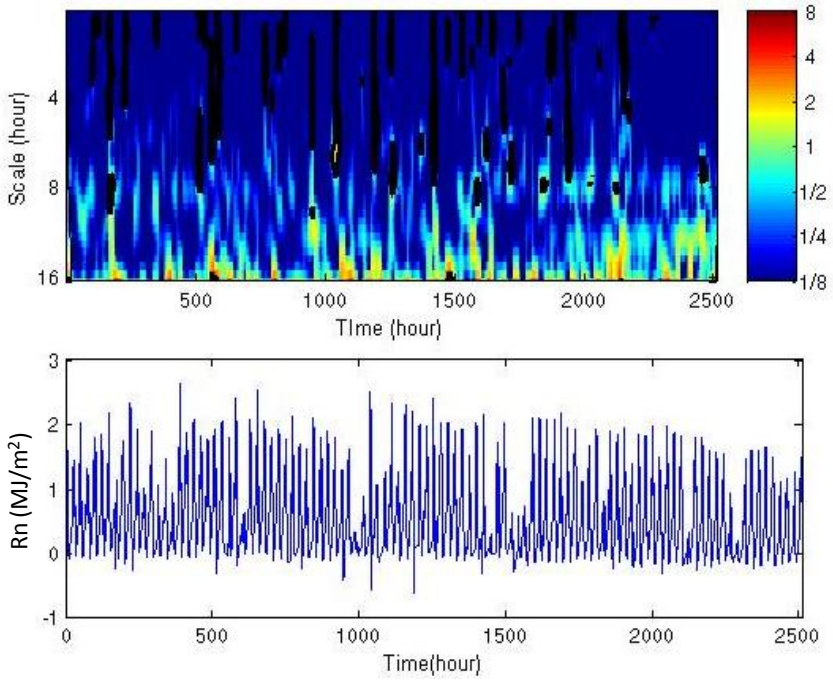

Figure 4.16. Continuous wavelet power spectrum (top) and time series of hourly R_n (bottom). The thick black contours show the 95% confidence level against red noise.

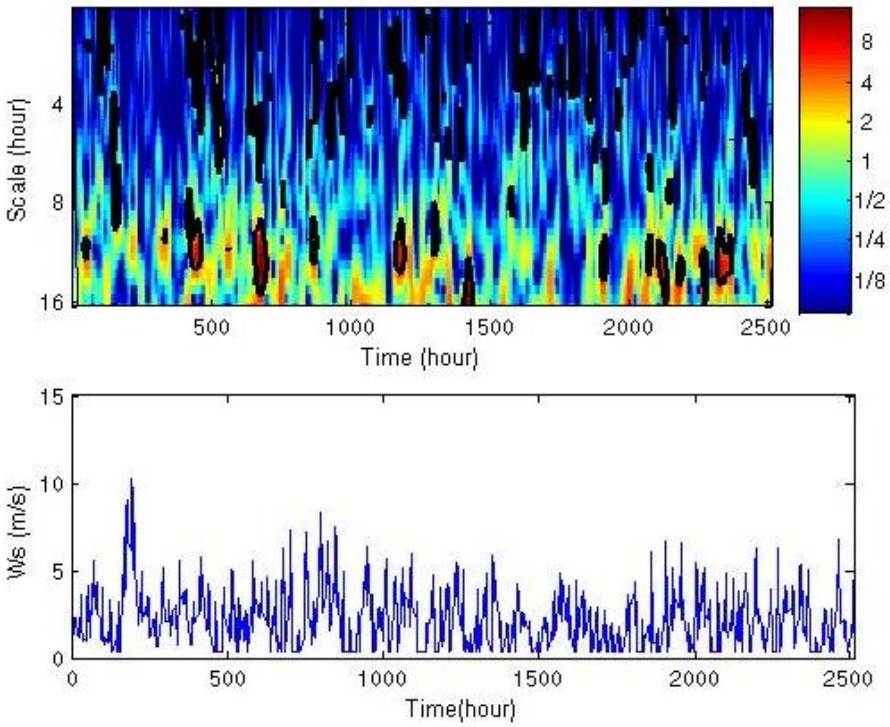

Figure 4.17. Continuous wavelet power spectrum (top) and time series of hourly W_s (bottom). The thick black contours show the 95% confidence level against red noise.

Out of the analyzed time series, the AET, R_n, RH, and W_s exhibited frequent small-scale cyclic features, which were found to be significantly different from the background red noise. No specific significant small-scale cyclic features were detected in the wavelet spectra of T_g and T_a, which could be attributed to two possible reasons. First, temporal variations of air and ground temperature signals do not involve considerable small-scale cyclic features and are mostly generated by larger-scale cyclic trends. Second, the likely existing small-scale cyclic variations are not large enough, in magnitude (because of slight changes of these variables in small time scales), to be differentiated from the background red noise and consequently, cannot be detected as significant cyclic features in the wavelet power spectrum.

As it was discussed earlier in this section, although several small-scale cyclic features were found in the wavelet spectra of the time series, they might not substantially contribute to the temporal variations of the considered signals. The reason is that larger-

scale features (scales of 16 to 32 hours) were observed to induce the major temporal variations in most of the studied time series (Appendix A).

4.3.3 Cross wavelet analysis

It can be seen from the cross wavelet spectrum of AET-R_n (Fig. 4.18) that both time series have common significant powers at scales of 2 to 8 hours along the studied period. This demonstrates the significant linear correlation between AET and R_n signals at small scales at 95% confidence level. To be more specific, the significant AET-R_n correlations appeared at particular time locations but not continuously along the time axis. This means that the linear covariation of these two time series becomes significantly different from red noise only at some periods of time, which is more likely due to the low magnitude of variations at small scales compared to that of larger scales (e.g. diurnal). In other words, there might be non-noise small-scale covariances between the time series; however, since they are not major source of variations in the time series and are low in magnitude, associated cross wavelet powers cannot be distinguished from background noise. Significant powers of AET-R_n cross wavelet spectrum imply that small-scale variation of AET can be explained by R_n time series. Phase information is provided in the cross wavelet spectra using arrows. Pointing right and left arrows show, in order, in-phase and anti-phase relationship between the two time series. Pointing straight down arrows indicate that one time series leads the other by 90^o. Fig. 4.18 indicates the in-phase relationship between AET and R_n at significant areas. By in-phase, it means that the two time series are positively correlated. The relationship between AET and R_n was observed to be not necessarily in-phase over all detected significant areas, since there are some cases when other involved factors affect the conventional cause and effect relationship between the two signals. Varying (not fixed) phase information was also observed in the cross wavelet spectra between AET and other considered meteorological signals, which might be attributed to the range of studied scales (small-scales). Small-scale cyclic events are not the dominant source of variation in the studied time series and consequently, might not carry solid phase information. Larger-scale features, which have more contribution to the temporal variations, contain less varying

and more reliable phase information. Associated cross wavelet spectra, which contain the phase information of extended range of scales of up to 48 hours, between AET and each of the five meteorological time series are provided in the Appendix C.

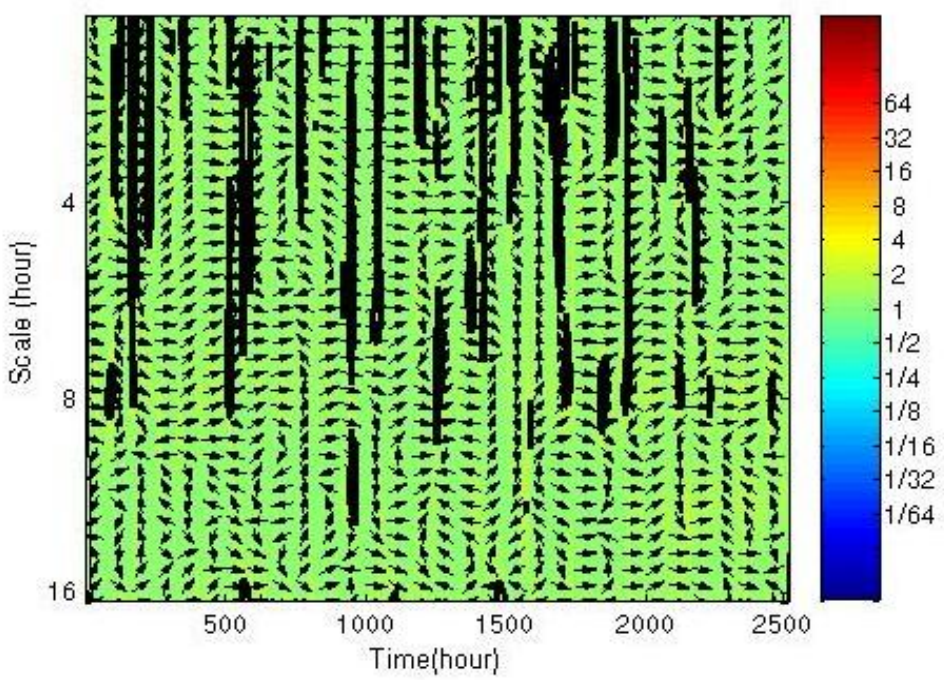

Figure 4.18. Cross wavelet transform of the AET-R_n time series. The thick black contours show the 95% confidence level against red noise. Pointing right and left arrows show in-phase and anti-phase relationship, respectively.

Cross wavelet transform of AET and *RH* exhibited significant common features at the scale band of 2 to 8 hours (Fig. 4.19). Significant correlation between AET and *RH* indicates that the *RH* signal can describe some of the small-scale variations of AET. Although the magnitude of linear correlation between the two time series might not be identified quantitatively, it is seen that *RH* has a significant cause and effect relationship with the AET signal at small scales. Similar to the AET-R_n cross wavelet spectrum, phase relationship between AET and *RH* was not stable. However, some anti-phase relationship can be observed at specific time-scale locations. By anti-phase it means that the AET and *RH* are negatively correlated to each other. Unstable phase relationship, at low scales, also demonstrates the complexity that exists in the short-time variations of AET and its relationship with the involved meteorological factors, which cannot be easily explored by using the cross wavelet transformation. More consistence anti-phase

relationship was observed between AET and *RH* time series at larger-band scale of 16 to 32 (Fig. C.3, Appendix C).

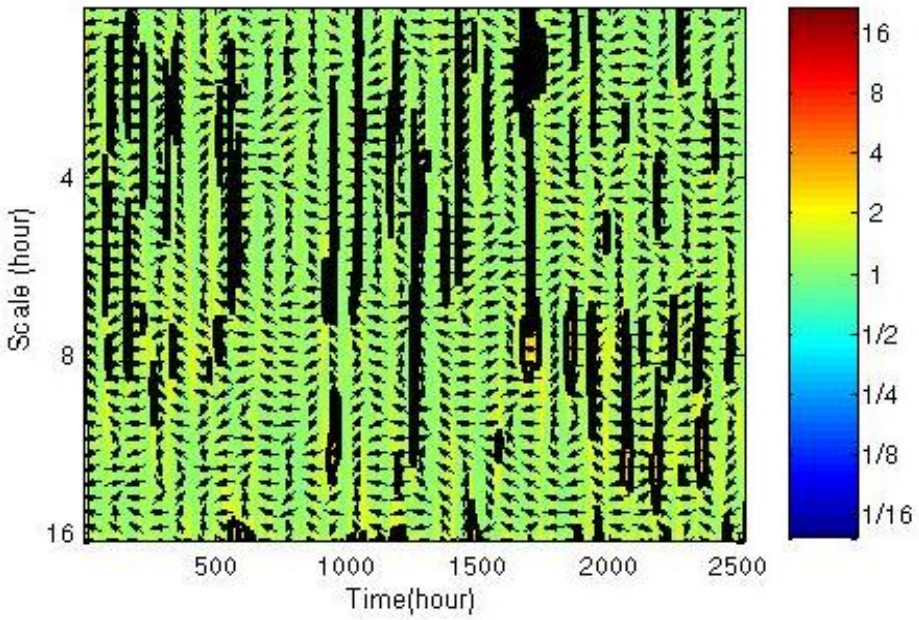

Figure 4.19. Cross wavelet transform of the AET-*RH* time series. The thick black contours show the 95% confidence level against red noise. Pointing right and left arrows show in-phase and anti-phase relationship, respectively.

W_s time series also exhibited significant covariances with AET signal at scales of 2 to 8 hours (Fig. 4.20), which were more frequent at scales less than 4 hours. All of the significant small-scale features found in individual wavelet transform of the W_s time series were not detected as common features between AET and W_s at 95% confidence level. It indicates that only specific numbers of short-time cyclic variations of W_s are linearly correlated to the small-scale cyclic variations of AET. Overall, the results of cross wavelet analysis of AET and W_s demonstrate the existence of linear correlation at small scales. Phase information of AET-W_s spectrum illustrates both in-phase and anti-phase relationship between the variations of the two analyzed signals.

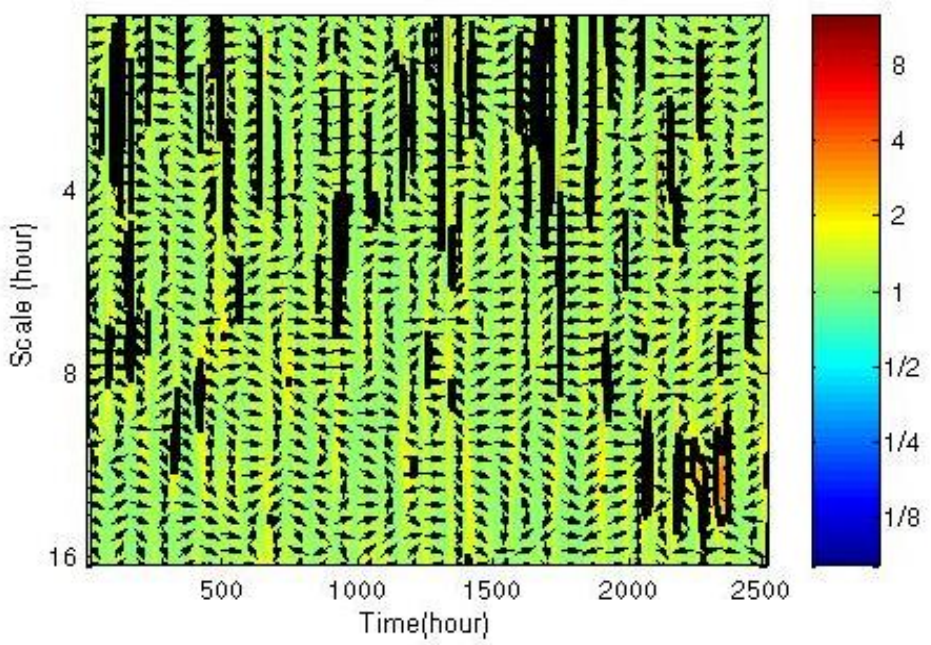

Figure 4.20. Cross wavelet transform of the AET-W_s time series. The thick black contours show the 95% confidence level against red noise. Pointing right and left arrows show in-phase and anti-phase relationship, respectively.

As it was expected from the individual wavelet spectra of AET and T_g, no specific significant common power was found at small scales in the cross wavelet transform of AET-T_g (Fig. 4.21). This might be attributed to two possible reasons; first, the presence of non-linear correlation between AET and T_g at small scales, which cannot be identified by the current cross wavelet analysis. Second, for a time series like T_g, which is not varying much over short time intervals (e.g. hourly), small-scale cyclic features do not have high powers at scales of 2-8 hours and result in low cross wavelet powers of AET-T_g spectrum that cannot be differentiated from background red noise.

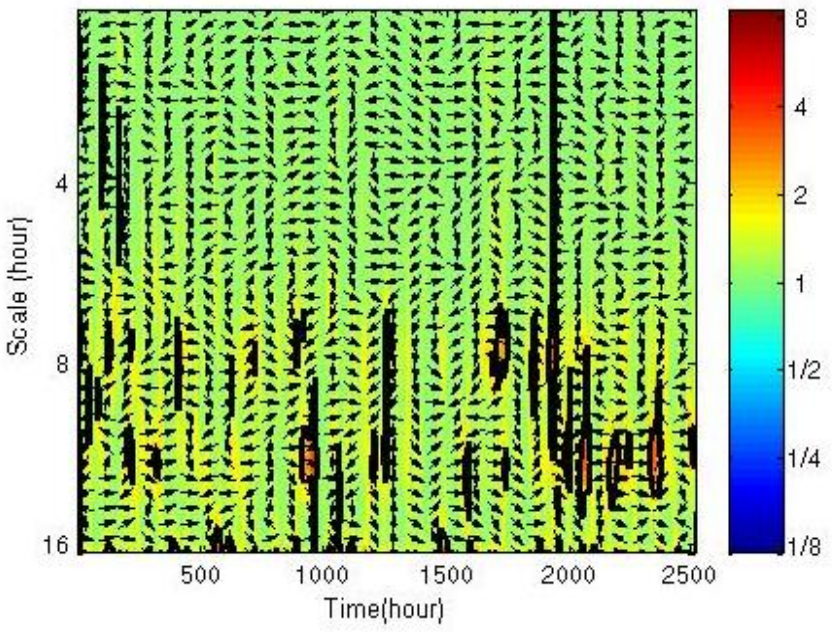

Figure 4.21. Cross wavelet transform of the AET-T_g time series. The thick black contours show the 95% confidence level against red noise. Pointing right and left arrows show in-phase and anti-phase relationship, respectively.

Cross wavelet spectrum of AET-T_a shows limited detected features in the time-scale domain in which the two signals were linearly correlated and the power was significantly different from red noise at 95% confidence level compared to those of AET-R_n, AET-RH, and AET-W_s (Fig. 4.22). Considering the rare significant peaks detected in the band scales of 2 to 8 hours of T_a univariate power spectrum (Fig. 4.14), the identified powers in the cross wavelet spectrum might not indicate significant covariations between the two signals. The significant common powers in the cross wavelet spectrum of AET-T_a were most probably caused by the strong powers of univariate AET spectrum only, which were more frequent than those of T_a over the studied time period. Consequently, no specific and reliable cause and effect relationship can be perceived between AET and T_a time series at small scales. However, strong linear correlation, which was significantly different from background red noise, was observed between AET and T_a at about diurnal scale (scale band of 16 to 32 hours) when the range of studied scales was extended up to 48 hours, Fig. 4.23. The same strong correlation was also observed between AET and T_g at band scale of 16 to 32 hours, which the associated spectrum is provided in Fig. C.2 in Appendix C. Similar cross

wavelet spectra between AET and other considered meteorological signals, for the scale rang of 2 to 48 hours, are available in Appendix C.

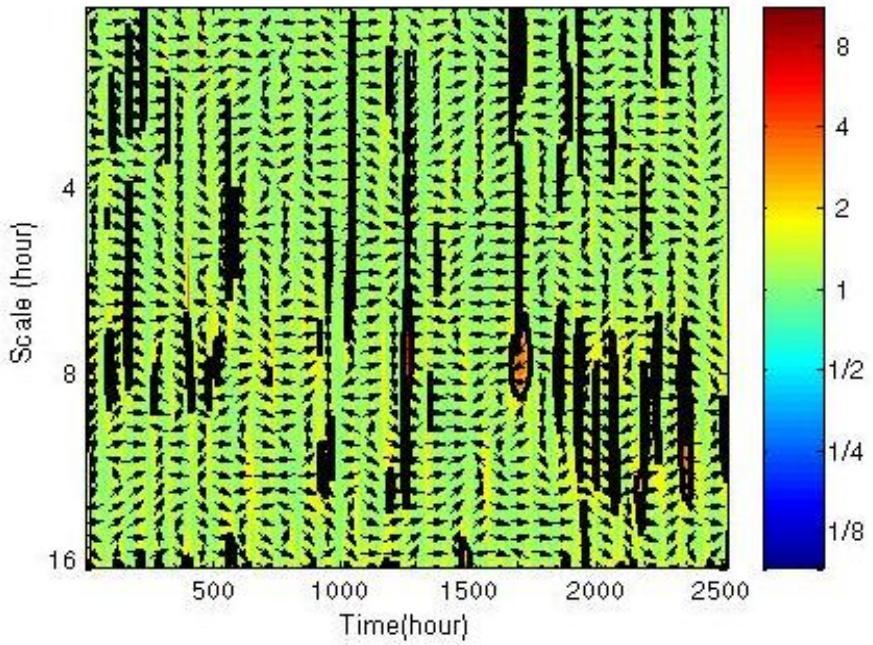

Figure 4.22. Cross wavelet transform of the AET-T_a time series. The thick black contours show the 95% confidence level against red noise. Pointing right and left arrows show in-phase and anti-phase relationship, respectively.

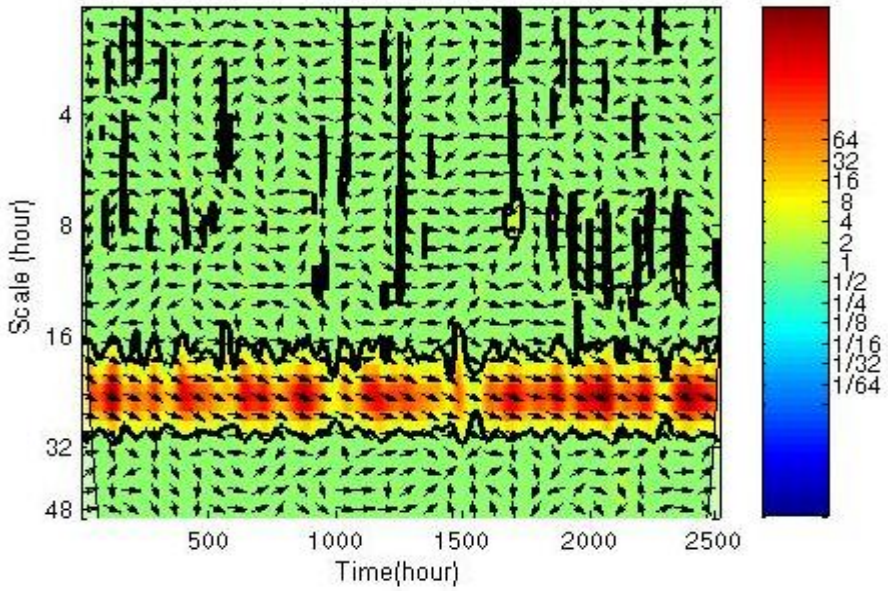

Figure 4.23. Cross wavelet transform of the AET-T_a time series for the scale range of 2 to 48 hours. The thick black contours show the 95% confidence level against red noise. Pointing right and left arrows show in-phase and anti-phase relationship.

The results of the cross wavelet analysis determined, to some extent, the meteorological variables that have significant linear correlation with the AET signal at small scales at 95% confidence level. Based on the cross wavelet analysis, R_n, *RH*, and W_s time series exhibited significant correlation with the AET signal and therefore, they are the important variables in the prediction of small-scale AET variations. Based on the values provided on the scales (color bars) of the cross wavelet spectra, R_n exhibited stronger correlation with AET than *RH*, which is stronger than W_s, with maximum cross wavelet power magnitudes of 256, 16, and 8, respectively. Unfortunately, the results of the cross wavelet analysis cannot be interpreted in a precise quantitative way to identify the importance of one variable over others in the prediction of AET at specific scales (or band scales). In addition, significant powers detected in the univariant wavelet spectra must always be considered when significant cross wavelet powers are interpreted. This is to avoid false common powers, which might be created by the large magnitude powers of one univariate spectrum only.

Based on the cross wavelet analysis, ground temperature has no important linear correlation with the AET time series at small scales. As a result, one might not select T_g as a predictor in the estimation of AET. However, the results of the data driven modeling demonstrated the importance of ground temperature in the prediction of AET. This inconsistency might be attributed to the previously mentioned ability of cross wavelet analysis in identifying only linear correlations between time series. As a result, any existing non-linear correlation between each pair of signals remains undiscovered using cross wavelet analysis. Another possible reason for insignificant common powers in AET-T_g cross wavelet spectrum is that the cross wavelet analysis can investigate the correlation between only two time series at a time (not multiple time series), which ignores the possible effect of other factors interacting with the considered signals. The importance of interaction effects, which exist among the variables involved in the AET process, was observed in the results of the data driven modeling. The above-mentioned limitations of cross wavelet analysis affect the accuracy of the correlation analysis of time series for determining the most important AET predictors.

The other issue, which most probably resulted in the inconsistency between the findings of wavelet analysis and data driven modeling is the time-scale at which the temporal variations of signals were investigated using wavelet analysis or modeled by data driven techniques. The results of the cross wavelet analysis at the larger-scales (scale range of 16 to 32 hours, Appendix C) were in agreement with the results of the data driven models, regarding the most effective variables in the prediction of AET. Cross wavelet analysis exhibited strong linear correlation between AET and T_g at about diurnal scale approximately over the whole studied period. As a result, it can be perceived that the proposed data driven models mainly characterized the larger-scale variations of AET (the dominant cyclic patterns) for which R_n and T_g were found to be the most effective predictors. The cross wavelet analysis, conducted in the present study, concerned more about the small-scale variations of AET. The results obtained using the WA at small scales might be useful in the development of AET models that aim to characterize the small-scale temporal variations.

Wind speed is another example of which the time-scale of its variations is of high importance to be considered in the analysis and may result in some conflict. Wavelet analysis demonstrated that W_s is one of the important variables in the prediction of AET at the small-scale bands (e.g. 2-8 hours). However, W_s was rarely identified by the data driven models, GP and MLR, to be an important variable in the estimation of AET. Simple visual comparison between AET and W_s time series (Fig. B.2, Appendix B), and the univariate wavelet spectrum of W_s at larger scales (Fig. A.4, Appendix A) indicated that larger-scale cyclic features (e.g. diurnal) are not the dominant source of variations in the W_s time series. Consequently, it is less probable, for W_s, to be identified as important input variable by the data driven models, which capture mainly the larger-scale cyclic patterns. The above-mentioned discussion highlights the importance of the time-scale of temporal variations, which might be of interest to be investigated, analyzed, and modeled. Depending on the specific time-scale of variations one is interested in, the employed modeling technique and/or, for instance, the range of studied scales in the wavelet analysis may vary. As a result, it is important to have better understanding of different types of temporal variation exist in the investigated time series prior to the signal analysis and/or modeling.

The correlation between AET and a combination of multiple predictor time series can be investigated by using cross wavelet transform between observed AET and GP models-predicted AET time series. The results of this specific analysis can highlight the importance of multiple combined predictors, rather than individual predictors, in explaining the small-scale cyclic variations of AET. The GP-evolved predictor signals are composed of different combinations of meteorological variables, which consider the effect of multiple predictors together (interaction effects). These GP-predicted AET signals also include the non-linear combinations of inputs by which the importance of non-linear correlations can also be investigated in the cross wavelet transform.

The four GP models, which were used as combined predictor signals, are given as follow:

$$AET = \frac{0.02T_g\left(0.1W_S + 0.38R_n\right)}{0.723 + 0.1W_S + 0.1W_S\left(3.09RH + 0.036T_g + 0.38R_n - 2\right)} \quad [4.20]$$

$$AET = 0.005T_g + 0.024T_g\left[0.383R_n - 0.147\left(1.03RH - \left(1 - 0.77R_n\right)\frac{0.097W_S\left(1.03RH - 1\right)}{1.03RH}\right)\right] \quad [4.21]$$

$$AET = 0.009R_nT_g + 0.00033R_n \times {T_g}^2\left(0.58 - 0.0296T_a\right) + 0.0045T_a \quad [4.22]$$

$$AET = 0.015T_g + 0.16R_n - 0.185 \quad [4.23]$$

Cross wavelet transform of observed AET and combined predictors (GP models) is shown in Fig.4.24. Significant common features were found to be different from red noise at small-scale band of 2 to 8 hours for all four GP-evolved signals. Identified cross wavelet powers demonstrate the significant linear correlation between the observed AET and combined predictor time series (obtained from GP models). Significant cyclic features in the individual wavelet transform of AET (Fig. 4.11) appeared to be significant in the cross wavelet spectra of Fig. 4.24, which demonstrates the ability of all four combined predictor signals in the estimation of small-scale cyclic variations of AET. In other words, the GP technique, which was found to mainly characterize the

large-scale (e.g. diurnal) variations of AET, can also capture some of the small-scale variations. This can also be observed in the time series comparison of the observed and GP-predicted AET signals (Fig. 4.25). The GP models are performing well in the estimation of variations that occur at time-scales of less than daily such as the event occurred between the data point of 668 to 688 in Fig. 4.25.

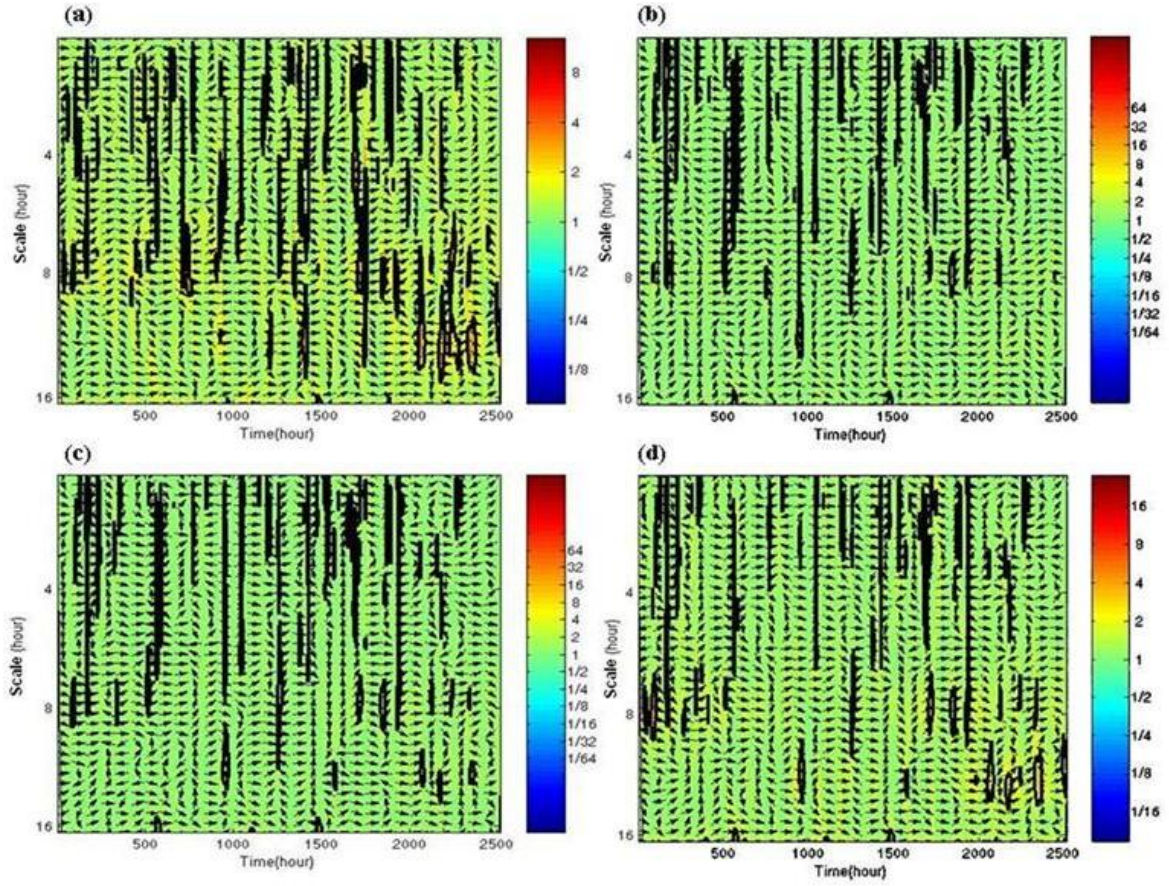

Figure 4.24. Cross wavelet transform of the AET and GP-evolved time series by (a) Eq. (4.20), (b) Eq. (4.21), (c) Eq. (4.22), and (d) Eq. (4.23). The thick black contours show the 95% confidence level against red noise. Pointing right and left arrows show in-phase.

Although, based on the conducted cross wavelet analysis, R_n, RH, and W_s are the most important variables in the prediction of AET, the GP-evolved signal of only R_n and T_g (Eq. 4.23) was able to fairly capture the small-scale cyclic variations of AET and exhibited significant correlation with the AET time series (Fig.4.24d). The same was true when the input combination of R_n, T_g and T_a was used as GP-evolved predictor time series (Eq. 4.22, Fig. 4.24c). This verifies the importance of the effect of variables'

interaction and/or multiple variables combination (linearly or nonlinearly) in the AET mechanism rather than that of each variable individually. For instance, the T_g variable might exhibit some covariations with the AET signal at small scales when other variables, which are physically interacting with T_g, are also considered simultaneously with the T_g time series. Phase information demonstrates the in-phase relationship between AET and GP-evolved signals at most of the significant power areas. Based on the largest magnitude of the powers in the cross wavelet spectra (color bars of Fig. 4.24), AET time series generated by the GP models of Eq.(4.21) and (4.22) exhibited stronger covariances with the observed AET than Eq.(4.20) than Eq.(4.23).

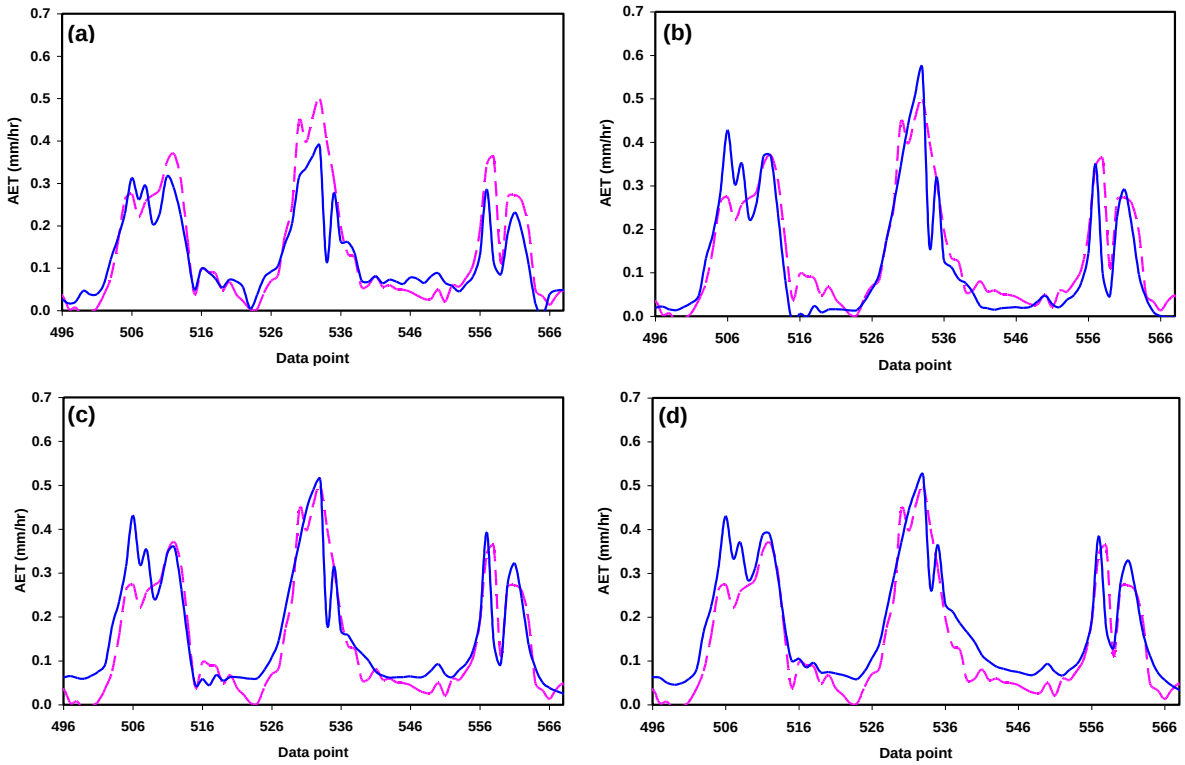

Figure 4.25. Visual comparison between the observed and the GP-evolved AET time series by (a) Eq. (4.20), (b) Eq. (4.21), (c) Eq. (4.22), and (d) Eq. (4.23) over a typical time-window of 72 hours: --, observed values; —, predicted values.

Identification of the most important predictor variables, a priori, to describe the temporal variations of AET might not be a straightforward task using the cross wavelet analysis. In order to identify the important input variables, prior to modeling, it is

important to consider, in advance, the capabilities/limitations of the wavelet analysis as well as the complexity of the mechanism under consideration.

4.4 Discussion

Among the proposed models in this study, the GP and MLR models are both equation-based. Such explicit equation-based models are more appealing to hydrological practitioners because of the transparency and the simplicity of their application. The variables that were observed to have the largest contribution to the AET prediction are almost the same for both equation-based modeling techniques; indicating that both GP and MLR techniques are able to adequately capture the most suitable meteorological variables. Based on the GP and MLR models, the meteorological variables, which were dominantly contributing to the prediction of AET variations (mainly large-scale, e.g. diurnal), include net radiation (R_n) and ground temperature (T_g). R_n is a known variable, which is the source of energy and is one of the essential elements in the evapotranspiration mechanism. The other important elements that shapes the physics of the evaporation are characterized by the surface soil moisture, surface soil temperature, and turbulent sensible heat flux (Wang et al., 2004).

Strong land-atmosphere interaction results in dynamic feedbacks among the involved processes in which the land surface states contain important signal of the near surface atmospheric condition. Sensible heat flux represents the free and forced turbulent transport of heat to the atmosphere caused by surface thermal instabilities and turbulent eddies of wind, respectively. Sensible heat flux as an indication of turbulent transport in the evaporation mechanism (Obukhov, 1946, cited by Wang et al., 2004) is physically related to the state variables of soil moisture and soil temperature (Wang et al., 2004). Wang et al. (2004) also found that the near surface humidity condition can be captured by the surface variables, such as soil moisture and soil temperature. Soil moisture is not easily measurable for most case studies, especially when short temporal scale is required for consistency with the time resolution of other variables. For this study, the hourly data of soil moisture was not available, and temporal downscaling

(disaggregation) of large time-scale soil moisture data to hourly data involves uncertainty. Although no information on soil moisture level was considered for the modeling purposes, it was observed that the net radiation and soil temperature variables (as the dominant inputs in the explicit proposed models) were able to properly compensate for the absence of soil moisture information and sufficiently estimate the variation of AET. This can be attributed to the influence of the upper soil layer moisture on the net radiation, Bowen ratio, and subsequently ground temperature.

Physical description of the AET mechanism, which can be found in many texts and literature (e.g. Dingman 2002; Wang et al., 2004), properly explains the importance of soil moisture element and its complex interaction with other land-atmosphere variables in the AET process. It was of interest to investigate the level of cause and effect relationship between the variations of AET and soil moisture condition in comparison with that of AET and meteorological variables, such as R_n and T_g, at small time-scales. In order to conduct this comparison, the time series of AET, soil water content, R_n, and T_g were visually compared over a typical time-window. Since only the six-hourly information of soil moisture was available, the comparison was conducted using the six-hour time resolution of data. Figure 2.26 shows the temporal variations of six-hour R_n, T_g, soil water content, and AET data series for a typical time-window of 13 days, which includes the data of daytime only. As it is expected from the physics of soil moisture time series, the soil water content varies slightly in time compared to R_n, T_g, and AET variables (Fig.4.26). It can be seen that over the time period of 13 days the soil water content is decreasing gradually, which results in a reduction in the AET value at the end of the time period compared to that at the beginning. Consequently, it is difficult to say if the soil moisture would influence the estimation of AET over shorter-time periods, e.g. daily or less.

Temporal intermittent variations observed in the data series of AET, R_n, and T_g (Fig. 4.26) mainly reflect the diurnal scale variations, since only daytime six-hour data (11:16 AM and 5:16 PM) were considered. Both examined meteorological variables, R_n and T_g, exhibit strong correlation with AET at this scale, which confirms the results of the data driven models and the wavelet analysis (at larger-scales) regarding the most

effective input variables. Figure 4.26 shows that the variations of AET is sometimes highly influenced by the variations of R_n, e.g. between June 27th to July 3th, and sometimes not, e.g. between June 22th to June 24th. This indicates that a single signal of R_n, for instance, might not be able to capture most of the variations in AET, and both R_n and T_g signals are required for estimation of most temporal variations in the AET signal. This means that R_n and T_g time series do not carry exactly the same information although diurnal variation is the major cyclic pattern in both signals.

Comparison of temporal variations of time series raises the question of "does the soil moisture considerably affect the small-scale, e.g. six-hour/hourly, variations of AET?" A model-based test could be implemented to investigate this question and to examine the sensitivity of the AET prediction models to the soil moisture information. The test was conducted for the modeling of six-hour AET, and several GP-based models were developed in two approaches; using and not-using the water content as a predictor. The meteorological variables; R_n, T_g, T_a, RH, and W_s, were the fixed predictors in the modeling process. The water content information used as input variable was associated with the top five centimetres of the soil.

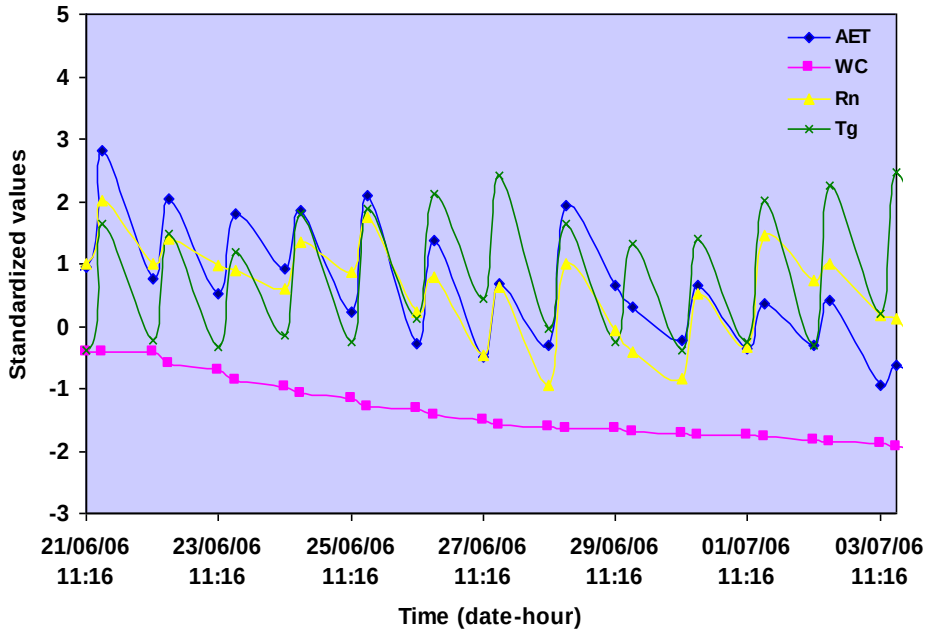

Figure 4.26. Visual comparison of six-hour (day-time) variations of water content (WC), R_n, T_g, and AET versus time.

It was observed that the soil moisture data might not necessarily improve the prediction accuracy of the AET estimation models. Table 4.16 provides a comparison between the possible ranges of performance statistics of the two types of developed AET models. The detailed results of this test are presented in Appendix D. The time resolution of the data in this test was larger than the already analyzed hourly data. It can therefore be perceived that for smaller time resolutions, such as hourly, soil moisture might not be a highly required input variable. It should also be mentioned that the test was conducted using the data of only 2006, which cannot be representative of all possible climatic conditions that may happen on the site. As a result, it is recommended to extend the test for different possible climatic conditions (dry and wet) to obtain more reliable results.

Table 4.16. Performance statistics of two types of AET models using testing subset of six-hour data.

Model	RMSE (MJ/6-hour)			MARE			R		
	Mean	Max.	Min.	Mean	Max.	Min.	Mean	Max.	Min.
Including WC* in input set	0.07	0.08	0.07	0.16	0.18	0.15	0.93	0.94	0.92
Not including WC in input set	0.08	0.09	0.08	0.16	0.17	0.15	0.92	0.93	0.91

*Water content

Another issue of interest is the vegetation factor (representation of transpiration) in the AET mechanism, which was not directly considered in the current modeling study. The vegetation factor of leaf area index (*LAI)* is not readily available variable, especially when short time-scale variations; e.g. hourly, are of interest. In order to investigate the influence of *LAI* on the prediction of short-time AET variations, the disaggregated hourly time series of *LAI*, which was already created as an input for the HYDRUS-1D model, were compared with the AET time series. Figure 4.27 illustrates a comparison between the hourly time series of AET and *LAI* over a typical time-window of six days. It is apparent that transpiration surface area (leaf-area) is not changing significantly over short-time intervals; therefore, its contribution to hourly AET might be something similar to that of soil moisture factor or even less. The temporal variation of *LAI* might become important and effective, in the estimation of AET, at the larger

scales; e.g. weekly or monthly. Visual comparison between the time series of *LAI* and AET over the whole studied period, growing season of 2006, is provided in Appendix E.

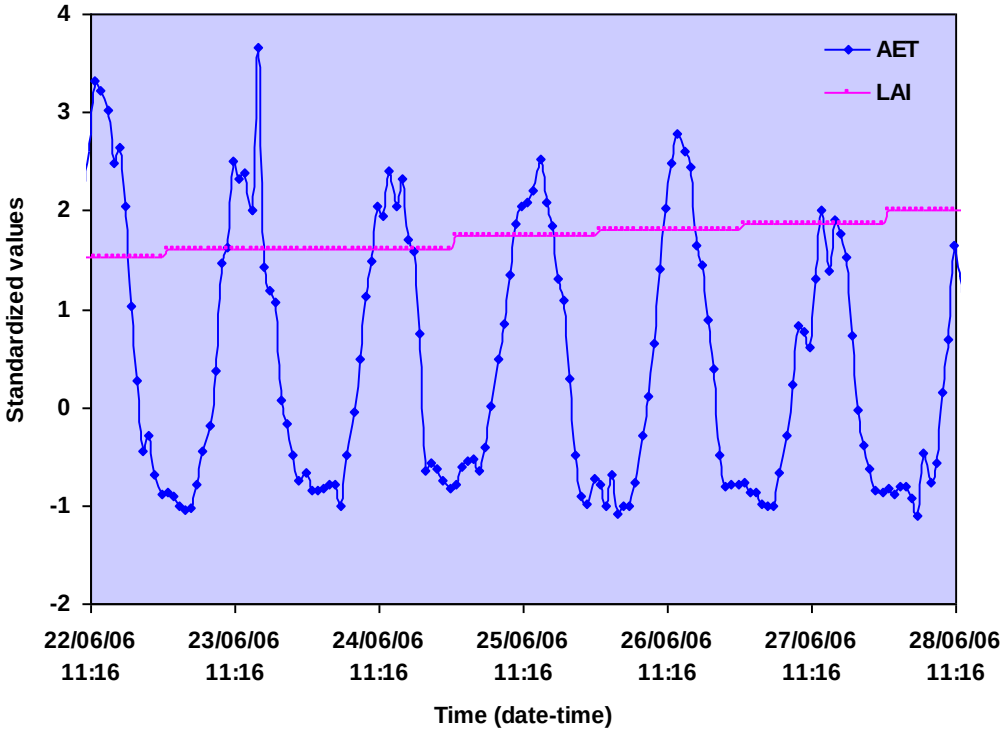

Figure 4.27. Visual comparison between hourly variations of leaf area index (*LAI*) and AET versus time.

Since the information of *LAI* cannot be directly considered in small-scale AET prediction models without uncertainty (associated with disaggregated *LAI* data), other readily available variables can be employed as surrogate factors to carry the information of vegetation in the AET models. Strong land-atmosphere interaction can be investigated to find the links between transpiration and easy-to-measure variables involved in the AET mechanism. The rate of transpiration from a canopy is controlled by different factors, such as light, vapor-pressure deficit, leaf temperature, and leaf water content (Stewart, 1989), which together control the vegetation conductance (leaf resistance), and the density of the leaf (foliar) areas (*LAI*), which in turn controls the extent of transpiration surface. The former factors can be represented by solar radiation, relative humidity, air temperature, and soil moisture, respectively. The latter factor, leaf area density, changes through the growing season and has interaction with ambient

hydrometeorological functions, such as the effect of transpiration area on the meteorological variables; e.g. relative humidity and ground temperature. Leaf area increases through the growing season and shelters the underlying ground area from the sun, which affects the variable of ground temperature. The study conducted by Sanchez-Carrillo et al. (2001) demonstrated that more than 75% of the hourly variance of transpiration (in their case study) can be explained by solar radiation and the residues can be explained by relative humidity and air temperature.

The not fully understood process of actual evapotranspiration makes it very difficult to mechanistically capture the interactions existed among the state variables to present a mathematical relationship between AET and highly correlated meteorological variables. Explicit data driven models (e.g. GP and MLR) exhibited their capability in efficiently capturing the variations of AET, and inducing symbolic estimation models, which are mostly dominated by net radiation and ground temperature. The equation-based GP technique, which was presented in this study, is not the only capacity of the GP as an evolutionary data driven technique. GP can also be implemented to evolve program-based models, which can be presented in a code format, but not as explicit mathematical expressions (Elshorbagy and El-Baroudy, 2009). The program-based type of GP has the advantage of using conditional, comparison, and logical operators in addition to the arithmetic operators, which may enhance the predictive capability of the model to capture more aspects of the investigated process. This means that the utility of GP technique can also be examined using a different implementation tool (e.g., Discipulus^{TM}) to investigate any further improvement in the prediction accuracy.

The cross wavelet analysis may not be essentially strong in determining the optimum input variables for modeling the small-scale AET variations a priori. However, it has the potential to provide deep insight for studying the larger scale variations of AET, e.g. diurnal. Among the examined techniques, GP exhibited to be more efficient than others in identifying the most relevant meteorological predictors. It should also be considered that there is no single data driven technique that could capture all complex processes at all times (Elshorbagy and El-Baroudy, 2009). Consequently, different

techniques might be capable of efficiently predicting different challenging components of the hydrological processes.

CHAPTER 5. SUMMARY AND CONCLUSION

This chapter summarizes the work described in this thesis, which includes the data driven models for the prediction of actual evapotranspiration (AET), and wavelet analysis for investigating the intermittent variations in the AET and meteorological time series. Conclusions of the results and analysis, the contribution of the conducted research, possible future research, and limitations of the study are also provided in this chapter.

5.1 Summary of the study

The research presented in this thesis focused on the modeling and analysis of hourly actual evapotranspiration (AET) in a reconstructed landscape, located in northern Alberta, Canada. The study was conducted in two main parts; data driven modeling of AET and multiresolution analysis of AET and meteorological time series. Hourly eddy covariance (EC)-measured AET data were investigated as the target function, whereas the meteorological variables of net radiation, ground temperature, air temperature, relative humidity, and wind speed were examined as possible predictors.

In the first part of the study, AET prediction models were developed using three different data driven techniques; artificial neural networks (ANNs), genetic programming (GP), and multilinear regression (MLR). The performances of the developed AET models were evaluated and a comparative analysis was conducted, with regard to the predictive and generalization abilities of the models, to identify the possible superiority of one modeling approach over the others. In addition, the result of the data driven models were compared with those of HYDRUS-1D; a physically-based model, as a possible alternative to the proposed data driven models for the estimation of AET.

In the second part of the study, the capability of the wavelet analysis was examined for possible identification of the most important variables in the modeling of AET, a priori. This was implemented by performing the continuous wavelet

transformation for multiresolution analysis of the temporal variations of the various signals, and for exploring the dominant frequency events. Then, cross wavelet analysis was performed between the AET time series and each of the meteorological signals, in order to find any significant covariances, which show the strong cause and effect relationship between them.

5.1.1 Data driven modeling

The ANN model with eight hidden neurons trained by Bayesian-regularization algorithm was found to be the best ANN model, with reasonable generalization ability. The optimum models generated by GP were linear and non-linear equations predicting AET as a function of net radiation, ground temperature, air temperature, and relative humidity. Although some of the GP-evolved models were nonlinear and contained interactions and/or second orders of variables, the models were all linear in parameters. Thus, it can be said that GP was able to model the complex process of AET as semi-linear functions of meteorological variables, which also had good predictive abilities. Almost half of the optimum GP models estimated AET only as a function of net radiation and ground temperature. The statistical analysis also revealed that net radiation and ground temperature were the most dominant climatic variables for predicting actual evapotranspiration. Furthermore, interaction effects of some meteorological variables were shown to be important in the modeling of AET. The contribution of the interaction effects in the estimation models was sometimes even more than those of the individual variables.

A comparative analysis of the models' predictive abilities indicated that the GP and MLR models have better generalization ability than the ANN models for estimating the hourly actual evapotranspiration as a function of meteorological variables in the case study presented in this thesis. In comparison with the data driven models, the HYDRUS-1D model performed on par to other models in one year of data (2005) but poorer in another year (2006) for the estimation of AET. This indicated that a physically-based model, such as HYDRUS-1D, might be inferior to the data driven models in terms of the

overall prediction accuracy. Compared to the ANNs, the important advantage of the GP and MLR models is the representation of the explicit equations, which can be easily interpreted. In addition, GP and MLR models are simpler in the application and usage than the ANN model. The GP-evolved models required fewer input variables than the MLR. The interesting point is that the performances of the GP and regression models are close to each other, although the numbers and combinations of the employed inputs are quite different for each model.

5.1.2 Wavelet analysis

In this study, wavelet analysis was mainly focused on the small-scale temporal variations of time series, since variations of AET at small time-scale (hourly) was of interest to be investigated and modeled. Wavelet analysis was also extended to larger-scales to have a brief overview of other possible cyclic variations exist in the time series. Continuous wavelet transformation was performed for the hourly time series of the AET and the five meteorological variables of R_n, T_g, T_a, RH, and W_s. The continuous wavelet spectra of AET, R_n, RH, and W_s exhibited significant powers at small scales (e.g. 2-8 hours); however, no specific cyclic features were detected in those of T_g and T_a. Extension of the range of scales to larger values demonstrated the presence of strong cyclic features at around diurnal scale in most of the studied time series, including T_g and T_a. It was observed that the contribution of larger-scale cyclic features to the total time series variations is considerably higher than those of small scales. In other words, larger-scale (e.g. diurnal) cyclic patterns can be perceived as the major source of temporal variations in the AET and most of the meteorological time series.

Cross wavelet analysis between AET and each of the meteorological time series over the range of small scales demonstrated significant linear covariations between AET and R_n, RH, and W_s time series. This implies that these meteorological variables are important in explaining the small-scale variations of AET. As it was expected from the univariate spectrum of T_g and T_a, cross wavelet spectra of AET-T_g and AET-T_a, did not exhibit any specific covariations at small scales. However, when the cross wavelet

analysis was extended to larger range of scales, stronger covariances were observed between AET and R_n, RH, T_g, and T_a time series, which were significant at the band scale of 16 to 32 hours (more likely due to diurnal variations). This indicates that the variables of T_g and T_a are important predictors for the estimation of larger-scale variations of AET. Consequently, prior-to-modeling identification of the most important input variables for the estimation of AET depends on the time-scale of variations, which is of interest to be modeled. It can subsequently be perceived that the GP and MLR models, which presented the T_g variable as one of the important inputs, may mainly capture the larger-scale variations of AET. The wavelet analysis, conducted in this study, revealed the importance of time-scale issue in the analysis and modeling of temporal variations exist it the AET and meteorological time series.

5.2 Conclusion

In conclusion, the investigated data driven modeling techniques were promising for the estimation of the hourly AET mechanism using the observed data, without assuming or applying significant knowledge of the physics of the process. The choice of the testing dataset was found to be important for realistically assessing the generalization ability of the proposed data driven models and also for the determination of the possible superiority of any of the modeling techniques over others. Among the examined data driven modeling techniques, genetic programming (GP) and MLR were found to perform similarly and better than the ANN model with regard to generalization ability. The GP-evolved models also had the advantage of being structurally simple and requiring fewer input variables, which is of interest for many hydrological practitioners.

Furthermore, the proposed equation-based models, using GP and MLR, showed that the AET process has the potential to be estimated by structurally simple (e.g. semi-linear) models. Equation-based AET models made it possible to extract some information about the physics of the process. It was observed that the meteorological variables of R_n and T_g have larger contribution, than other variables, to the estimation of

AET. In addition, the interaction effects of the meteorological variables were found to be important and effective in the estimation of AET.

The results of wavelet analysis improved the understanding of the AET mechanism by revealing the importance and contributions of different time-scale cyclic variations exist in the AET time series. This highlights the issue of time-scale and the importance of its consideration in the modeling and prior-to-modeling input selection procedure. Although several small-scale cyclic features were detected in the AET signal, larger-scale variations were found to be the major frequency events at which the predictant-predictor (AET-meteorological variables) correlation analysis was more clear and reliable. GP and MLR models were noted to mainly model the larger-scale (dominant) temporal variations of AET, although short time-scale (hourly) data were employed for training and developing the models.

Consistency between the results of data driven modeling (especially GP) and wavelet analysis, regarding the most important predictor variables, at large time-scales (e.g. diurnal) indicated that wavelet analysis can be employed as a guide for identifying the most linearly correlated predictors for the modeling of AET. However, limitations of such signal analysis tool should be considered when it is used for input determination prior to modeling. Wavelet analysis helped to perceive the difference between the predictive abilities of various models from a new perspective, which is the time-scale of variations that the models characterize. For instance, when the performances of two prediction models are compared, it should be noted if both models are capturing the same time-scale of variations. Consideration of this point can make the models' comparative analysis more accurate and fair.

5.3 Contribution of the research

In this study, actual evapotranspiration as one of the major components of the hydrological cycle was modeled using data driven modeling techniques in a reconstructed watershed. Determination of the most suitable and efficient prediction model is important for accurate assessment of AET in a reconstructed watershed in

which understanding of the various hydrological processes is essential for improvement and development of sustainable reclamation strategies.

The proposed AET data driven models can be used for practical estimation of the AET in the studied reconstructed site using the conventional meteorological variables. Using the developed equation-based GP models, the hourly values of AET can be estimated using a few and readily available numbers of meteorological variables, which are usually measured, or can be measured, in most weather stations. Although the proposed models were basically developed for the estimation of hourly AET, the AET values associated with larger time scales can also be obtained by aggregating the hourly AET values. The AET models represented in this study were local models, which might be applicable for AET estimations in similar case studies. However, it should be first verified if the climatic conditions and the general characteristics of the considered sites are similar to that of the site used for model development. Further studies can be conducted on assessing the performance of the locally proposed models on other reconstructed sites. In the case of availability of measured AET and meteorological variables, data driven techniques can be easily used for developing local AET models. This kind of modeling could be more efficient and easier than the physically-based and empirical modeling approaches, which require large number of measured inputs and estimation of models parameters.

Although data driven models do not require any knowledge about the underlying process, better understanding of the investigated function and identification of the most important predictor variables, prior to the modeling, can improve the efficiency and the predictive ability of the model. The results of this study demonstrated that wavelet analysis can be used as a tool for this purpose. This study also revealed the importance of the time-scale of variations, under consideration, in the analysis and modeling of hydrological time series. This finding could improve the current understanding of the AET variations as well as its correlation with the predictor variables, which can be very helpful in the interpretation of prediction models. Temporal variations of a hydrological time series might occur at different time-scales, and different prediction models might be suitable for capturing each of them. In addition, the cause and effect relationship

between hydrological predictant and predictors may vary when the investigated time-scale of variation is changed. This kind of information can be employed for the analysis and modeling of any hydrological time series, which enhances the success of the modeling procedures and consequently, improves the understanding and monitoring of the reconstructed watershed hydrology.

5.4 Future work

Some of the possible extensions to the current research study, associated with the inductive modeling of hydrological processes in the reconstructed watersheds, are as follows:

- Extending the GP modeling of AET and wavelet analysis of time series at different time-scales (e.g. daily or larger) would help to have better understanding of the GP models' prediction abilities at different time-scales and the applicability of wavelet analysis for prior-to-modeling determination of AET model inputs;

- Performing cross wavelet analysis between each pair of the meteorological variables can help to identify the input variables, which have inter-dependency and carry the same information to the model, and clean the final set of important input variables from redundant variables. This may help in redundancy handling and determining the most efficient and parsimonious set of model's important input;

- Studying the influence of soil moisture on the AET prediction models can be extended to include dry and wet years. Also, the soil moisture content data of the root zone of the soil layer should be included. This helps to investigate the effect of soil moisture on AET in dry conditions when required water mostly provided from lower layers of the soil; and

- Continuous and cross wavelet analysis can be employed for comparing the performances of different models in terms of their abilities in capturing different time-scales variations.

5.5 Study limitations

Some of the limitations and assumptions involved with this study are as follows:

- For the modeling and analysis of AET mechanism, only two years of data were available and used in this study, which might not be sufficient for accurate modeling and model assessment. Two years of data may not include all extreme conditions;

- The functional set selected for performing the GP algorithm was limited to simple arithmetic functions. Several different functional operators can be used for developing the equation-based GP models.

- For investigating soil moisture effect on the prediction of six-hour AET, the water content information of only top five centimetres of the soil was considered;

- In the HYDRUS model, crop coefficient was assumed to be one, which means that the vegetation was assumed to have similar aerodynamic and surface characteristics as reference surface in the PM equation. This assumption was made because the mentioned information was not available for the vegetation cover in the studied site; and

- For the statistical analysis, time series data were assumed to have normal distribution.

REFERENCES

Abrahart, R.J. and White, S. 2001. Modelling Sediment Transfer in Malawi: Comparing Backpropagation Neural Network Solutions Against a Multiple Linear Regression Benchmark Using Small Data Sets. Phys. Chem. Earth (B) **26(1)**: 19–24.

Akaike, H. 1974. A new look at statistical model identification. IEEE Trans. Automat. Contr., AC, **19**: 716-722.

Allen, M.R. and Smith, L.A. 1996. Monte Carlo SSA: Detecting irregular oscillations in the presence of coloured noise, J. Clim., **9**: 3373–3404.

Allen, R.G., Pereira, L.S., Raes, D., and Smith M. 1998. Crop evapotranspiration: guidelines for computing crop water requirements. Irrig. and Drain. Paper No. 56. Rome: FAO.

Anctil, F. and Coulibaly, P. 2004. Wavelet analysis of the interannual variability in Southern Quebec streamflow. Journal of Climate **17 (1)**: 163–173.

Anctil, F. and Tape, D.G. 2004. An exploration of artificial neural network rainfall-runoff forecasting combined with wavelet decomposition. J. Environ. Eng. Sci., **3**: S121–S128.

ASCE. 2000a. Artificial Neural Networks in Hydrology. I. Preliminary Concepts. J. Hydrol. Eng., **5(2)**: 115–123.

ASCE. 2000b. Artificial Neural Networks in Hydrology. II. Hydrologic Applications. J. Hydrol. Eng., **5(2)**: 124–137.

ASCE Environmental and Water Resources Institute (ASCE-EWRI). 2004._The ASCE standardized reference evapotranspiration equation. Standardization of Reference Evapotranspiration Task Committee Final Rep., Reston, Va.

Aytek, A. and Kisi, O. 2008. A genetic programming approach to suspended sediment modeling. Journal of Hydrology, **351**: 288–298.

Aziz, A.R.A. and Wong, K.F.V. 1992. Neural network approach to the determination of aquifer parameters. Ground Water, **30(2)**: 164– 166.

Babovic, V. 2000. Data mining and knowledge discovery in sediment transport. Comput.-Aided Civ. Infrastruct. Eng., **15(5)**: 383–389.

Babovic, V. and Keijzer, M. 2002. Declarative and preferential bias in GP-based scientific discovery. Genet. Program. Evol. Mach., **3(1)**: 41-79.

Back, T., Hammel, U., and Schwefel, H.P. 1997. Evolutionary Computation: Comments on the History and Current State. IEEE Transactions on Evolutionary Computation, **1(1)**: 3-16.

Baldocchi, D.D. 2003. Assessing the eddy covariance technique for evaluating carbon dioxide exchange rates of ecosystems: Past, present and future. Global Change Biology, **9**: 479−492.

Baldocchi, D.D., Hicks, B.B., and Meyers, T.P. 1988. Measuring biosphere–atmosphere exchanges of biologically related gases with micrometeorological methods. Ecology, **69**: 1331−1340.

Baliunas, S., Frick, P., Sokoloff, D., and Soon, W. 1997. Time scales and trends in the Central England temperature data (1659– 1990) – a wavelet analysis. Geophysical Research Letters, **24**: 1351–1354.

Banzhaf, W., Nordin, P., Keller, R.E., and France, F. 1998. Genetic Programming: An Introduction. Morgan Kaufmann Publishers, Inc. San Francisco, California, USA.

Baptist, M.J., Babovic, V., Uthurburu, J.R, Keijzer, M., Uittenbogaard, R.E., Mynett, A., and Verwey, A. 2007. On inducing equations for vegetation resistance. Journal of Hydraulic Research, **45(4)**: 435–450.

Bernatowicz, S., Leszczynski, S., and Tyczynska, S. 1976. The influence of transpiration by emergent plants on the water balance in lakes. Aquat. Bot., **2**: 275-288.

Bhakar, S.R, Oiha, S., Singh, R.V., and Ansari, A. 2006. Estimation of evapotranspiration for wheat crop using artificial neural network, Proceedigs, 4th World Congress on Computers in Agriculture, Orlando, FL, US.

Bhattacharya, B., Price, R.K., and Solomatine, D.P. 2005. Data-driven modelling in the context of sediment transport. Phys. Chem. Earth, **30(4–5)**: 297–302.

Birikundavy, S., Labib, R., Trung, H.T., and Rousselle, J. 2002. Performance of Neural Networks in Daily Streamflow Forecasting. J. Hydrol. Eng., **7(5)**: 392–398.

Blaney, H.F. and Criddle, W.D. 1950. Determining water requirements in irrigated area from climatological irrigation data. Soil Conservation Service Technical Paper no. 96. US Department of Agriculture, Washington DC, USA.

Boese, C. 2003. The design and installation of a field instrumentation program for the evaluation of soil-atmosphere water fluxes in a vegetated cover over saline/sodic shale overburden. M.Sc. Thesis, University of Saskatchewan, Saskatoon, SK, Canada.

Box, G.E.P. 1957. Evolutionary operation: A method for increasing industrial productivity. Appl. Statistics, **6(2)**: 81–101.

Bremermann, H.J. 1962. Optimization Through Evolution and Recombination, In M.C. Yovits et al, Editors, Self-Organizing Systems, Spartan Books, Washington, DC: 93-106.

Brunsell, N.A., Ham, J.M., and Owensby, C.E. 2008. Assessing the multi-resolution information content of remotely sensed variables and elevation for evapotranspiration in a tall-grass prairie environment. Remote Sens. Environ., **112(6)**: 2977-2987.

Brutsaert, W.H. 1982. Evaporation into the Atmosphere. D. Reidel, Dordrecht, The Netherlands.

Cahill, A.T. 2002. Determination of changes in streamflow variance by means of a wavelet-based test. Water Resour. Res., **38(6)**: 1065-1078.

Campolo, M., Andreussi, P., and Sodalt, A. 1999. River stage forecasting with a neural network model. Wat. Res. Res., **35(4)**: 1191–1197.

Campolo, M., Soldati, A., and Andreussi, P. 2003. Artificial neural network approach to flood forecasting in the River Arno. Hydrol. Sci. J., **48(3)**: 381–398.

Carey, S.K. 2008. Growing season energy and water exchange from an oil sands Overburden reclamation soil cover, Fort McMurray, Alberta, Canada. Hydrol. Process, **22**: 2847–2857.

Chauhan, S. and Shrivastava, R.K. 2009. Performance Evaluation of Reference Evapotranspiration Estimation Using Climate Based Methods and Artificial Neural Networks. Water Resource Management, **23(5)**: 825-837.

Chaikowsky, C.L.A. 2003. Soil moisture regime and salinity on a tailing sand storage facility. M.Sc. Thesis, University of Alberta, Edmonton, Alberta, Canada.

Chen, X. and Liu, D. 2008. Wavelet analysis on inter-annual variation of precipitation in Guangdong, China. IAHS publication, **319**: 3-9.

Cheng, B. and Titterington, D.M. 1994. Neural networks: A review from a statistical perspective. Statistical Science, **9(1)**: 2–54.

Compagnucci, R.H., Blanco, S.A., Figliola, M.A., and Jacovkis, P.M. 2000. Variability in subtropical Andean Argentinean Atuel river: a wavelet approach. Environmetrics, **11**: 251–269.

Coulibaly, P. 2004. Downscaling daily extreme temperatures with genetic programming. Geophysical Research Letters, **31**, L16203, doi:10.1029/2004GL020075.

Coulibaly, P. 2006. Spatial and temporal variability of Canadian seasonal precipitation (1900-2000). Advances in Water Resources, **29**: 1846–1865.

Coulibaly, P. and Burn, D.H. 2004. Wavelet analysis of variability in annual Canadian streamflows. Water Resource Research **40,** W03105, doi:10.1029/2003WR002667.

Cousin, N. and Savic, D.A. 1997. A rainfall-runoff model using genetic programming. Centre for Systems and Control Engineering; Report No. 97/03, School of Engineering, University of Exeter, Exeter, United Kingdom.

Cybenko, G. 1989. Approximation by superposition of a sigmoidal function. Math. Control Signals Syst. **2**: 303–314.

Dai, X., Shi, H., Li, Y., Ouyang, Z., and Huo Z. 2009. Artificial neural network models for estimating regional reference evapotranspiration based on climate factors. Hydrological processes, **23(3)**: 442-450.

Daniel, T.M. 1991. Neural networks—applications in hydrology and water resources engineering. Proceedings, Int. Hydrol. and Water Resour. Symp., Institution of Engineers, Perth, Australia.

Dartus, D., Courivaud, J.M., and Dedecker, L. 1993. Use of a neural net for the study of a flood wave propagation in an open channel. J. Hydr. Res., **31(2)**: 161-169.

Daubechies. I. 1988. Orthonormal Bases of Compactly Supported Wavelets. Comm. Pure Appl. Math., **41**: 906-966.

Daubechies, I. 1992. Ten Lectures on Wavelets. Society for Industrial and Applied Mathematics, 357 pp.

Davis, L. (Ed.) 1991. Handbook of Genetic Algorithms. Van Nostrand Reinhold, N.Y.

Dawson, C.W. and Wilby, R.L. 2001. Hydrological modelling using artificial neural networks. Progress in Physical Geography **25(1)**: 80–108.

De Jong, K.A. 1975. An analysis of the behavior of a class of genetic adaptive systems. Ph.D. dissertation, Univ. of Michigan, Ann Arbor, Diss. Abstr. Int. 36(10), 5140B (University Microfilms No. 76 9381).

De Jong, K.A. 1987. On using genetic algorithms to search program spaces, Proceedings, 2nd Int. Conf. on Genetic Algorithms and Their Applications, Hillsdale, NJ.

Denmead O.T. and Shaw R.H. 1962. Availability of soil water to plants as affected by soil moisture content and meterological conditions. Agron J, **45**: 385 – 390.

Devito, K., Creed, I., Gan, T., Mendoza C., Petrone R., Silins U., and Smerdon B. 2005. Aframework for broad-scale classification of hydrologic response units on the Boreal Plain: is topography the last thing to consider? Hydrological Processes, **19**: 1705-1714.

Dingman, S.L. 2002. Physical Hydrology. Prentice-Hall, Inc., Upper Saddle River, NJ.

Dolan, T.J., Hermann, A.J., Bayley, S.E., and Zoltek, J., Jr. 1984. Evapotranspiration of a Florida, U.S.A., freshwater wetland. J. Hydrol., **74**: 355-372.

Doorenbos, J. and Pruitt, W.O. 1977. Guidelines for predicting crop water requirements. FAO Irrig. and Drain. Paper No. 24. Rome: FAO.

Drexler, J.Z., Snyder, R.L., Spano, D. and Paw, K.T. 2004. A review of models and micrometeorological methods used to estimate wetland evapotranspiration. Hydrol. Processes, **18**: 2071-2101.

Droogers, P. 2000. Estimating actual evapotranspiration using a detailed agro-hydrological model. Journal of Hydrology, **229 (1-2)**: 50-58.

El-Baroudy, I., Elshorbagy, A.**,** Carey, S., Giustolisi, O. and Savic, D. 2009. Comparison of Three Data-driven Techniques in Modelling Evapotranspiration Process. Journal of Hydroinformatics. In press.

Elshorbagy, A. 2006. Multicriterion decision analysis approach to assess the utility of watershed modeling for management decision. Water Resour. Res., **42**, W09407, doi:10.1029/2005WR004264.

Elshorbagy, A. and El-Baroudy, I., 2009. Investigating the Capabilities of Evolutionary Data-Driven Techniques Using the Challenging Estimation of soil Moisture Content. Extraordinary. Issue of the Journal of Hydroinformatics **11**(3-4): 237-251.

Elshorbagy, A. and Parasuraman, K. 2008. On the Relevance of Using Artificial Neural Networks For Estimating Soil Moisture Content. Journal of Hydrology, **362**(1-2): 1-18.

Elshorbagy, A., Jutla, A., Barbour, L., and Kells, J. 2005. System dynamics approach to assess the sustainability of reclamation of disturbed watersheds. Canadian Journal of Civil Engineering, **32**: 144-158.

Elshorbagy, A., Jutla, A., Kells, J. 2007. Simulation of the hydrological processes on reconstructed watersheds using system dynamics. Hydrological Sciences Journal, **52(3)**: 538-562.

Elshorbagy, A.**,** Simonovic, S.P. and Panu, U.S. 2000. Performance Evaluation of Artificial Neural Networks for Runoff Prediction. Journal of Hydrologic Engineering, ASCE, ***5*(4)**: 424-427.

Elshorbagy, A.**,** Simonovic, S.P. and Panu, U.S. 2002. Estimation of Missing Streamflow Data Using Principles of Chaos Theory. Journal of Hydrology, **255**(**1-4)**: 123-133.

FAO (Food and Agriculture Organization of the United Nations), 1990. Expert consultation on revision of FAO methodologies for crop water requirements, ANNEX V, FAO Penman-Monteith Formula, Rome, Italy.

Farge, M. 1992. Wavelet transforms and their applications to turbulence. Annu. Rev. Fluid Mech., **24**: 395–457.

Fausett, L. 1994. Fundamentals of neural networks. Prentice Hall, Englewood Cliffs, N.J.

Fauske, K.J. 2006. TikZ examples, http://www.texample.net/tikz/examples/neural-network, accessed on January 2010.

Flood, I. and Kartam, N. 1994. Neural networks in civil engineering. I: Principles and understandings. J. Comp. in Civ. Engr. ASCE., **8(2)**: 131–148.

Flood, I. and Kartam, N. 1997. Systems. In I. Flood and J. H. Garrett Jr., Editors, Artificial Neural Networks for Civ. Engrs.: Fundamentals and Applications, Kartam, ASCE, New York: 19–43.

Fogel, L.J. 1962. Autonomous automata. Ind. Res., **4**: 14–19.

Forrest, S. and Mitchell, M. 1993. What makes a problem hard for a genetic algorithm? Some anomalous results and their explanation. Mach. Learn., **13**: 285–319.

Foufoula-Georgiou, E. and Kumar, P. 1994. Wavelets in Geophysics. Academic press, San Diego, Calif.

French, M.N., Krajewski, W.F., and Cuykendal, R.R. 1992. Rainfall forecasting in space and time using a neural network. J. Hydrol., **137**: 1–37.

Friedberg, R.M. 1958. A learning machine: Part I. IBM J., **2(1)**: 2–13.

Friedberg, R.M., Dunham, B., and North, J.H. 1959. A learning machine: Part II. IBM J., **3(7)**: 282–287.

Gamage, N. and Blumen, W. 1993. Comparative analysis of low level cold fronts: wavelet, Fourier, and empirical orthogonal function decompositions. Monthly Weather Review, **121**: 2867–2878.

Gang, L., Liu, J., Rong, Z., and Zhang, Q. 2008. Analysis of periodical variation of Lancang river base on wavelet transform. Journal of Computer engineering and application, **44(7)**: 236-237.

Gaucherel, C. 2002. Use of wavelet transform for temporal characterisation of remote watersheds. Journal of Hydrology, **269(3-4)**: 101–121.

Gavin, H. and Agnew, C.A. 2004. Modelling actual, reference and equilibrium evaporation from a temperate wet grassland. Hydrol. Proc., **18 (2)**: 229–246.

Gilley, J.E., Gee, G.W., Bauer, A., Willis, W.O., and Little, R.A. 1977. Runoff and erosion characteristics of surface mined sites in western North Dakota. Transactions of American Society of Agricultural Engineers, **20(4)**: 697-704.

Giustolisi, O. 2004. Using genetic programming to determine Chezy resistance coefficient in corrugated channels, J. Hydroinform, **6(3)**: 157–173.

Goldberg, D.E. 1985. Genetic algorithms and rule learning in dynamic system control. Proceedings, 1st Int. Conf. on Genetic Algorithms and Their Applications, Hillsdale, NJ.

Goldberg, D.E. 1989. Genetic Algorithms in Search, Optimization and Machine Learning. Addison-Wesley, Reading, MA.

Goldberg, D.E., Deb, K., Kargupta, H., and Harik, G. 1993. Rapid, accurate optimization of difficult problems using fast messy genetic algorithms. Proceedings, 5th Int. Conf. on Genetic Algorithms, San Mateo, CA.

Govindaraju, R.S. 2000. Artificial Neural networks in Hydrology. I: Preliminary Concepts. Journal of Hydrologic Engineering, **5(2)**: 115-123.

Granger, R.J. and Gray, D.M. 1989. Evaporation from natural non-saturated surface. J. Hydrol., **111**: 21–29.

Graps, A. 1995. An introduction to wavelets. Computational Science & Engineering, IEEE, **2(2)**: 50-61.

Grefenstette, J.J. 1986. Optimization of control parameters for genetic algorithms. IEEE Trans. Syst., Man Cybern., SMC-**16(1)**: 122–128.

Grindley J. 1969. The calculation of actual evaporation and soil moisture deficit over specified catchment areas. Hydrol. Mere., **38**. Meteorological Office, Bracknell, Berkshire.

Grinsted, A., Moor, J.C., and Jevrejeva, S 2004. Application of the cross wavelet transform and wavelet coherence to geophysical time series. Nonlinear Processes in Geophysics, **11**: 561-566.

Gu, D. and Philander, S.G. 1995. Secular changes of annual and interannual variability in the tropics during the past century. Journal of Climate, **8**: 864–876.

Guitjens, J.C. 1982. Models of Alfalfa Yield and Evapotranspiration. Journal of the Irrigation and Drainage Division, Proceedings of the American Society of Civil Engineers, **108(IR3)**: 212–222.

Gupta, V.K. and Waymire, E. 1990. Multiscaling properties of spatial rainfall and river flow distribution. Journal of Geophysical Research, **95**: 1999−2009.

Guven, A., Azamathulla, H.Md., and Zakaria, N.A. 2009. Linear genetic programming for prediction of circular pile scour. Ocean Eng., **36(12-13)**: 985-991.

Guyodo, Y., Gaillot, P., and Channell, J.E.T. 2000. Wavelet analysis of relative geomagnetic paleointensity at ODP Site 983. Earth and Planetary Science Letters, **184**: 109–123.

Haigh, M.J. 2000. The aim of land reclamation. Land Reconstruction and Management, A.A.Balkema Publishers, Rotterdom, The Netherlands, **1**:1-20.

Harbeck Jr., G.E. 1962. A Practical Field Technique for Measuring Reservoir Evaporation Utilizing Mass-transfer Theory. U.S. Geol. Surv., **272-E**: 101–105.

Hargreaves, G.H. and Samani, Z.A. 1985. Reference crop evapotranspiration from temperature. Applied Engineering in Agriculture, **1**: 96-99.

Hasselmann, K. 1976. Stochastic climate models: part I. theory. Tellus, **28(6)**: 473–85.

He, Y., Guo, R., and Si, B.C. 2007. Detecting grassland spatial variation by a wavelet approach. Int. J. Remote Sens., **28**:1527–1545.

Hettiarachchi, P., Hall, M.J., and Minns, A.W. 2005. The extrapolation of artificial neural networks for the modelling of rainfall-runoff relationships. J. Hydroinformatics, **7(4)**: 291–296.

Holland, J.H. 1962. Outline for a logical theory of adaptive systems. J. Assoc. Comput. Mach., **3**: 297–314.

Holland, J.H. 1975. Adaptation in Natural and Artificial Systems. Univ. of Michigan Press, Ann Arbor, MI.

Holland, J.H. and Reitman J.S. 1978. Cognitive systems based on adaptive algorithms. In D.A. Waterman and F. Hayes-Roth, Editors, Pattern-Directed Inference Systems, Academic Press, New York: 313-329.

Hong, Y.S. and Rosen, M.R. 2002. Identification of an urban fractured-rock aquifer dynamics using an evolutionary self-organizing modeling. Journal of Hydrology, **259(1-4)**: 89-104.

Hong, Y.S.T., White, P.A., and Scott, D.M. 2005. Automatic rainfall recharge model induction by evolutionary computational intelligence. Water Resour. Res., 41, W08422, doi:10.1029/2004WR003577.

Hopfield, J.J. 1982. Neural networks and physical systems with emergent collective computational abilities. Proceedings, Nat. Academy of Sciences of the United States of America, **79**: 2554-2558.

Hornik, K., Stinchcombe, M., and White, H. 1989. Multilayer feedforward networks are universal approximators. Neural Networks, **2(5)**: 359–366.

Hsu, K., Gupta, H.V., Sorooshian, S., and Gao, X. 1996. An artificial neural network for rainfall estimation from satellite infrared imaginary. Proceedings, 3rd Int. Workshop

on Applications of Remote Sensing in hydrol., NHRI Symp. No. 17, NASA, Greenbelt, Md.

Hsu, K., Gao, X., Sorooshain, S., and Gupta, H.V. 1997. Precipitation estimation from remotely sensed information using artificial neural networks. J. Appl. Meteorology, **36(9)**: 1176–1190.

Huang, W., Xu, B., and Chad-Hilton, A. 2004. Forecasting flows in Apalachicola River using neural networks. Hydrol. Processes, **18(13)**: 2545–2564.

Hutton, P.H., Sandhu, N., and Chung, F.I. 1996. Predicting THM formation with artificial neural networks. Proceedings, North Am. Water and Envir. Conf., ASCE, New York.

HYDRUS-1D Software Package User's Manual, 2008. Department of Environmental Sciences, University of California Riverside, Riverside, USA.

Irmak, S. and Haman D.Z. 2003. Evapotranspiration: Potential or Reference? (ABE 343), Lecture notes, Agricultural and Biological Engineering Department, Florida Cooperative Extension Service, Institute of Food and Agricultural Sciences, University of Florida. Gainesville, FL, USA.

Izadifar, Z. and Elshorbagy, A. 2010. Prediction of hourly actual evapotranspiration using neural networks, genetic programming, and statistical models. Hydrological Processes, in press, DOI: 10.1002/hyp.7771.

Jackson, R.D. 1985. Evaluating evapotranspiration at local and regional scales. Proceedings, IEEE, Geoscience and Remote Sensing Society, **73(6)**: 1086–1096.

Jain, A.K., Jianchang, M., and Mohiuddin, K.M. 1996. Artificial Neural Networks: A Tutorial. IEE Computer Society, **29(3)**: 31-44.

Jain, S.K., Nayak, P.C., and Sudheer, K.P. 2008. Models for estimating evapotranspiration using artificial neural networks, and their physical interpretation. Hydrological Processes, **22(13)**: 2225-2234.

Jenkins, G.M. and Watts, D.G. 1968. Spectral Analysis and Its Applications. Holden-Day, USA.

Jensen, M.E. and Haise, H.R. 1963. Estimation of Evapotranspiration from Solar Radiation. Journal of Irrigation and Drainage Division, Proc. Amer. Soc. Civil Eng. **89**: 15–41.

Jensen, M.E. and Allen, R.G. 2000. Evolution of practical ET estimating methods. Proceedings. 4th National Irrigation Symposium, St. Joseph, Mich., ASAE: 52−65.

Jensen, M.E., Burman, R.D., and Allen, R.G. 1990. Evapotranspiration and Irrigation Water Requirements. ASCE Manual and Reports on Engineering Practice No. 70, Am. Soc. Civil Engr., New York.

Jothiprakash, V., Ramachandran, M.R., and Shanmuganathan, P. 2002. Artificial neural network model for estimation of REF-ET. Journal of the Institution of Engineers (India), Part CV, Civil Engineering Division, **83(1)**: 17-20.

Ju, Q., Yu, Z., Hao, Z., She, C., Ou, G., and Liu, D. 2008. Streamflow Simulation with an Integrated Approach of Wavelet Analysis and Artificial Neural Networks. Proceedings, 4th International Conference on Natural Computation (ICNC 2008), Jinan, China.

Jutla, A. 2006. Hydrological modeling of reconstructed watersheds using a system dynamic approach. M.Sc Thesis, University of Saskatchewan, Saskatoon, SK, Canada.

Jutla, A., Elshorbagy, A., and Kells, J. 2006. Simulation of the hydrological processes on reconstructed watershed using system dynamics. Center for Advance Numerical Simulation (CNASIM) series report No. CAN-06-01.

Kaheil, Y.H., Rosero, E., Gill, M.K., McKee, M., and Bastidas, L.A. 2008. Downscaling and forecasting of evapotranspiration using a synthetic model of wavelets and support vector machines. IEEE Trans. Geosci.Remote Sens., **46(9)**: 2692-2707.

Kang, K.W., Kim, J.H., Park, C.Y., and Ham, K.J. 1993. Evaluation of hydrological forecasting system based on neural network model. Proceeding, 25th Congress of Int. Assoc. for Hydr. Res., International Association for Hydraulic Research, Delft, The Netherlands.

Karunanithi, N., Grenney, W.J., Whitley, D., and Bovee, K. 1994. Neural networks for river flow prediction. J. Comp. in Civ. Engr., ASCE, **8(2)**: 201–220.

Keshta, N. and Elshorbagy, A. 2009. A comparative Application of SWAT and a System Dynamics Watershed Model Using a Lumped Set of Data. Proceeding, the 33rd IAHR Congress, Vancouver, Canada.

Keshta, N., Elshorbagy, A**.,** and Carey, S. 2009. A Generic System Dynamics Model For Simulating and Evaluating the Hydrological Performance of Reconstructed Watersheds. Hydrology and Earth System Sciences**, 13(6)**: 865-881.

Khu, S.T., Liong, S.Y., Babovic, V., Madsen, H., and Muttil, N. 2001. Genetic programming and its application in realtime runoff forecasting. J. Am. Water Resour. Assoc., ASCE, **8(2)**: 201–220.

Kim. T.W. and Valdes, J.B. 2003. Nonlinear model for drought forecasting based on a conjunction of wavelet transforms and neural networks. Journal of hydrologic engineering, **8(6)**: 319-328.

Kirkup, H., Pitman, A.J., Hogan, J., and Brierley, G. 2001. An initial analysis of river discharge and rainfall in Coastal New South Wales, Australia, using wavelet transforms. Australian Geographical Studies, **39(3)**: 313-334.

Kisi, O. 2006. Evapotranspiration estimation using feed-forward neural networks. Nordic Hydrol., **37(3)**: 247-260.

Kizhisseri, A.S., Simmonds, D., Rafiq, Y., and Borthwick, M. 2005. An Evolutionary computation approach to sediment transport modeling. Proceedings, 5th International Conference on Coastal Dynamics, April 4–8, Barcelona, Spain.

Koerselman, W. and Beltman, B. 1988. Evapotranspiration from fens in relation to Penman's potential free water evapotranspiration (E_o) and pan evaporation. Aquatic Botany, **31**: 307-320.

Koza, J.R. 1989. Hierarchical genetic algorithms operating on populations of computer programs. Proceedings, 11th Int. Joint Conf. on Artificial Intelligence, N.S. Sridharan, Ed. San Mateo, CA.

Koza, J.R. 1992. Genetic Programming: On the Programming of Computers by Means of Natural Selection. MIT Press, Cambridge, MA.

Kuligowski, R.J. and Barros, A.P. 1998. Experiments in short-term precipitation forecasting using artificial neural networks. Monthly Weather Rev., **126(2)**: 470–482.

Kumar, M., Bandyopadhyay, A., Raghuwanshi, N.S., and Singh, R. 2008. Comparative study of conventional and artificial neural netwrok-based ET_o estimation models. Irrig. Sci., **26(6)**: 531-545.

Kumar, M., Raghuwanshi, N.S., Singh, R., Wallender, W.W., and Pruitt, W.O. 2002. Estimating evapotranspiration using artificial neural network. Journal of Irrigation and Drainage Engineering, **128(4)**: 224-233.

Kumar, P. and Foufoula-Georgiou, E. 1993a. A multicomponent decomposition of spatial rainfall fields 1. Segregation of large-and small-scale features using wavelet transforms. Water Resources Research, **29(8)**: 2515−2532.

Kumar, P. and Foufoula-Georgiou, E. 1993b. A multicomponent decomposition of spatial rainfall fields 1. Self-similarity in fluctuations. Water Resources Research, **29(8)**: 2533−2544.

Kumar, P. and Foufoula-Georgiou, E. 1997. Wavelet analysis for geophysical applications. Rev. Geophys., **35(4)**: 385–412.

Labat, D. 2005. Recent advances in wavelet analyses: Part 1. A review of concepts. J Hydrol., **314**: 275–288.

Labat, D. 2006. Oscillations in land surface hydrological cycle. Earth and Planetary Science Letters, **242(1-2)**: 143-154.

Labat, D. 2008. Wavelet analysis of the annual discharge records of the world's largest rivers. Adv. Water Resour., **31(1)**:109-117.

Labat, D., Ababou, R., and Mangin, A. 2000. Rainfall–runoff relations for karstic springs. Part II: Continuous wavelet and discrete orthogonal multiresolution analyses. Journal of Hydrology, **238**: 149–178.

Labat, D., Ronchail J., and Guyot, J.L. 2005. Recent advances in wavelet analyses: Part 2 – Amazon, Parana, Orinoco and Congo discharges time scale variability. J Hydrol., **314(1–4)**: 289–311.

Labat, D., Ronchail, J., Callede, J., Guyot, J.L., De Oliveria, E., and Guimaraes, W. 2004. Wavelet analysis of Amazon hydrological regime variability. Geophysical Research Letter, **31**, L02501. doi:10.1029/2003GL018741.

Lachtermacher, G. and Fuller, J.D. 1994. Backpropagation in hydrological time series forecasting. In K.W. Hipel, A.I. MacLeod, U.S. Panu and V.P. Singh, Editors., Stochastic and Statistical Methods in Hydrology and Environmental Engineering, Vol. 3, Time Series Analysis in Hydrology and Environmental Engineering, Kluwer Academic, Dordrecht: 229–242.

Lafreniere, M. and Sharp, M. 2003. Wavelet analysis of inter-annual variability in the runoff regimes of glacial and nival stream catchments, Bow Lake, Alberta. Hydrological Processes, **17(6)**: 1093–1118.

Landeras, G., Ortiz-Barredo, A., and Lopez, J.J. 2008. Comparison of artificial neural network models and empirical and semi-empirical equations for daily reference evapotranspiration estimation in the Basque Country (Northern Spain). Agricultural Water Management, **95(5)**: 553-565.

Lange, N.T. 1999. New Mathematical Approaches in Hydrological Modeling- An Application of Artificial Neural Networks. Phys. Chem. Earth (b), **24(1-2)**: 31-35.

Lau, K.M. and Weng, H.Y. 1995. Climate signal detection using wavelet transform: How to make a time series sing. Bull. Amer. Meteor. Soc., **76(12)**: 2391–2402.

Laverty, W. 2009. Statistical methods in research (STAT 845), Lecture notes, Department of Mathematics and Statistics, University of Saskatchewan, SK, Canada.

Levenberg, K. 1944. A method for the solution of certain problems in least squares. Quart. Appl. Math. **2**: 164–168.

Linacre, E.T. 1976. Swamps. Vegetation and Atmosphere, In J.L. Monteith (Editor), Vol. 2: Case Studies. Academic Press, London: 329-347.

Liong, S.Y., Gautam, T.R., Soon, T.K. Babovic, V., Keijzer, M., and Muttil, N. 2002. Gentic Programming: A new paradigm in rainfall runoff modeling. Journal of American Water Resources Associatio, **38(3)**: 705-718.

Lui, A.T.Y. 2002. Multiscale phenomena in the near-Earth magnetosphere. Journal of Atmospheric and Solar-Terrestrial Physics, **64**: 125–143.

MacKay, D. 1992. A practical bayesian framework for backproparation networks. Neural Computation, **4(3)**: 448-472.

Maier, H.R. and Dandy, G.C. 1996. The use of artificial neural networks for the prediction of water quality parameters. Water Resour. Res., **32(4)**: 1013–1022.

Maier, H.D. and Dandy, G.C. 2000. Neural network for the prediction and forecasting of water resource variables: a review of modeling issues and applications. Environmental Modelling & Software, **15**: 101–124.

Maier, H.R. and Dandy. G.C. 2001. Neural network based modelling of environmental variables: A systematic approach. Mathematical and Computer Modelling, **33(6-7)**: 669-682.

Makkeasorn, A., Chang, N.B., and Zhou, X. 2008. Short-term streamflow forecasting with global climate change implications – A comparative study between genetic programming and neural network models. Journal of Hydrology, **352(3-4)**: 336-354.

Makkeasorn, A., Chang, N.B., Beaman, M., Wyatt, C., and Slater, C. 2006. Soil moisture estimation in a semiarid watershed using RADARSAT-1 satellite imagery and genetic programming. Water Resource Research, **42(9)**: W09401.1-W09401.15.

Makkink, G.F. 1957. Testing the Penman Formula by Means of Lysimeters. J. Instit. Water Engineers, **11**: 277–288.

Mallat, S. 1989. Multiresolution approximations and wavelet orthonormal bases of L^2(R).Transaction of the American Mathematical Society, **315(1)**: 69-87.

Marquardt, D. 1963. An algorithm for least squares estimation of non-linear parameters. J. Ind. Appl. Math. **11(2)**: 431–441.

MATLAB software, Version [6.5.1]. Copyright © 1994-2009. MathWorks, Inc., 3 Apple Hill Drive, Natick, MA, USA.

McCulloch, W.S. and Pitts, W. 1943. A logical calculus of the ideas imminent in nervous activity. Bulletin of Mathematical Biophysics, **5**: 115–33.

McNamara. J. 2009. Hydrology (GEOL/CE/GEOPH 416/516), Lecture notes, Department of Geosciences, Boise State University, Idaho, USA.

Meyer, Y. 1993. Wavelet and Operators. Cambridge University Press, Cambridge, U.K.

Miao, C.Y., Wang, Y.F., and Zheng, Y.Z. 2007. Wavelet-based analysis of characteristics of summer rainfall in Nenjiang and Harbin. Journal of Ecology and Rural Environment, **23(4)**: 29-32.

Minnes, A.W. and Hall, M.J. 1996. Artificial neural networks as rainfall-runoff models. Hydrol. Sci. J., **41(3)**: 399–416.

Minsky, M. and Papert, S. 1969. Perceptrons: An lntroduction to Computational Geometry. MIT Press, Cambridge, Mass.

Mitchell, M. 1996. An Introduction to Genetic Algorithms. MIT Press, Cambridge, MA.

Monteith, J.L. 1965. Evaporation and environment. In: The State and Movement of Water in Living Organisms. XIXth Symposium of the Society of Experimental Biology, Cambridge University Press, Swansea: 205–234.

Monteith, J.L. 1973. Principles of Environmental Physics. Edward Arnold, London.

Monteith, J.L. 1981. Evaporation and surface temperature. Quarterly J. Royal Meteo. Soc., **107**: 1-27.

Monteith, J.L. and Unsworth, M.H. 1990. Principles of Environmental Physics, Edward Arnold, London.

Muttiah, R.S., Srinivasan, R., and Allen, P.M. 1997. Prediction of two-year peak stream discharges using neural networks. J. Am. Water Resour. Assoc., **33(3)**: 625–630.

Nagy, H.M., Watanabe, K., and Hirano, M. 2002. Prediction of Sediment Load Concentration in Rivers using Artificial Neural Network Model. J. Hydraul. Eng., **128(3)**: 588–595.

Neural Network Toolbox User's Guide, 2009. MathWorks, Inc., 3 Apple Hill Drive, Natick, MA, USA.

O'Kane, M., Wilson, G.W., and Barbour, S.L. 1998. Instrumentation and monitoring of an engineered soil cover system for mine waste rock. Canadian Geotechnical Journal, **35**: 828-846.

Obukhov, A.M. 1946. Turbulence in an atmosphere of non-homogenus temperature, Trans. Inst. Theor. Geophys. USSR, **1**: 95-115.

Parasuraman, K. 2007. Hydrological prediction using pattern recognition and soft-computing techniques. Ph.D Thesis, University of Saskatchewan, Saskatoon, SK, Canada.

Parasuraman, K., Elshorbagy, A., and Carey, S.K. 2006. Spiking modular neural networks: A neural network modeling approach for hydrological processes. Water Resour. Res., **42**, W05412, doi:10.1029/2005WR004317.

Parasuraman, K., Elshorbagy, A., and Carey, S.K. 2007. Modeling the dynamics of the evapotranspiration process using genetic programming, Hydrological Sciences Journal, **52**: 563-578.

Parasuraman, K. and Elshorbagy, A. 2008. Toward improving the reliability of hydrologic prediction: Model structure uncertainty and its quantification using ensemble-based genetic programming framework. Water Resour. Res., 44, W12406, doi:10.1029/2007WR006451.

Partal, T. and Cigizoglu H.K. 2008. Estimation and forecasting of daily suspended sediment data using wavelet-neural networks. Journal of hydrology, **358(3-4)**: 317-331.

Pauwels V.R.N. and Samson, R. 2006. Comparison of different methods to measure and model actual evapotranspiration rates for a wet sloping grassland. Agricultural Water Management, **82**: 1-24.

Penman, H.L. 1948. Natural evapotranspiration from open-water, bare soil and grass. Proc. R. Soc. Acad., **193**: 120-145.

Poff, N.L., Tokar, S., and Johnson, P. 1996. Steam hydrological and ecological responses to climate change assessed with an artificial neural network. Limnol. and Oceanog., **41(5)**: 857–863.

Polikar, P. 1996. The wavelet tutorial, http://www.site.uottawa.ca/~qingchen/wavelet/p2.htm, accessed on July 2008.

Poulovassilis, A., Anadranistakis, M., Liakatas, A., Alexandris, S., and Kerkides, P. 2001. Semi-emprical approach for estimating actual evapotranspiration in Greece. Agricultural Water Management, **51**: 143–152.

Priestley, C.H.B. and Taylor, R.J. 1972. On the assessment of surface heat flux and evaporation using large-scale parameters. Mon. Weather Rev., **100**: 81-92.

Ranjithan, S., Eheart, J.W., and Rarret Jr., J.H. 1993. Neural networkscreening for groundwater reclamation under uncertainty. Water Resour. Res., **29(3)**: 563–574.

Rechenberg, I. 1965. Cybernetic solution path of an experimental problem, Royal Aircraft Establishment, Library translation No. 1122, Farnborough, Hants., U.K.

ReliaSoft's DOE++ software User's Guide, 2008. ReliaSoft Corporation, Worldwide Headquarters, Eastside Loop. Tucson, USA. http://www.weibull.com/DOEWeb/multiple_linear_regression_analysis.htm, accessed on February, 2010.

Riad, S., Mania, J., Bouchaou, L., and Najjar, Y. 2004. Predicting catchment flow in a semi-arid region via an artificial neural network technique, Hydrol. Processes, **18(13)**: 2387–2393.

Rick, G. 1995. Closure consideration in environmental impact statements. Mineral Industry International, **1022**: 5-10.

Rizzo, D.M. and Dougherty, D.E. 1994. Characterization of aquifer properties using artificial neural networks: neural kriging. Water Resour.Res., **30(2)**: 483–497.

Rogers, L.L. 1992. Optimal groundwater remediation using artificial neural network and the genetic algorithm. PhD disertation, Stanford University, Stanford, Calif.

Rogers, L.L. and Dowla, F.U. 1994. Optimization of groundwater remediation using artificial neural networks with parallel solute transport modeling. Water Resour. Res., **30(2)**: 457–481.

Rohwer, C. 1931. Evaporation from Free Water Surface. USDA Tech. Null., **217**: 1–96.

Rumelhart, D.E. and McClelland, J.L., editors. 1986. Parallel distributed processing: explorations in the microstructures of cognition. Vol. 1., MIT Press, Cambridge, MA.

Russo. D, Bresler, E., Shani, U., and Parker J.C. 1991. Analysis of infiltration events in relation to determining soil hydraulic properties by inverse problem, methodology. Water Resour. Res. **27**:1361-1373.

Saco, P. and Kumar, P. 2000. Coherent modes in multiscale variability of streamflow over the United States. Water Resour.Res., **36(4)**: 1049-1067.

Salerno, F. and Tartari, G. 2009. A coupled approach of surface hydrological modelling and Wavelet Analysis for understanding the baseflow components of river discharge in karst environments. Journal of hydrology, **376 (1-2)**: 295-306.

Sanchez-Carrillo, S., Alvarez-Cobelas, M., and Benitez, M. 2001. A simple method for estimating water loss by transpiration in wetlands. Hydrological Sciences, **46** (4): 537-552.

SAS/STAT software, Version [9.1] of the SAS System for Windows. Copyright © 2002-2003 SAS Institute Inc. SAS and all other SAS Institute Inc. product or service names are registered trademarks or trademarks of SAS Institute Inc., Cary, NC, USA.

Savic, A.D., Walters, A.G., Davidson, J.W., 1999. A genetic programming approach to rainfall-runoff modeling, Water Resour. Manage. **13**: 219–231.

Schaefli, B., Maraun, D., and Holschneider, M. 2007. What drives high flow events in the Swiss Alps? Recent developments in wavelet spectral analysis and their application to hydrology. Advances in Water Resources, **30(12)**: 2511-2525.

Schalkoff, R.J. 1997. Artificial neural networks. McGraw-Hill, N.Y.

Schmuller, J. 1990. Neural networks and environmental applications. In Expert systems for environmental applications. (Hushon, J.M., ed.), American Chemical Society, Washington, D.C.

Schwefel, H.P. 1968. Project MHD-ramjet pipe: Experimental optimization of a Zweiphasend use, Part 1, Technical report 11.034/68, 35, AEG Forschungsinstitut, Berlin, Germany.

Senthil Kumar, A.R., Sudheer, K.P., Jain, S.K., and Agarwal, P.K. 2005. Rainfall-runoff modelling using artificial neural networks: comparison of network types. Hydrol. Processes, **19(3)**: 1277–1291.

Sette, S. and Boullart, L. 2001. Genetic programming: principles and applications. Engineering Application of Artificial Intelligence, **14**: 727-736.

Shurniak, R.E. 2003. Predictive modeling of moisture movement within soil cover systems for saline/sodic overburden piles. M.Sc. Thesis, University of Saskatchewan, Saskatoon, SK, Canada.

Shuttleworth, W.J. and Wallace, J.S, 1985. Evaporation from sparse crops — an energy combination theory. Quart. J. R. Meteorol. Soc., **111**: 839–855.

Si, B.C. 2003. Spatial and scale-dependent soil hydraulic properties: A wavelet approach. In Ya. Pachepsky et al., Editors, Scaling methods in soil physics. CRC Press, New York: 163–178.

Si, B.C. 2008. Spatial Scaling Analyses of Soil Physical Properties: A Review of Spectral and Wavelet Methods. Vadose Zone Journal, **7(2)**: 547-562.

Si, B.C. 2009. Personal correspondence.

Si, B.C. and Zeleke T.B. 2005. Wavelet coherency analysis to relate saturated hydraulic properties to soil physical properties. Water Resour Res., **41(11)**: W11424. doi:10.1029/2005WR004118.

Silva, S., 2005. GPLAB—a genetic programming toolbox for MATLAB. http://gplab.sourceforge.net.

Simunek, J., van Genuchten, M. T. and Sejna, M. 2006. The HYDRUS Software Package for Simulating the Two- and Three-Dimensional Movement of Water, Heat, and Multiple Solutes in Variable-saturated Media. University of California, Riverside, CA.

Sivapragasam, C., Vincent, P., and Vasudevan, G. 2007. Genetic programming model for forecast of short and noisy data. Hydrol. Process, **21(2)**: 266-272.

Slabbers, P.J. 1980. Practical Prediction of Actual Evapotranspiration. Irrigiation Science, **1**: 185- 196.

Smith, L.C., Turcotte, D.L., and Isacks, B.L. 1998. Stream flow characterization and feature detection using a discrete wavelet transform. Hydrological Processes, **12**: 233–249.

Starrett, S.K., Najjar, Y.M., and Hill, J.C. 1996. Neural networks predict pesticide leaching. Proceedings, American Water and Environment Conference, ASCE, New York.

Stephens, J.C. and Stewart, E.H. 1963. A comparison of procedures for computing evaporation and evapotranspiration. In Publication 62, International Association of Scientific Hydrology, International Union of Geodesy and Geophysics, Berkeley, California, USA: 123–133.

Stewart, J.B. 1989. On the use of the Penman-Monteith equation for determining areal evapotranspiration. In T.A. Black et al., Editors, Estimation of Areal evapotranspiration. Wallingford, Oxon., U.K., International Association of Hydrological Sciences Publications **177**: 3-12.

Strangeways, I. 2003. Measuring the Natural Environment. Cambridge University Press, Cambridge, UK.

Sudheer, K.P., Gosain, A.K., and Ramasastri, K.S. 2003. Estimating actual evapotranspiration from limited climatic data using neural computing technique. Journal of Irrigation and Drainage Engineering, ASCE, **129**: 214-218.

Swingler, K. 1996. Applying neural networks: A practical guide, Academic press, London.

Taylor, J.G. (ed.) 1996. Neural networks and their applications. Wiley, Chichester, U.K.

Thirumalaian, K. and Deo, M.C. 1998. River stage forecasting using artificial neural networks. J. Hydrol. Engng., **3(1)**: 26–32.

Thornthwaite, C.W. 1948. An approach toward a rational classification of climate. Geography Rev., **38(1)**: 55-94.

Tohma, S. and Igata, S. 1994. Rainfall estimation from GMS imagery data using neural networks. In W.R. Blain and K.L. Katsifarakis, Editors, Hydraulic engineering software V, Vol. 1, Computational Mechanics, Southampton, U.K.: 121–130.

Tokar, A.S. and Johnson, P.A. 1999. Rainfall-runoff modeling using artificial neural networks. ASCE, J. Hydrol. Engng., **4(3)**: 232–239.

Torrence, C. and Compo, G.P. 1998. A practical guide to wavelet analysis. Bull. Am. Met. Soc., **79**: 61-78.

Trajkovic, S. 2005. Temperature-based approaches for estimating reference evapotranspiration. ASCE, Journal of Irrigation and Drainage Engineering, **131(4)**: 316–323.

Trajkovic, S., Todorovic B., and Stankovic, M. 2003. Forecasting reference evapotranspiration by artificial neural networks. ASCE, Journal of Irrigation and Drainage Engineering, **129(6)**: 454–457.

Van Genuchten, M.Th. 1978. Mass transport in saturated-unsaturated media: one-dimensional solutions. Research Rep. No. 78-WR-11, Water Resources Program, Princeton Univ., Princeton, NJ.

Walter, I.A., Allen, R., Elliott,G.R., Itenfisu,D., Brown, P., Jensen, M.E., Mecham, B., Howell, T.A., Snyder, R., Echings, S., Spofford, T., Hattendorf, M., Martin, D., Cuenca, R.H. and Wright, J.L. 2001. The ASCE standardized reference evapotranspiration equation. Environmental and Water Resources Institute (EWRI) of the ASCE. ASCE, Standardization of Reference Evapotranspiration Task Committee Report. Reston, Va.: ASCE.

Wang, J., Salvucci, G.D., Bras, R.L. 2004. An extremum principle of evaporation. Water Resour. Res. **40**, W09303,doi:10.1029/2004WR003087.

Wang, W.C., Chau, K.W., Cheng, C.T., and Qiu, L. 2009. A comparison of performance of several artificial intelligence methods for forecasting monthly discharge time series. Journal of Hydrology, **374(3-4)**: 294-306.

Wang, W.G. and Luo, Y.F. 2007. Wavelet network model for Reference Crop Evapotranspiration forecasting. Proceedings, International Conference on Wavelet Analysis and Pattern recognition, China.

Wang, Y., Traore, S., and Kerh, T. 2008. Neural network approach for estimating reference evapotranspiration from limited climatic data in Burkina Faso. WSEAS, Transactions on Computers, **7(6)**: 704-713.

Waymire, E., Gupta, V.K., and Rodriguez-lturbe, I. 1984. A spectral theory of rainfall intensity at meso-13 scale. Water Resources Research, **20**: 1453−1465.

Werbos, P. 1974. Beyond Regression: New tools for prediction and analysis in the behavioral sciences. PhD thesis, Dept. of Applied Mathematics, Harvard University, Cambridge, Mass.

Westra, S. and Sharma, A. 2006. Dominant modes of interannual variability in Australia rainfall analyzed using wavelets. Journal of Geophysical Research-part D: Atmospheres, **111(5)**: D05102, doi:10.1029/2005JD005996.

Whigham, P.A. and Crapper, P.F. 1999. Time series modeling using genetic programming: an application to rainfall-runoff models. In L. Spector et al., Editors, Advances in Genetic Programming, The MIT Press, Cambridge, MA: 89–104.

Whigham, P.A. and Crapper, P.F. 2001. Modeling rainfall-runoff using genetic programming. Math. Comput. Model., **33**: 707–721.

Wright, J.L. 1982. New evapotranspiration crop coefficients. J. of Irrig. and Drain. Div., **108(1)**: 57−74.

Wright, J.L. 1996. Derivation of alfalfa and grass reference evapotranspiration., Proceedings, International Conference on Evapotranspiration and Irrigation Scheduling, eds. C. R. Camp, E. J. Sadler, and R. E. Yoder. St. Joseph, Mich.: ASAE.

Xiaomei, S., Yueqing, X., and Changrong, Y. 2006. Wavelet analysis of rainfall variation in the Yellow River Basin. Acta Scientiarum Naturalium Universitatis Pekinensis, **42(4)**: 503-509.

Yang, C.C., Prasher, S.O., Lacroix, R., Sreekanth, S., Patni, N.K., and Masse, L. 1997. Artificial neural network model for subsurfacedrained farmland. J. Irrig. and Drain. Engrg., ASCE, **123(4)**: 285–292.

Yitian, L. and Gu, R.R. 2003. Modeling Flow and Sediment Transport in a River System Using an Artificial Neural Network. Environ. Manage., **31(1)**: 122–134.

Yokoyama, Y., Yamazaki, T. 2000. Geomagnetic paleointensity variation with a 100 kyr quasi-period. Earth and Planetary Science Letters, **181**: 7–14.

Zahner R. 1967. Refinement in empirical functions for realistic soil-moisture regines under forest cover. Stopper WE, Hull HW (eds) Forest hydrology. Pergamon Press, Oxford: 261–274.

Zanchettin, D., Traverso, P., and Tomasino, M. 2008. Po River discharges: A preliminary analysis of a 200-year time series. Climatic Change, **89(3-4)**: 411-433.

Zanetti, S.S., Sousa, E.F., Oliveira, V.P.S., Almeida, F.T., and Bernardo, S. 2007. Estimating evapotranspiration using artificial neural network and minimum climatological data. J. Irrig. and Drain. Engrg., **133(2)**: 83-89.

Zhu, M., Fujita, M., and Hashimoto, N. 1994. Application of neural networks to runoff prediction. In K.W. Hipel et al., Editors, Stochastic and statistical method in hydrology and environmental engineering, Vol. 3, Kluwer, Dordrecht, The Netherlands: 205–216.

Appendix A

Continuous wavelet transformation of meteorological variables of T_g, T_a, RH, and W_s for the scale range of 2 to 48 hours are presented here. In the following figures, the thick black contour lines enclose the areas in which the wavelet power is significant at the confidence level of 95%.

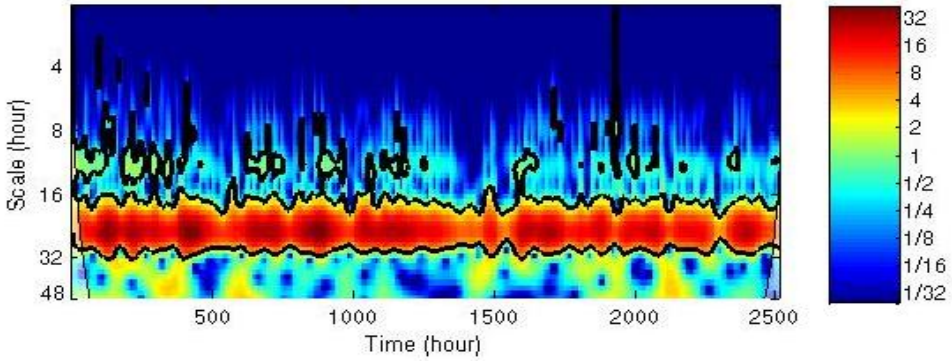

Figure A. 1. Continuous wavelet power spectrum of hourly T_g time series for the scale range of 2 to 48 hours. The thick black contours show the 95% confidence level against red noise.

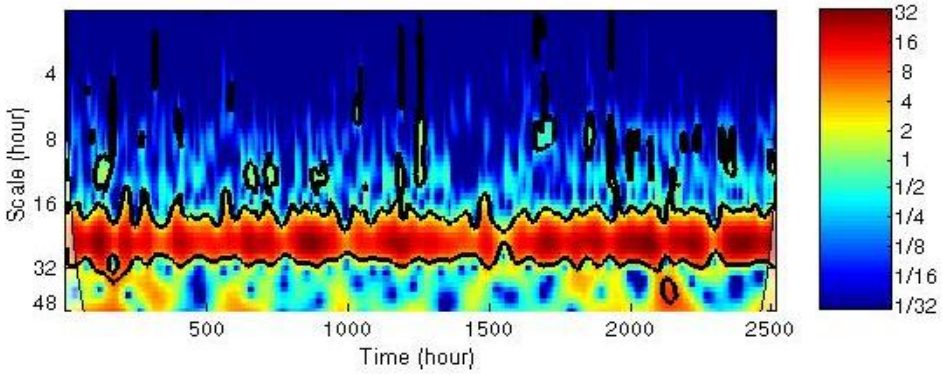

Figure A. 2. Continuous wavelet power spectrum of hourly T_a time series for the scale range of 2 to 48 hours. The thick black contours show the 95% confidence level against red noise.

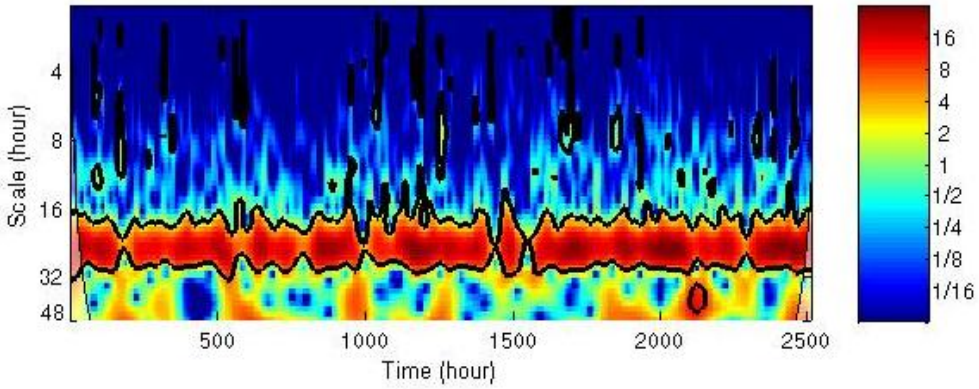

Figure A. 3. Continuous wavelet power spectrum of hourly *RH* time series for the scale range of 2 to 48 hours. The thick black contours show the 95% confidence level against red noise.

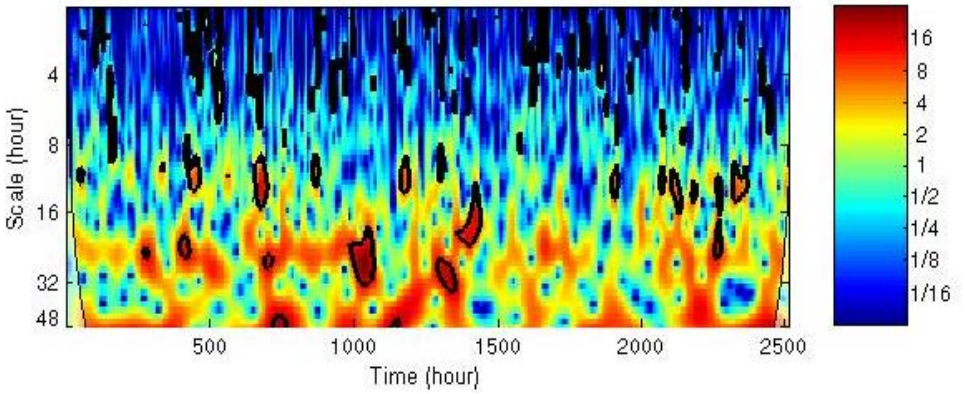

Figure A. 4. Continuous wavelet power spectrum of hourly W_s time series for the scale range of 2 to 48 hours. The thick black contours show the 95% confidence level against red noise.

Appendix B

A visual comparison between AET and meteorological time series of *RH*, W_s, T_a, and R_n for a typical time-window of 48 hours are presented here in the following figures.

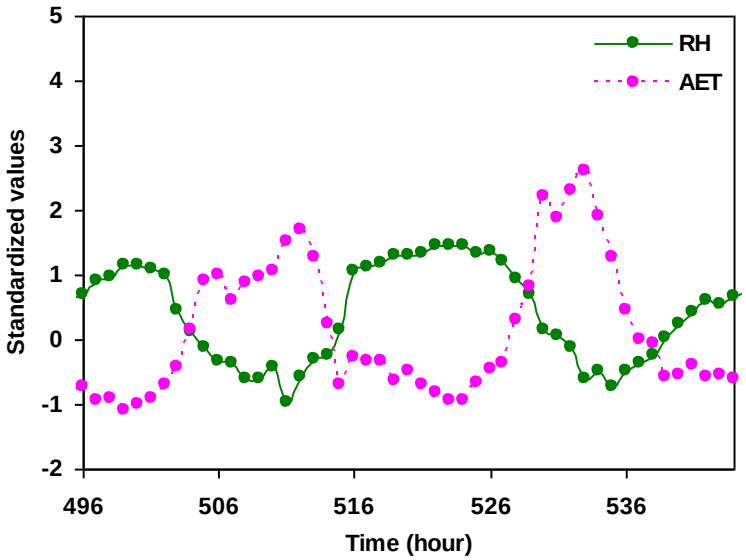

Figure B. 1. Time series of AET and *RH* for a typical time-window of 48 hours.

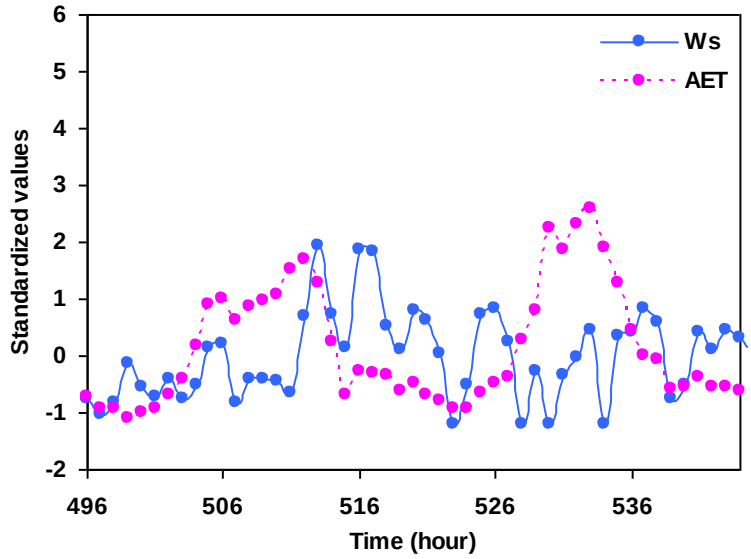

Figure B. 2. Time series of AET and W_s for a typical time-window of 48 hours.

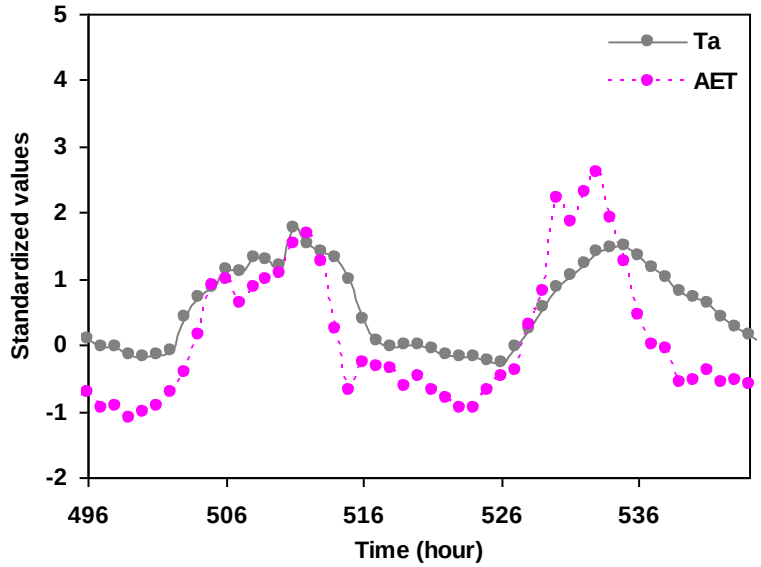

Figure B. 3. Time series of AET and T_a for a typical time-window of 48 hours.

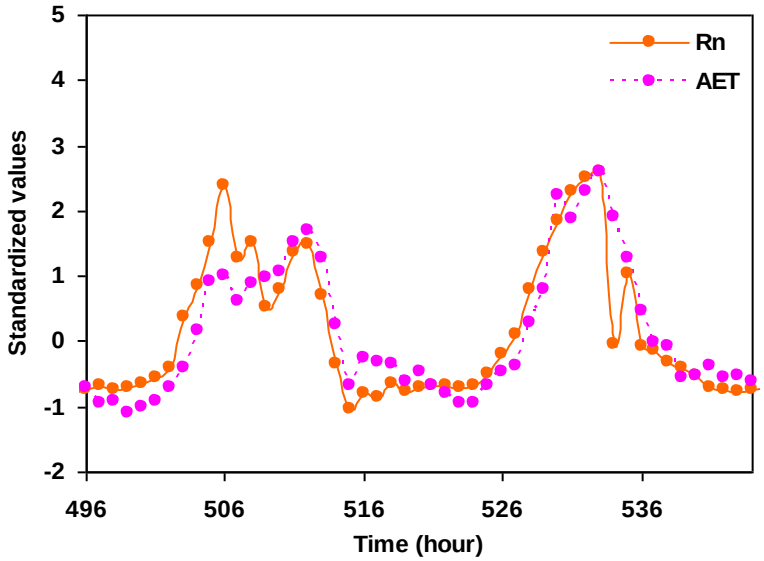

Figure B. 4. Time series of AET and R_n for a typical time-window of 48 hours.

Appendix C

Cross wavelet spectra of AET and the meteorological signals of R_n,T_g, RH, and W_s, for an extended range of scales of 2 to 48 hours are presented here in the following figures.

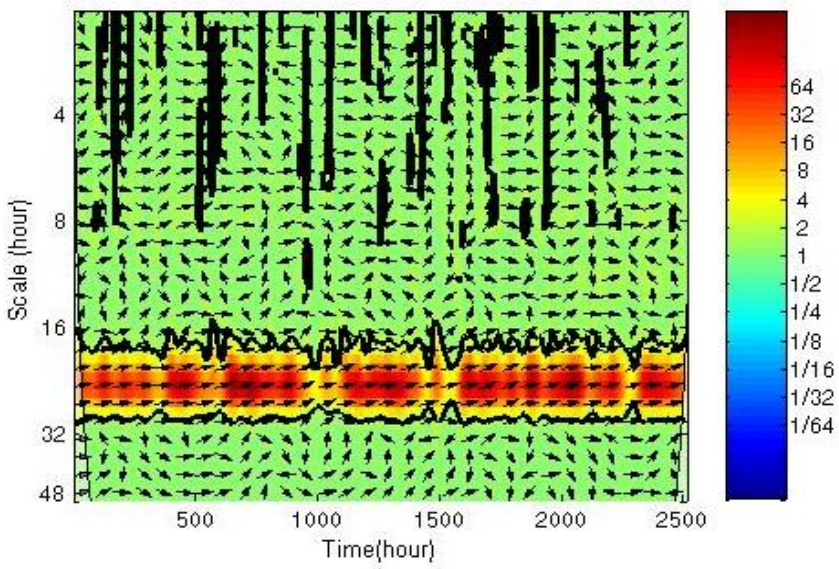

Figure C. 1. Cross wavelet spectrum between AET and R_n time series for the scale range of 2 to 48 hours.

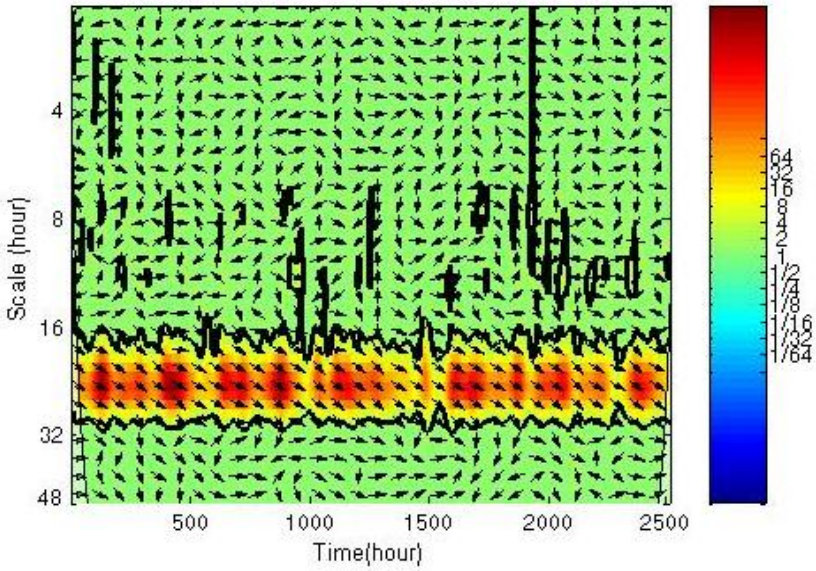

Figure C. 1. Cross wavelet spectrum between AET and T_g time series for the scale range of 2 to 48 hours.

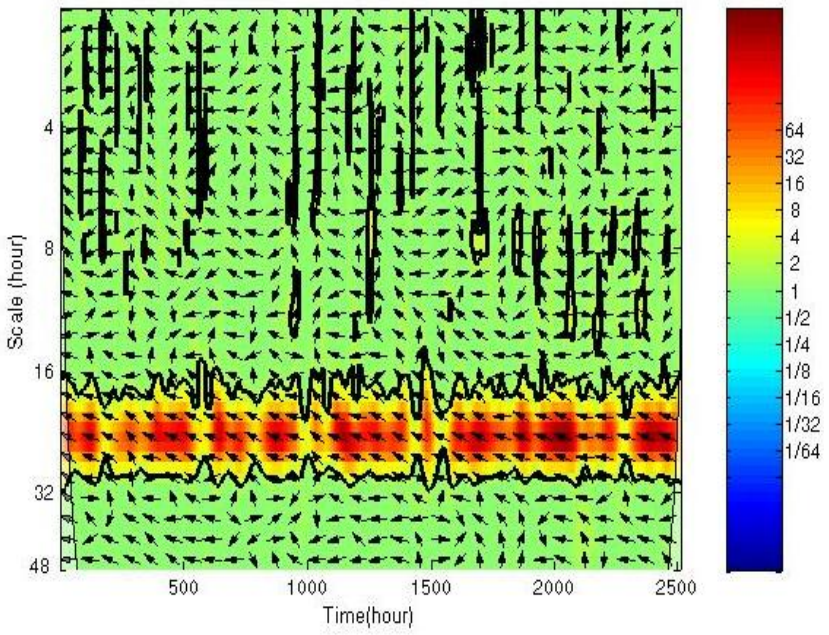

Figure C. 3. Cross wavelet spectrum between AET and *RH* time series for the scale range of 2 to 48 hours.

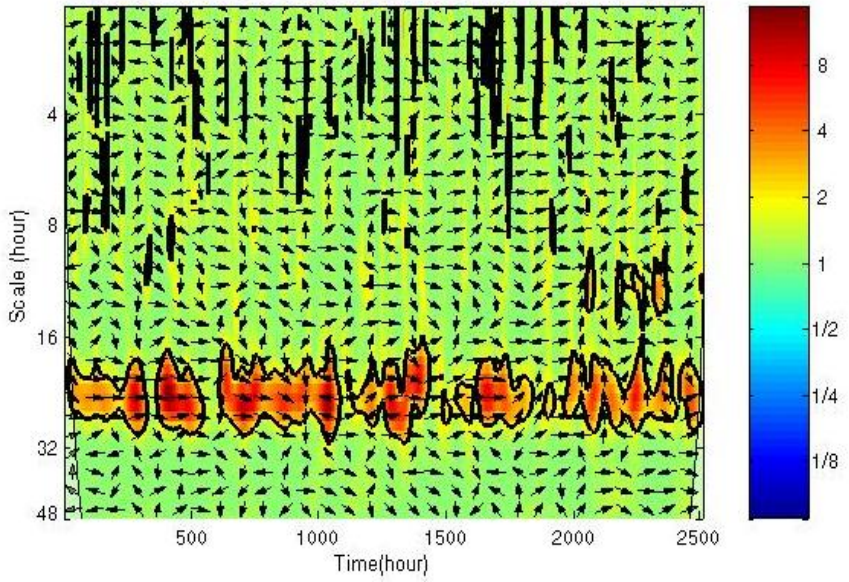

Figure C. 2. Cross wavelet spectrum between AET and W_s time series for the scale range of 2 to 48 hours.

Appendix D

The results of a model-based test in which the importance of soil moisture in the prediction of six-hour AET was assessed, are presented here. In this test, the six-hour eddy covariance (EC)-measured latent heat was modeled using GP technique in two approaches; using and not-using the water content information as input. In the first approach, the predictor set, namely 5-input set, include the meteorological variables of net radiation (R_n), ground temperature (T_g), air temperature (T_a), relative humidity (RH), and wind speed (W_s). In the second approach, in addition to the above mentioned meteorological variables, the soil water content at the current prediction time and at the previous six and 12 hours were also included in the input set (8-input set). The water content data were associated with the top five centimetres of the soil. The dataset that was used for this test includes the six-hour day-time data of the year 2006. Disregarding the missing data, the total number of instances for this test was 193, which was randomly divided into two data subsets of training and testing. The training and testing subsets constitute of 129 instances (67%) and 64 instances (33%) of the data, and were employed for developing and testing the GP models, respectively. Several equation-based GP models were generated at about 50 different levels of GP parameters, and the best six models, corresponding with both investigated approaches, were selected based on the testing sub dataset and are given as follows:

i. Not considering the water content factor in the input set (5-input set):

$$AET = 0.435\left[R_n + T_g\left(1.175 - RH\right)\right] \qquad [D.1]$$

$$AET = \frac{R_n T_g}{T_a RH + R_n} \qquad [D.2]$$

$$AET = R_n\left[T_g + 0.315\left(2T_g - R_n\right)\left(\frac{W_S\left(0.986 - T_g\right)}{R_n\left(RH^2 + 0.512{W_S}^2\right)}\right)\right] \qquad [D.3]$$

$$AET = R_n - R_n{}^2 RH\left(\frac{0.974}{T_g} - 0.783\right) \quad [D.4]$$

$$AET = \frac{0.921T_g}{0.795\left(\frac{T_g}{R_n} + \frac{RH}{0.938}\right)} \quad [D.5]$$

$$AET = 0.076T_g\left[3 - R_n - T_g + RH\left(0.259 - 2T_g - R_n - RH\right)\left(T_g + R_n\right)\right] + T_g R_n + T_g^2 W_S\left(1 - T_g\right) \quad [D.6]$$

ii. Considering water content factor in the input set (8-input set):

$$AET = R_n WC\left[T_g + \frac{0.1272}{0.1807 + R_n\left(2R_n RH + RH\right)\left(2R_n RH + \frac{0.1272}{0.1807 + 2R_n RH}\right)}\right] \quad [D.7]$$

$$AET = \frac{R_n T_g WC}{0.708R_n + T_a RH} \quad [D.8]$$

$$AET = R_n\left\{WC_1 - RH\left[\left(R_n + \frac{4R_n{}^2}{WC}\left(WC_2 - T_g\right)\right)\left(WC_2 - T_g\right)\right]\right\} \quad [D.9]$$

$$AET = WC\left[R_n T_g + 0.108 + 0.031\left(3 + 5W_S - RH\left(WC_2 + 3 + 2Rn\right) - R_n T_g\left(T_g + RH\right)\right)\right] \quad [D.10]$$

$$AET = T_g WC_1(0.144 + R_n) \quad [D.11]$$

$$AET = R_n T_g\left(WC_1 - R_n WC\left(0.879 - R_n WC_1 + WC\right) + WC_1\right) \quad [D.12]$$

where $AET, WC, WC_1, WC_2, R_n, T_g, T_a, RH$, and W_s are, in order, the rate of actual evapotranspiration [MJ], water content at current time, at six hours lag, and at 12 hours lag, net radiation [MJ], ground temperature [^{o}C], air temperature [^{o}C], relative humidity, and wind speed [m/s].

A comparison between the performance statistics of the GP models, obtained from the two different approaches, is presented in Table D.1. No considerable improvement can be perceived from the 8-input AET models in terms of error measures and correlation coefficient compared to the 5-input models. General statistical characteristics of the models errors (Table D.2) also demonstrate the similarity between the performances of 8-input and 5-input models. This indicates that inclusion of water content information, as predictor variable, may not be effective in improving the prediction ability of the six-hour AET models.

Table D. 1. Performance statistics of two types of AET models using testing subset of six-hour data.

Model	RMSE			MARE			R		
	Mean	Max.	Min.	Mean	Max.	Min.	Mean	Max.	Min.
8- input set	0.07	0.08	0.07	0.16	0.18	0.15	0.93	0.94	0.92
5-input set	0.08	0.09	0.08	0.16	0.17	0.15	0.92	0.93	0.91

Table D. 2. General statistical characteristics of errors obtained from the best six models of each type of GP models.

Model	Mean	Variance	Minimum	Maximum
8-input set	0.01	0.005	-0.22	0.23
5-input set	0.02	0.006	-0.24	0.27

Scatter plots of predicted AET values by 8- and 5-input set GP models versus observed data (Fig. D 1), and visual comparison among modeled and observed data series (Fig. D. 2) also confirms the similarity between the predictive abilities of the AET models. Furthermore, the errors produced by the 8-input and 5-input GP models follow similar probability distribution (Fig. D. 3).

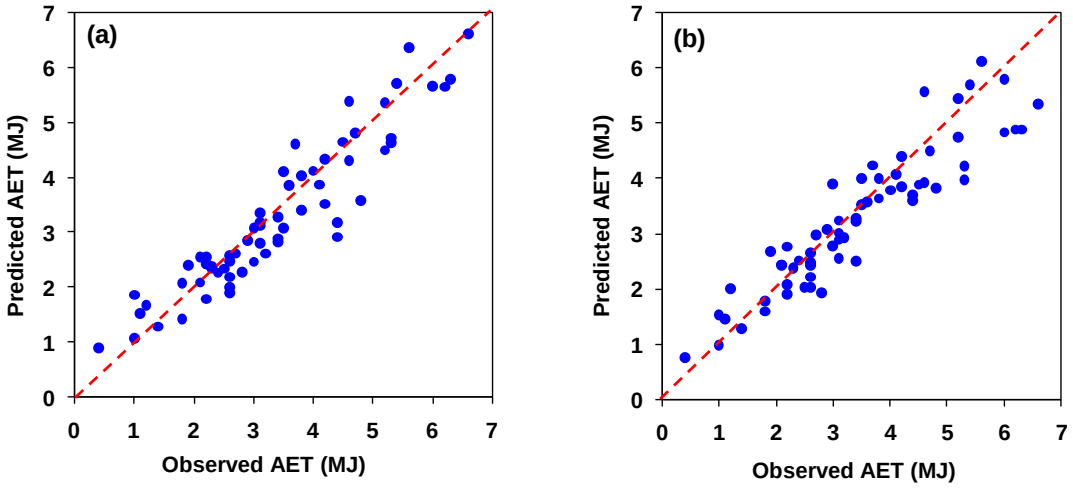

Figure D. 1. Scatter plots of predicted values resulted from (a) 8-input model (Eq. D.7) and (b) 5-input model (Eq. D. 1) versus measured data using testing subset.

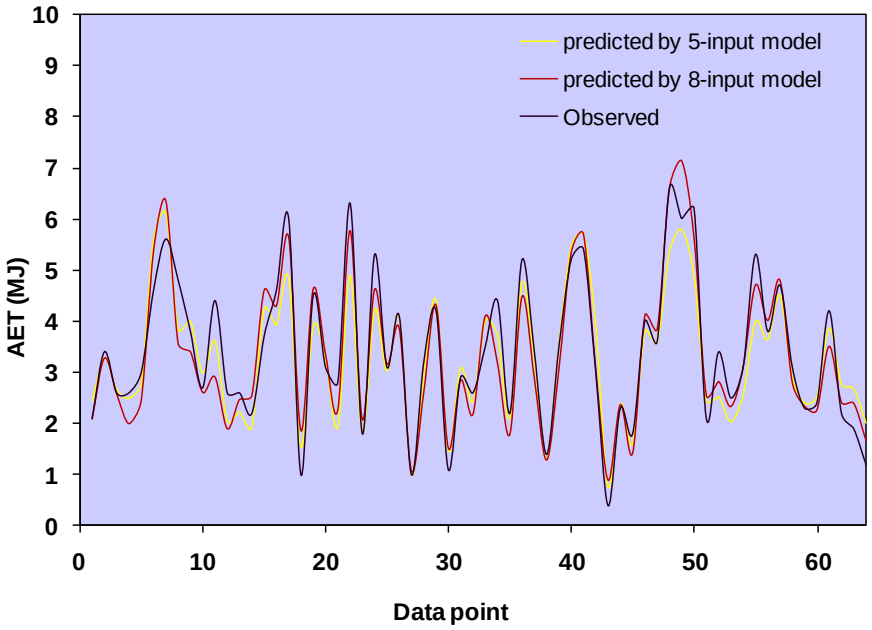

Figure D. 1. Visual comparison among the observed and the GP predicted AET values of testing subset using 8-input model (Eq. D. 7), red line, and 5-input model (Eq. D. 1), yellow line.

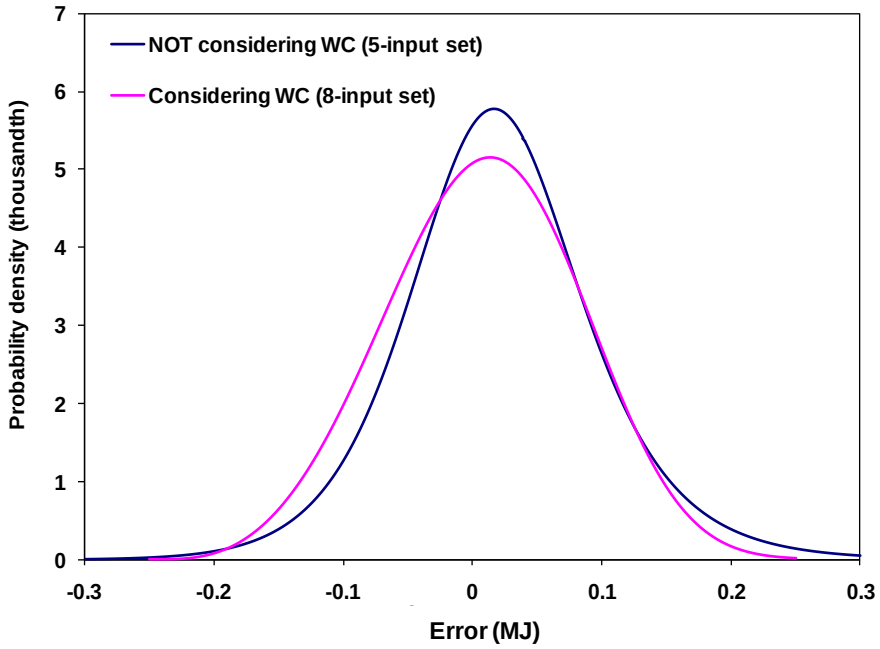

Figure D. 3. Probability distribution of the GP-evolved AET models errors.

Appendix E

The LAI and AET data in the below figure are normalized values by subtracting the data from the associated mean value and dividing by the standard deviation.

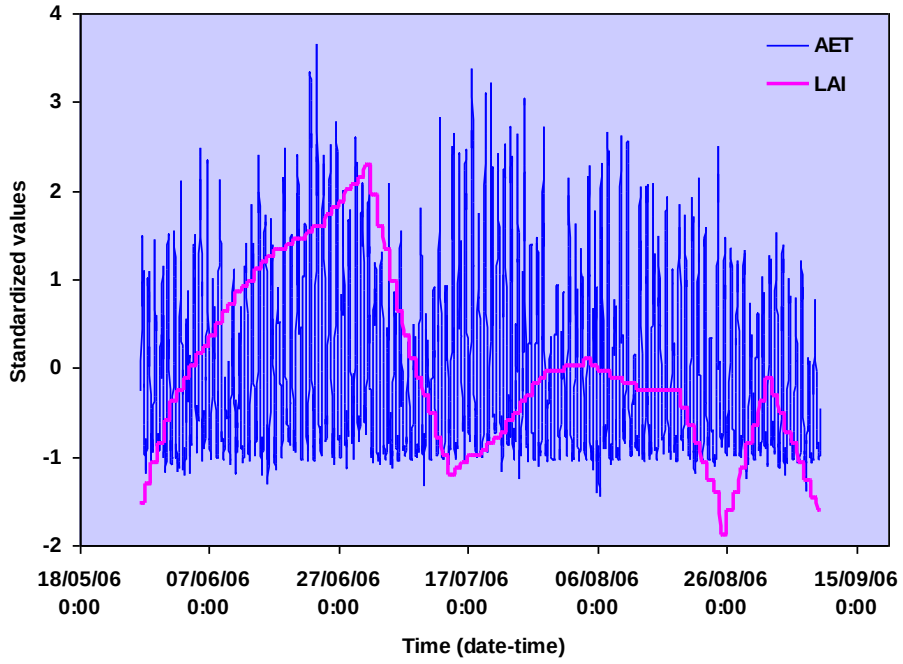

Figure E.1. Visual comparison between hourly variations of leaf area index (*LAI*) and AET versus time over the entire studied period.